MEASUREMENT OF NATURAL MAGNESIUM ISOTOPE EFFECTS IN HUMAN URINE BY GRAVIMETRIC SPIKING-ISOTOPE DILUTION ANALYSIS

CHEW CHIN NA GINA

NATIONAL UNIVERSITY OF SINGAPORE

2014

MEASUREMENT OF NATURAL MAGNESIUM ISOTOPE EFFECTS IN HUMAN URINE BY GRAVIMETRIC SPIKING-ISOTOPE DILUTION ANALYSIS

CHEW CHIN NA GINA

B.Sc. (Hons.), NUS

A THESIS SUBMITTED

FOR THE DEGREE OF DOCTOR OF PHILOSOPHY

NUS GRADUATE SCHOOL FOR INTEGRATIVE SCIENCES AND ENGINEERING

NATIONAL UNIVERSITY OF SINGAPORE

2014

DECLARATION

I hereby declare that this thesis is my original work and it has been written by me in its entirety. I have duly acknowledged all the sources of information which have been used in the thesis.

This thesis has also not been submitted for any degree in any university previously.

CHEW CHIN NA GINA

25 April 2014

ACKNOWLEDGEMENTS

It would not have been possible to complete this PhD without many important people in my life. I thank my supervisor, Assoc. Prof Thomas Walczyk for giving me a challenging project to take on and having the faith in me that I will see it to completion. His requirement for perfection, patience in clarifying, words of encouragement and devotion to scientific excellence has helped me to become a better scientist. I also want to thank Assoc. Prof Thomas Osipowicz and Prof Li Fong Yau Sam for being part of my Thesis Advisory Committee.

I am grateful to our collaborators, Dr Jimmy Teo and Dr Priscilla How, both from the National University of Singapore (NUS) and the National University Hospital (NUH), and Mr Toh Qi Chun from NUH for their input on the practicalities involved in carrying out a clinical study. This allowed me to apply the method that I developed into the real world setting. The experience was a valuable learning journey for me.

My parents George and Katherine, and my brother Billy have been constant supporters of all my decisions in life, including the one to embark on this PhD programme. My husband, Chee Heng's encouragement meant a lot to me during some of my toughest moments. I was fortunate to have spent most of my time in the laboratory with fellow postgraduate students at Nutritrace – Fransiska Dewi, Chen Jie Hua, Ren Yao, Bay Lian Jie, Li Bin, Ji Xiang and Dong Xiao as well as our dear Research Assistant Nadia Nur Singh. I will always remember the fond memories I have with each and every one of them.

I acknowledge my scholarship board, the NUS Graduate School of Integrative Sciences and Engineering (NGS) for their financial support in this PhD programme and sponsorship to attend conferences in Israel and Japan. I am thankful for the opportunity to meet great friends among fellow PhD students and NGS staff while organizing one of the NGS L.O.R symposiums. Last but not least, I would like to thank Dr Lee Tong Kooi, Director of the Chemical Metrology Division, Health Sciences Authority (HSA), for allowing me to take four years of no-pay leave to complete my PhD. I am sure that what I have learnt during the past four years would allow me to contribute to the team that implements the chemical metrology programme for Singapore.

TABLE OF CONTENTS

I. SUMMARY

Subtle variations in the isotopic composition of elements carry unique information about physical and chemical processes in nature and are now exploited widely in diverse areas of research. Reliable measurement of natural isotope abundance variations is among the biggest challenges in inorganic mass spectrometry as they are highly sensitive to methodological bias. For decades, double spiking of the sample with a mix of two stable isotopes has been considered the reference technique for measuring such variations both by multi-collector inductively coupled plasma mass spectrometry (MC-ICP-MS) and multi-collector thermal ionization mass spectrometry (MC-TIMS). However, this technique can only be applied to elements having at least four stable isotopes. Magnesium being a co-factor for more than 300 enzymes is an important but less studied essential nutrient for the human body as compared to other essential elements such as calcium or iron. Having only three stable isotopes excludes it from the investigation of natural isotope fractionation effects by double spiking techniques. This limitation is overcome by the novel Gravimetric Spiking-Isotope Dilution Analysis (GS-IDA) technique which has been developed in this thesis. Methodological parameters were optimized using Monte Carlo Simulations for which we have developed an easy-to-apply technique using commercial spreadsheet software that can be adopted for any question that requires error propagation analysis of complex analytical processes. Using these techniques we could show for the first time that human Mg metabolism is sensitive to the small differences in mass between Mg isotopes. Our final study involving twenty healthy Chinese males showed that magnesium isotope effects vary with age. The kidney is the primary homeostatic organ of Mg and it is known that renal function declines with age. The Mg isotope effect observed in urine may be explained by a Rayleigh fractionation process in which ultrafilterable Mg is reabsorbed from the tubular fluid into serum. Because most Mg is reabsorbed and only a small fraction (<5%) is excreted in urine, the difference in isotope effect between the ultrafilterable Mg in serum and Mg in urine

may reflect differences in the efficiency of renal Mg reabsorption between individuals. Such a mechanism, if confirmed, may lead ultimately to a new class of biomarkers to assess kidney function.

II. LIST OF TABLES

LITERATURE REVIEW

MANUSCRIPT 2

MANUSCRIPT 3

III. LIST OF FIGURES

LITERATURE REVIEW

MANUSCRIPT 1

MANUSCRIPT 2

MANUSCRIPT 3

1. INTRODUCTION

Stable isotopes are the building blocks of nature and most elements are made up of more than one of them. There are two types of isotopes – radioactive and stable, of which the latter are the subject of interest of this thesis. Although isotopic abundances of the stable isotopes of an element are fairly constant in nature, small variations can be observed. When there is an incomplete transfer process of matter, changes in isotopic abundances of an element or isotopic fractionation effects may occur if the transport process is sensitive to the masses of the atoms/molecules transferred.

The study of isotopic fractionation effects for the light elements such as carbon, hydrogen and oxygen is well-established and used in several ways such as dating of archaeological samples or to establish the geographical origin of a food product[1]. As the magnitude of isotope effects is not determined by the absolute but the relative mass difference of the isotopes or isotopologues, it was only with the advent of advanced mass spectrometric techniques such as Multi-Collector Thermal Ionization Mass Spectrometry (MC-TIMS) and Multi-Collector Inductively-Coupled Plasma Mass Spectrometry (MC-ICP-MS), that isotope fractionation effects of the heavier stable isotopes can be studied.

The study of naturally occurring isotopic fractionation effects is an established field of research in the geosciences but an emerging field in biomedical research. Iron [2-4] and calcium[5] were the first two elements to be examined for isotope effects in humans as markers of metabolic processes and research was recently expanded to include other essential elements in the body such as copper[6] and zinc[7]. Magnesium (Mg) is a promising candidate for isotope effects to occur during metabolic processes due to its relatively large mass differences between its three stable isotopes (^{24}Mg, ^{25}Mg, ^{26}Mg) and the central role of the kidneys in maintaining Mg homeostasis. According to isotope fractionation theory[8-10], an isotope effect in the source compartment of a mass transfer process is greater when more of an element/compound is transferred from the source compartment to the

target compartment. Ninety-five percent of filtered Mg is reabsorbed from the tubular fluid (source) back into serum (target). Remaining Mg in the tubular fluid is excreted in urine (approx. 5% of filtered Mg). Based on the assumption that Mg reabsorption in the kidneys is mass sensitive, we hypothesized that Mg in human urine should have a distinct isotope composition that should be linked to the efficiency of Mg reabsorption in the kidney making Mg isotope effects in urine a potential biomarker of kidney function.

The challenge of measuring Mg isotope effects, however, is the instrumental mass bias induced during measurement of the sample. Since both natural isotope fractionation effects and instrumental mass bias follow the same or indistinguishable fractionation laws in practice, a mathematical correction technique is necessary to differentiate the two. Various techniques have been formulated to correct for instrument fractionation effects but they have their limitations. The reference technique known as the “double spiking” technique[11] is only applicable to elements with four or more isotopes, which excludes Mg that has only three stable isotopes.

It is the aim of this thesis to develop and apply a novel technique for measuring isotope effects that requires isotope abundance ratio measurements of only three stable isotopes using Mg as a potential candidate element for isotope effects in human urine. This included a) the derivation and validation of a set of equations that can correct for instrumental mass bias effects by gravimetric mixing of the sample with an isotopic spike in different proportions and by applying principles of isotope dilution mass spectrometry for data analysis b) the development of procedures to determine the optimal mixing proportions of sample and spike that will give the lowest measurement uncertainty in the determination of Mg isotope effects and c) the application of the newly developed technique within a clinical study to investigate age-related Mg isotope effects in the urine of healthy Chinese males and to study a possible link to the renal reabsorption process.

In the following literature review, we will focus on the theory of isotope fractionation effects to establish the foundation for which this thesis is based on (Chapter 2.1), the homeostasis of Mg in the human body with a special focus on the role of the kidneys (Chapter 2.2), how Mg isotope effects arise in nature (Chapter 2.3) and the measurement of Mg isotope fractionation effects using multi-collector mass spectrometric techniques (Chapter 2.4). The three manuscripts describing the experimental work in this thesis address the use of Monte Carlo Simulations (Manuscript 1) for optimization of parameters for the novel instrumental mass bias correction technique developed in this thesis (Manuscript 2) and the application of this technique in a clinical study to establish the links between Mg isotope effects and renal function (Manuscript 3).

2. LITERATURE REVIEW

2.1 Isotope Fractionation Theory

2.1.1 Characteristics of Isotopes

Isotopes are the building blocks of nature. Isotopes of the same element have the same number of protons but different number of neutrons, hence they have different isotopic masses. Apart from chemical elements that only have a single stable isotope such as sodium (^{23}Na) and manganese (^{55}Mn), elements can have up to 10 stable or non-radioactive isotopes.

Isotopes can be distinguished as being “stable” or “radioactive”. Stable isotopes, compared to radioactive isotopes, do not spontaneously undergo decay. The stability of isotopes is governed mainly by two rules. First is the symmetry rule which states that nuclei for which the ratio of protons to neutrons is either approximately 1 for light elements (atomic number < 20) or between 1 to 1.5 for heavier elements (atomic number > 20) tend to be stable. The second rule is known as the *Oddo-Harkins* rule which states that stable isotopes tend to have an even number of protons and neutrons in the nucleus[9].

Scientists mostly consider stable isotope abundances and, thus, the Standard Atomic Weight of an element as listed in most Periodic Systems as a natural constant. In fact, this is only the case for mono-isotopic elements for which the atomic weight equals the atomic mass of a single nuclide. For all other elements, isotopic abundances and atomic weights may vary slightly. Isotope variations occur in nature either when one of the isotopes is the mother or the daughter nuclide of a natural nuclear reaction (radioactive decay) or due to isotope fractionation effects.

Natural isotope variations caused by radioactive decay have been studied extensively over the past century. They gave us insight into the history of our planet and the universe by allowing us to date

back processes that took place billions of years ago[12]. Other common applications include the dating of archaeological findings using ^{14}C such as the Alpine Iceman[13] and tracing the origin of foodstuff in forensic sciences using imprints of geographical differences in ^{87}Sr abundance[14]. This thesis, however, focuses on isotope fractionation effects as described in the following literature review.

2.1.2 Isotope Fractionation

The isotopic composition of an element is altered when matter is transferred between two compartments and when transfer efficiency is mass sensitive. Such a phenomenon is known as isotope fractionation. As an example, surface water contains slightly more of the heavier oxygen (^{17}O, ^{18}O) and hydrogen (^{2}H) isotopes as compared to condensed water (^{16}O, ^{1}H) in clouds. Isotopic fractionation occurs because isotopically lighter water evaporates faster than isotopically heavier water. This raises the question of why the physicochemical properties of isotopes of the same element differ.

According to classical theory, the chemical properties of an element are determined by its electronic structure, whereas its physical properties (e.g. boiling point, density, reaction rate) are determined by the nature of its nucleus. Since isotopes have the same number of electrons, they are expected to have the same chemical properties but slightly different physical properties. This can be explained by quantum theory[15] which states that the energy of an atom or molecule is restricted to certain discrete energy levels. Let us consider the energy of a diatomic molecule as a function of the distance between two atoms as illustrated in Fig. 1. The zero point energy (difference between the potential energy well represented by the minimum point and the ground vibration energy state) is different for two isotopes of the same element. The ground vibration energy state is determined by $½h\nu$, where h is Planck's constant and ν is the frequency with which the atoms in the molecule vibrate with respect to one another which depends on the isotope's mass. Although a diatomic molecule can undergo rotation, translation and vibration, only vibrational energy states yield

different zero point energy for different isotopes. Bonds formed by the light isotope are weaker than bonds involving the heavy isotope of the same element. Thus, for an equilibrium reaction, it would favour the reactant or product depending on which side bears the heavier isotope (more stable). On the other hand, during a chemical reaction, molecules bearing the lighter isotope will, in general, react slightly more readily than those with the heavy isotope.

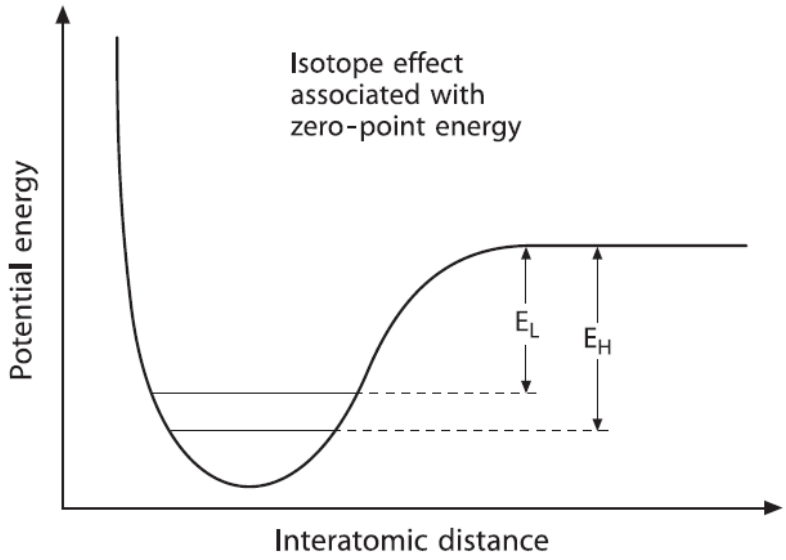

Figure 1. Schematic potential energy curve for the interaction of two atoms in a stable, diatomic molecule. E_L and E_H represent the dissociation energy for the lighter and heavier molecule respectively. The difference between E_L and E_H determines the isotope fractionation behavior (illustration adopted from Hoefs, 2009).

2.1.3 Nomenclature

2.1.3.1 Delta Notation

The isotopic composition of an element is commonly studied in a mass spectrometer in which the isotope abundances of two isotopes of an element are compared by measuring the ratio of their ion currents after ionization of the sample in the ion source. The delta ($\delta^i E$) notation is commonly used to report the relative difference in isotopic ratios of the element E, where the ratio of interest in the

sample ${}^{1/j}R_{sample}$ is expressed as a relative deviation from the ratio of the referencing standard ${}^{i/j}R_{ref}$. By convention, the subscript i denotes the heavier isotope (numerator) whereas the subscript j denotes the lighter isotope (denominator). The referencing standard is a reference material chosen by the scientific community which has been assigned a δ-value of zero absolute to allow for interlaboratory comparisons.

$$\delta({}^{i}E) = \frac{{}^{i/j}R_{sample}}{{}^{i/j}R_{ref}} - 1 \qquad (1)$$

If the δ-value is negative (for an isotope abundance ratio in which the lighter isotope abundance is in the denominator), it implies that the sample is enriched in the lighter isotopes relative to the reference material. On the other hand, if it is positive, the heavier isotopes are enriched. Since natural variations in isotope ratios are usually very small, delta values are expressed in per mill (‰) or parts per thousand by multiplying the δ-value calculated using Eqn. (1) with 1,000. Ideally, the reference standard for reporting δ-values is an isotopically homogenous material that has been certified for absolute isotope composition to ensure data comparability over space and time and that is freely available. Because of a lack of such a material for Mg, IUPAC has recommended recently DSM-3, an uncertified aqueous Mg standard solution kept at the University of Cambridge (UK), as the anchor point of the δ-scale carrying a δ-value of zero absolute[16].

2.1.3.2 Isotope fractionation factor

The isotope fractionation factor, $\alpha_{A\text{-}B}$ which reflects the difference in isotopic compositions between two substances/phases A and B, in either the equilibrium or non-equilibrium state, is defined in Eqn. (2) as:

$$\alpha_{A-B} = \frac{{}^{i/j}R_A}{{}^{i/j}R_B} \qquad (2)$$

where ${}^{i/j}R_A$ and ${}^{i/j}R_B$ are the isotopic ratios of mass *i* to mass *j*, in substance/phase A and B respectively.

In order to describe isotope fractionation effects with a mathematical expression, $\alpha_{A\text{-}B}$ can be expressed in terms of the δ-value (given in units of per mil) as:

$$\alpha_{A-B} = \frac{\delta^i E_A + 1}{\delta^i E_B + 1} \tag{3}$$

Taking $\ln$ on both sides of Eqn. (3),

$$\ln \alpha_{A-B} = \ln(\delta^i E_A + 1) - \ln(\delta^i E_B + 1) \tag{3a}$$

Since the δ-values are small, we can make use of the Maclaurin series expansion of

$$\ln(x+1) = x + \frac{x^2}{2} - \frac{x^3}{3} + \ldots + (-1)^n \left(\frac{x^n}{n} \right) + \ldots \tag{3b}$$

And ignore higher orders of *x* to obtain the approximation:

$$\ln(x+1) \approx x \tag{3c}$$

Isotopic fractionations can thus be described by simply subtracting the $\delta^i E$ values of substances A and B.

$$\ln \alpha_{A-B} = \delta^i E_A - \delta^i E_B \equiv \Delta_{A-B} \tag{4}$$

This assumption is valid as long as calculated δ-values are not larger than several tens of per mil. Phenomena that can give rise to isotope effects are thermodynamic (equilibrium) reactions and kinetic processes that depend primarily on differences in reaction or transfer rates of isotopologues.

2.1.4 Thermodynamic (Equilibrium) Isotope Effects

An equilibrium isotope effect is one in which there is no net reaction but a change in distribution of isotopes between different chemical or physical states. It is a specific type of closed equilibrium system represented by Eqn. (5)

$$A_1 + B_2 \Leftrightarrow A_2 + B_1 \quad (5)$$

where the subscripts indicate that species or phase A and B contain either the light or heavy isotope 1 or 2, respectively. For the example of equilibrium fractionation in which the heavier isotopes are concentrated in liquid water relative to water vapour, A_1 refers to $H_2{}^{16}O\ (l)$, B_2 refers to $H_2{}^{18}O\ (g)$, A_2 refers to $H_2{}^{18}O\ (l)$ and B_1 refers to $H_2{}^{16}O\ (g)$.

The equilibrium constant K, which is α_{A-B} for equilibrium isotope effects, is given by:

$$\alpha_{A-B} = K = \frac{\left(\frac{A_2}{A_1}\right)}{\left(\frac{B_2}{B_1}\right)} \quad (6)$$

α_{A-B} can be characterized mathematically by changes in energy and/or changes in δ-values. As the energy of a molecule is restricted to certain discrete energy levels, the Boltzmann distribution is used to predict how energy is distributed among the molecules. The most probable distribution of populations between two different available states, i and j with energies E_i and E_j, respectively, is given by:

$$\frac{n_i}{n_j} = e^{-(E_i - E_j)/k_B T} \quad (7)$$

where n refers to the number of molecules, T is the temperature and k_B is the Boltzmann's constant defined to be 1.38 x 10^{-23} J·K^{-1}.

Since the equilibrium constant is a function of the difference in energy and the difference in number of available states between the reactants and the products, we can apply the Boltzmann distribution directly to obtain:

$$K = e^{-\Delta E / k_B T} \tag{8}$$

where $\Delta E = E_i - E_j$

The driving force for chemical reactions, the Gibbs free energy is approximately equal to the difference in energy between the reactants and products, ΔE. Since rotational and translational energy have negligible effects on isotope fractionation, ΔG can be defined solely in terms of the vibrational energy ΔE_{vib}.

$$\Delta G \approx \Delta E \approx \Delta E_{vib} \tag{9}$$

The equilibrium constant is related to the Gibbs free energy difference ΔG (per mole) according to this relationship:

$$\Delta G = - RT \ln K \tag{10}$$

where R, the universal gas constant = $N_A k_B$ (N_A is the Avogadro's number, 6.02 x 10^{23} molecules/mole). Therefore,

$$\alpha_{A-B} = K = \frac{\left(\frac{A_2}{A_1}\right)}{\left(\frac{B_2}{B_1}\right)} = e^{-\Delta G / RT} = e^{-\Delta E_{vib} / RT} \tag{11}$$

We see the dependence of the equilibrium constant K on temperature and that at very high temperatures, isotope fractionations tend to become zero. α_{A-B} can thus be calculated from the vibrational bond energies of the molecules. The above is for the simplest case where the stoichiometry of A and B for the light and heavy isotope is 1 : 1. When the stoichiometric coefficients are not equal to 1, a more complicated expression is used to convert between equilibrium constants and fractionation factors[17].

Another means to describe α_{A-B} mathematically is through the measured change in δ-values between two phases.

For an equilibrium reaction where A and B remain open to complete isotopic exchange during the process, the equilibrium can be described by:

$$\delta^i E_B \approx \delta^i E_{total} + f\,(\alpha_{B-A} - 1) \qquad (12)$$

where α_{B-A} is the B – A fractionation factor (negative value of α_{A-B}), $\delta^i E_{tot}$ is the $\delta^i E$ value for the total system and *f* is the fraction of A remaining (i.e. *f* equals to 1 for the absence of B). Due to the principles of mass conservation, the molar fraction of A remaining (*f)* equals the molar fraction of B formed (1 – *f).*

Eqn. (12) may be further simplified to

$$\delta^i E_B \approx \delta^i E_{total} + f\Delta_{B-A} \qquad (13)$$

where Δ_{B-A} is the negative value of Δ_{A-B} defined in Eqn. (4).

The change in the δ-value as the equilibrium shifts from substance A to B is represented in Fig. 2 below.

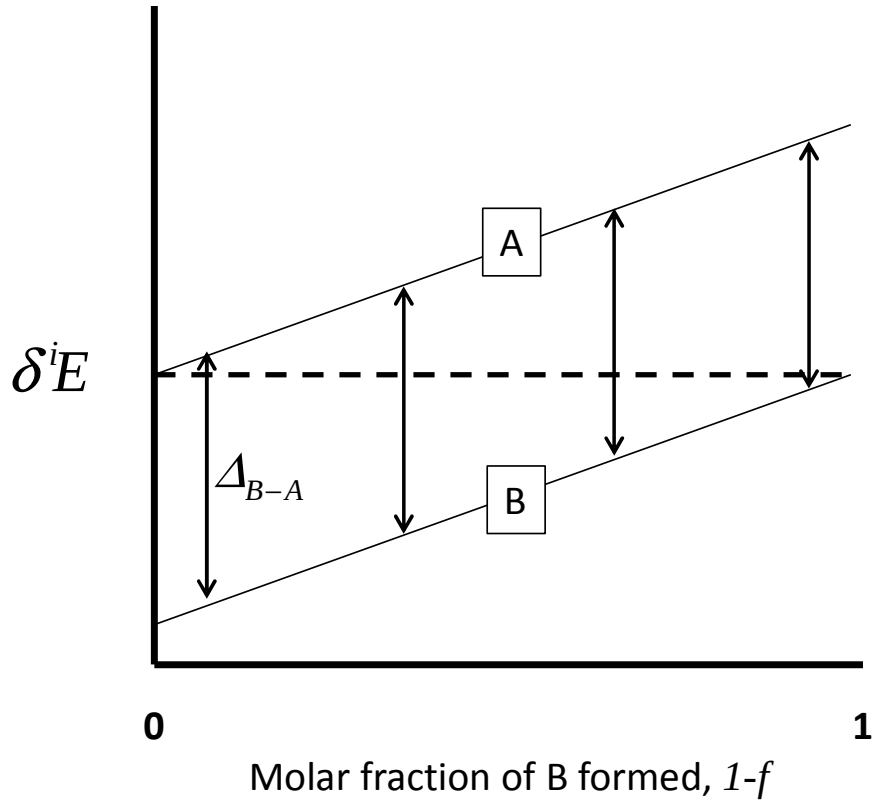

Figure 2. Isotope fractionation produced in an equilibrium fractionation process. The diagonal lines A and B represent the changes in isotopic composition of A and B respectively, as the molar fraction of B formed changes. Δ_{B-A} is a constant regardless of the position of the equilibrium. Due to the principle of conservation of mass, $\delta^i E_B$ will be equal to the initial value $\delta^i E_A$ if all of substance A is converted into substance B (Adapted from Johnson et al., 2004).

2.1.5 Kinetic Isotope Effects

Kinetic isotope fractionation effects are associated with incomplete and unidirectional mass transfer processes (e.g. evaporation, diffusion) or reactions (e.g. dissociation reactions, biologically mediated reactions). For the reaction of light and heavy isotopologues 1 and 2 between reactants and products, A and B respectively, the reactions or mass transfer processes can be written as:

$$A_1 \xrightarrow{k_1} B_1 \qquad (14)$$

and

$$A_2 \xrightarrow{k_2} B_2 \tag{15}$$

The rate constant of the process, k is determined by the activation energy E_A between reactants and products containing isotopes of different masses according to

$$k = Ae^{-E_A / RT} \tag{16}$$

where A is the Arrhenius constant.

As lighter isotopes have a higher zero point energy, the activation energy is smaller for molecules that contain the lighter isotope. Molecules that contain light and heavy isotopes will react at different rates, resulting in different k_1 and k_2 values.

The fractionation factor α_{A-B} of a kinetic isotope effect is the ratio of rate constants for the reaction of light and heavy isotope species $\frac{k_1}{k_2}$ which is proportional to the reduced masses μ of the isotope and the counteratom of the dissociating bond.

$$\alpha_{A-B} = \frac{k_1}{k_2} \propto \sqrt{\frac{\mu_1}{\mu_2}} \tag{17}$$

If the structure of the reactant and activated complex are similar, the fractionation factor can be calculated using the approximation:

$$\alpha_{A-B} \cong \sqrt{\frac{\mu_1}{\mu_2}} \tag{18}$$

The changes in isotopic composition of the components A and B, i.e. $\delta^i E_A$ and $\delta^i E_B$, in a kinetic isotope effect can be described by Rayleigh fractionation. For component A, the Rayleigh equation is:

$$\frac{\left({}^{i/j}R\right)_A}{\left({}^{i/j}R\right)_{A,0}} = f^{(\alpha_{B-A}-1)} \tag{19}$$

where $\left({}^{i/j}R\right)_{A,0}$ is the initial ratio and $\left({}^{i/j}R\right)_A$ is the ratio in A for molar fraction *f* remaining.

This can be expressed in terms of $\delta^i E$ values:

$$\frac{1+\delta^i E_A}{1+\delta^i E_{A,0}} = f^{(\alpha_{B-A}-1)} \tag{20}$$

To determine $\delta^i E_A$, the equation can be rearranged to:

$$\delta^i E_A = (f^{\alpha_{B-A}-1} \cdot (1+\delta^i E_{A,0})) - 1 \tag{21}$$

$$\delta^i E_B = (f^{\alpha_{B-A}-1} \cdot (1+\delta^i E_{B,0})) - 1 \tag{22}$$

$$\delta^i E_B = \delta^i E_A + \Delta_{B-A} \tag{23}$$

Equations (21) and (22) were used to plot Fig. 3. If Δ_{B-A} is constant, the instantaneous $\delta^i E$ values for A and the incremental formation of B will be constant as seen in Fig. 3. However in practice, it is the isotopic composition of total B after a given extent of reaction or mass transfer that is of interest. Changes in $\delta^i E$ of total B is more modest than for the incremental portions of B and is equal to $\delta^i E$ of initial A if the reaction or mass transfer process goes to completion. As a result, Δ_{B-A} increases dramatically towards the end of the reaction or mass transfer process. Hence for a

process in which the extent of reaction or mass transfer from A to B is large (close to 100%), we would expect a large value for Δ_{B-A}. On the other hand, if the process reaches completion, no net isotope fractionation will be observed.

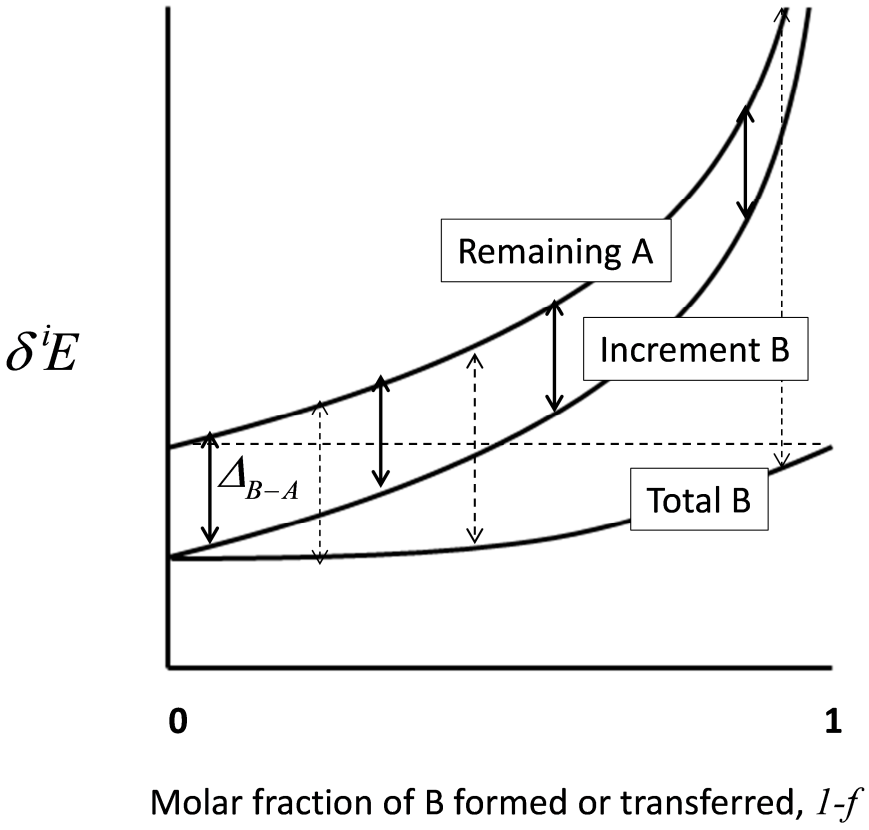

Figure 3. Plot of isotope composition $\delta^i E$ of remaining A, increment B and total B, against the molar fraction of B formed or transferred. In a kinetic isotope fractionation effect also known as an incremental Rayleigh fractionation process, increment B refers to the instantaneously formed/transferred B. Total B refers to the total formed/transferred fraction of B. Δ_{B-A} is a constant between remaining A and increment B (represented by the normal double arrow lines). On the other hand, Δ_{B-A} increases dramatically towards the end of the reaction (represented by the dashed double arrow lines). Adapted from Johnson et al. (2004).

2.1.6 Mass Dependent Fractionation (MDF)

In Mass Dependent Fractionation (MDF), differences in isotope ratios are proportional to the relative differences in mass between the isotopes or isotopologues involved. Mass Dependent Fractionation

(MDF) effects can be described by isotope fractionation laws. These laws relate the extent of isotope fractionation observed for one isotope ratio R_1 to a second isotope ratio R_2 of the same element, as a function of the masses of the relevant species. The general form of common mass fractionation laws[18-19] is:

$$\frac{(R_1)_M}{(R_1)_T} = b\left[\frac{(R_2)_M}{(R_2)_T}\right]^a \tag{24}$$

where the subscripts M and T refer to measured and true isotope ratios respectively. R_1 refers to the ratio of the abundances of the two isotopes $\frac{n(^{iso1}E)}{n(^{iso2}E)}$ where *n* refers to the number of moles and *iso1* and *iso2* are their physical masses m_1 and m_2 respectively. R_2 refers to the ratio of the abundances of the two isotopes $\frac{n(^{iso3}E)}{n(^{iso2}E)}$ where *n* refers to the number of moles and *iso2* and *iso3* are their physical masses m_2 and m_3 respectively. Both R_1 and R_2 share the same denominator. Different empirical laws have been suggested to describe isotopic fractionation as seen in Eqns. (25), (26) and (28). The Rayleigh law (Eqn. 27) was derived by linking evaporation of species with Rayleigh fractionation in the ion source of a mass spectrometer.

For the exponential fractionation law, $a = \frac{\ln(m_1/m_2)}{\ln(m_3/m_2)}$, b =1 (25)

For the power law, $a = \frac{m_1 - m_2}{m_3 - m_2}$, b = 1 (26)

For the Rayleigh law, $a = \frac{1-(m_2/m_1)^{1/2}}{1-(m_2/m_3)^{1/2}}$, $b = \frac{(m_2/m_1)^{1/2}}{\left[(m_2/m_3)^{1/2}\right]^a}$ (27)

The linear law can be written in the form:

$$\frac{(R_1)_M}{(R_1)_T} - 1 = a\left[\frac{(R_2)_M}{(R_2)_T}\right] \text{ where } a = \frac{m_1 - m_2}{m_3 - m_2} \quad (28)$$

It is generally agreed that the exponential law best describes fractionation effects in nature and in the ion source of a mass spectrometer. From the exponent, it can be seen that the difference between fractionated and unfractionated ratios is greater for isotopes that have a large relative mass difference which are more common for the lighter elements (e.g. carbon, hydrogen, oxygen and nitrogen). Conversely, natural isotope variations of the heavier elements are smaller and therefore more difficult to detect.

2.1.7 Mass Independent Fractionation (MIF)

A deviation from MDF is known as Mass Independent Fractionation (MIF) which has been a topic of discussion in recent years[20]. In MIF, the magnitude of separation of isotopes does not change in proportion with the difference in the masses of the isotopes. Compared to MDF, MIF processes are less common and seem to occur mainly in photochemical reactions and spin-forbidden reactions. MIF is supposed to be caused either by the nuclear field shift (NFS), also known as nuclear volume effect, or by nuclear spin effects in the heavier elements. Isotopes experience a nuclear field shift when the binding energy between the electron and its nucleus is affected by the heterogeneous distribution of protons inside the nucleus. For most isotopes, the relationship between the size of the nucleus versus number of neutrons is linear. However, deviations from this linear relationship are observed for elements with odd isotope numbers, such as mercury and thallium[21]. On the other hand, nuclear spin effects may arise from the interaction of the magnetic field associated with the spin angular momentum of an electron with the magnetic field associated with non-zero nuclear spin that occur during chemical reactions involving radical pairs, such as photolysis[22].

A majority of MIF observations in nature are for mercury in aquatic ecosystems where it undergoes reactions such as methylmercury degradation[23-24], in atomospheric samples[25-27], environmental samples such as sediment, soil and peat[26-27], and in laboratory experiments such as

photoreduction[23]. A review by Epov[20] showed that out of 37 publications related to MIF, 22 were based on investigations of mercury. The remaining publications reported on rare observations of MIF for other heavy elements - tin during methylation and demethylation reactions in aqueous solution under UV irradiation[28]; for cadmium during isotope exchange reaction with dicyclohexano-18-crown-6[29-30]; for strontium during isotope exchange reaction in liquid chromatography with a cryptand (2B,2,2) polymer[31]; for zinc during redox reactions and reaction with crown ether in different acidities[32]; and for ^{207}Pb isotope - during measurement of the lead isotopic composition by Thermal Ionization Mass Spectrometry (TIMS) at a high temperature (> 1175 °C)[33]. So far, MIF has not been thoroughly investigated for elements other than mercury and is still a topic of debate. MIFs that have been observed for the other elements may also be measurement artifacts induced during isotopic analysis, especially when using Multi Collector-Inductively Coupled Plasma-Mass Spectometry (MC-ICP-MS)[34-35].

2.2 Magnesium in the Human Body

2.2.1 Physiological Function

The physiologically active form of Mg is its divalent cation, Mg^{2+}. Mg^{2+} is a co-factor for more than 300 enzymatic reactions in the body. Mg^{2+} works synergistically with Ca^{2+} to activate phosphorylase kinase[36] which stimulates glycogen to break down to free glucose that enters glycolysis. In the Krebs cycle, Mg^{2+} activates acetyl-CoA synthetase to break down adenosine tri-phosphate (ATP) to adenosine mono-phosphate and the inorganic phosphate ions[37]. In the cell, Mg^{2+} activates ion transport pumps such as Ca^{2+}-ATPase[38-39], Na^{+}/K^{+}-ATPase[40] and K^{+}/H^{+} ATPase[41] located in the Sarco(endo)plasmic Reticulum membranes, by forming a complex with ATP so that it can be used as a substrate and also in the dephosphorylation of the enzyme.

Mg^{2+} competes with Ca^{2+} for binding sites on proteins and membranes and influences Ca metabolism. In muscular contraction, it helps to maintain a low intracellular Ca^{2+} concentration for proper cell functioning by non-competitive inhibition. In the nervous system, Mg exerts a depressant effect by competing with Ca and inhibiting the release of acetyl-choline necessary for the transmission of nervous signals[42]. When the balance is disturbed by low Mg serum concentration, it may give rise to neuromuscular and cardiovascular disorders[43].

Due to its relatively high positive charge-to-size ratio, it has a high affinity for the negatively charged ribose phosphate structure. It therefore helps to stabilize numerous ribonucleotides and deoxyribonucleotides which are important in cell replication processes such as DNA maintenance, duplication and transcription[44].

2.2.2 Magnesium Homeostasis

In an adult human, the amount of magnesium (Mg) present in the body is about 22 – 26 g. Mg is one of the major minerals in the human body and is responsible for important physiological functions. More than 99% of total body Mg is equally distributed between cells in muscle and soft tissue and bone, whereas less than 1% of total body Mg is present in the extracellular fluid[45] . Intracellular Mg is mainly bound to anionic compounds such as ATP, ADP, citrate, proteins, RNA and DNA or is sequestered within mitochondria and the endoplasmic reticulum. Only 0.5 to 5% of intracellular Mg exists in the free ionic form. In the circulatory system, Mg is found in red blood cells (0.5%) and in serum (0.3%). In serum, the concentration of Mg is 0.7 to 1.1 mmol/L[46]. Approximately 70-80% of serum Mg is unbound by proteins (i.e. exist as free Mg^{2+} ions or complexed with anions) and is therefore available for glomerular filtration by the kidney[47]. Under normal conditions, about 95% of the filtered load of Mg is reabsorbed by the kidney and about 5% is excreted in urine. Mg is not secreted by the renal tubules.

The following diagram (Fig. 4 Swaminathan 2003) illustrates uptake, distribution and excretion of Mg in the human body.

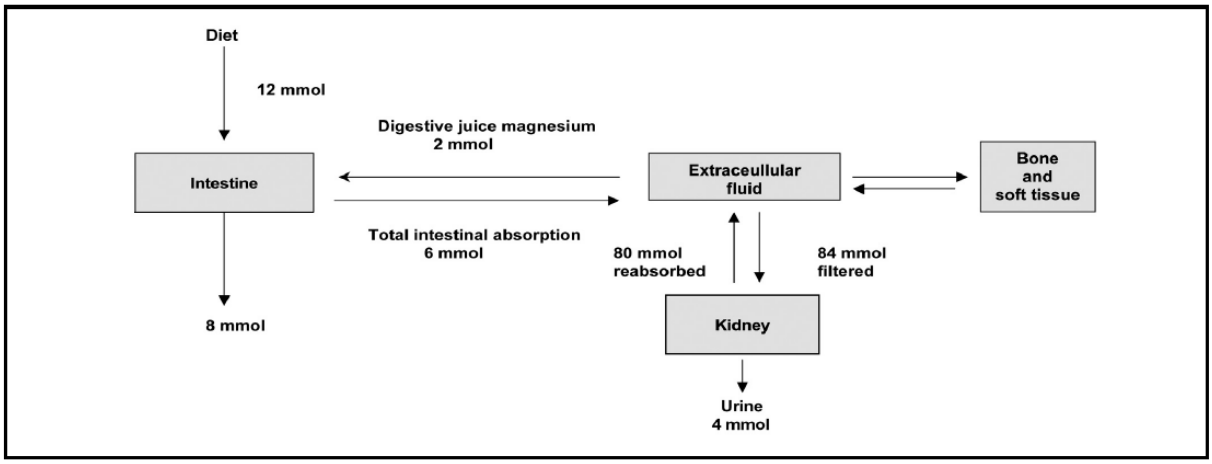

Figure 4. The distribution of Mg in the human body. Adapted from Swaminathan (2003).

The average adult diet consists of approximately 12 mmol (360 mg) of Mg per day. Approximately 8 mmol/day is undigested and lost in faeces. Approximately 2 mmol/day of magnesium is secreted into the intestinal tract in bile and pancreatic and intestinal juices. From this pool, 6 mmol is absorbed, giving a net absorption of approximately 4 mmol/day. To achieve Mg balance, the net excretion is approximately 4 mmol/day in urine.

However, there are several factors that influence Mg excretion. When glomerular filtration rate is increased but tubular reabsorption is unchanged, the Mg load to the kidneys increase and excess Mg is removed from the body in the urine. Mg reabsorption follows sodium and water. When extracellular fluid volume is increased, sodium and water reabsorption is decreased and less Mg is reabsorbed. Similarly, drugs such as furosemide (loop diuretics) which decrease sodium and water reabsorption, also increases Mg excretion. On the other hand, drugs such amiloride and chlorothiazide increase Mg reabsorption in the distal tubule. Magnesium homeostasis is not known to be regulated by any specific hormone. Instead, it is the concerted action of several hormones

together that affect Mg reabsorption and hence excretion. Hormones such as parathyroid hormone, calcitonin, antidiuretic hormone, glucagon and insulin have been found to increase Mg reabsorption at either the Thick Ascending Loop of Henle or the Distal Tubule[43]. Metabolic acidosis may induce renal losses of Mg regardless of Mg intake[48]. When plasma concentration of Mg and calcium are high, calcium-sensing receptors reduce Mg reabsorption and more Mg is excreted in the urine[49].

Dietary factors that affect Mg urinary excretion include ethanol, caffeine, proteins and sodium. It has been demonstrated that ethanol ingestion may increase urinary excretion of Mg[50] and patients suffering from chronic alcoholism frequently have low plasma Mg levels[51-52]. Caffeine is structurally similar to adenosine which functions as a mediator in the tubuloglomerular feedback response[53]. Caffeine inhibits adenosine and therefore reduces tubular reabsorption and increases urinary excretion of Mg, as well as other ions such as calcium, sodium and chloride. A study on adult males showed that there is a significant increase in urinary Mg with increase in dietary protein intake[54] probably due to an increased acid load which increases urinary Mg excretion. A high sodium intake increases renal Mg excretion[55-56].

To counteract Mg losses through the kidneys, about 30–40% of Mg from the diet is absorbed. At normal intakes, absorption is primarily passive. Depending on the body status, intestinal absorption may increase to 80% (magnesium deficiency) or may decrease to 20% (positive body Mg balance). Intestinal absorption follows a curvilinear kinetic resulting from two transport mechanisms: a saturable transcellular transport which is of functional importance at low intraluminal concentrations and a paracellular passive transport linearly rising with intraluminal magnesium concentrations[57] as shown in Fig. 5A. Factors controlling magnesium absorption are not well understood. Parathyroid hormone (PTH) may be involved in regulating Mg absorption whereas the role of Vitamin D and its metabolite (1,25)-di-hydroxy-vitamin D are more controversial.

Paracellular transport accounts for 80 – 90% of Mg renal reabsorption in the proximal convoluted tubule (PCT) and the thick ascending loop of Henle (TALH), see Fig. 5B. It involves the movement of the dehydrated Mg^{2+} ion through the small spaces between the epithelial cells[58]. The electrochemical gradient between the lumen of the renal tubule (positive transepithelial voltage) and serum (0.7 – 1.1 mmol/L) is the driving force for the passive transport of Mg[59]. In the kidney, Mg reabsorption requires a steeper concentration gradient compared to sodium or calcium. Hence the extent of Mg reabsorption increases as more and more water is reabsorbed along the nephron. It increases from 15 – 20% in the PCT to 65 – 75% in the TALH[56], see Fig. 5C.

On the other hand, the transcellular pathway involves the active transport of Mg^{2+} to the blood through the interior of the epithelial cell via the Transient Receptor Potential Channels, TRPM 6 and TRMP 7[60] (see Fig. 5D). When intestinal magnesium concentration is low, active transcellular transport prevails, primarily in the distal small intestine and the colon, and also in the distal convoluted tubule (DCT) of the kidney, in order to conserve Mg. Though only a minority of filtered magnesium (approximately 5 – 10%) is reabsorbed in the DCT, this nephron segment determines the final urinary magnesium concentration, as no reabsorption takes place beyond this segment[57].

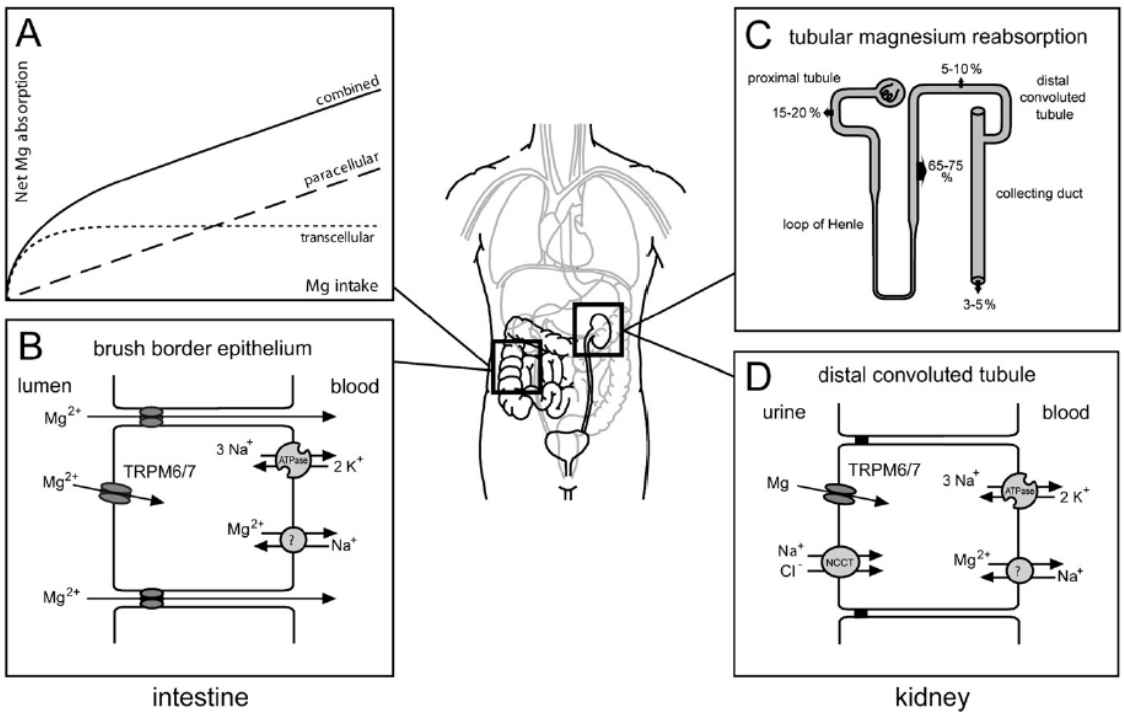

Figure 5. Epithelial magnesium transport in the intestine and the kidneys. (A) Relationship between net Mg absorption in the intestine and Mg intake (B) TRPM6/7 is a component of the active transcellular pathway in the brush border epithelium. (C) Magnesium transport along the nephron. (D) TRPM6/7 is a component of Mg transport in the distal convoluted tubule. Adapted from Schlingmann (2007).

Serum Mg levels are kept within a narrow range in the human body despite significant variations in daily dietary intake and excretion. The different processes involved in Mg homeostasis are gastrointestinal absorption, urinary excretion by the kidneys, and exchange between the bone reservoir and serum. Gastrointestinal absorption and urinary excretion involves short term (hourly /daily) and rapid adjustments of Mg serum levels, whereas the bone reservoir involves a slower turn-over rate and is more important in the longer term (days/weeks)[61]. In the skeleton, one third of intracellular Mg is free to enter the circulatory system when Mg concentration is low, such as in times of poor dietary supply. However, the mechanism by which Mg enters and leaves bone is not well understood. The kidneys play a major role in controlling Mg reabsorption so that urinary excretion is balanced with dietary intake and gastrointestinal absorption[61].

When dietary magnesium intake is poor, the kidney can compensate by increasing fractional reabsorption from the filtered load, mainly in the TALH with further reabsorption in the DCT. Normally, plasma magnesium is filtered at the glomeruli apart from the fraction bound to albumin. Reabsorption of the filtered load can vary depending on the body store, being lowest when body stores are adequate to maximum in deficiencies. Prolonged periods of poor dietary intake, however, would eventually lead to a decline in intracellular magnesium concentration and hence in Mg status[62-63].

2.2.3 Recommendations for Dietary Mg Intake

2.2.3.1 Dietary sources

Mg is found in all unprocessed foods in different proportions. It has the highest concentration in whole seeds such as nuts, legumes, and unmilled grains[64]. More than 80% of the Mg is lost in cereal grains when the germ and outer layers are removed[65]. Green vegetables, which contain Mg in the form of the porphyrin complex in chlorophyll, are also a good source of Mg. Relatively poor sources of Mg include fish, meat, milk and fruits apart from bananas. In general, diets high in vegetables and unrefined grains are much higher in Mg than diets that include mainly refined foods, meat, and dairy products[66]. Apart from food, “hard” water may also be a major source of Mg for populations who live in areas where water rich in Mg salts are found.

2.2.3.2 Bioavailability

The human diet is complex and contains various organic and inorganic substances that may affect the bioavailability of Mg. Bioavailability is the amount of Mg which is available for use by the body and determines the Recommended Dietary Allowance (RDA) for Mg (see below). Factors that affect intestinal absorption are more significant than those that affect urinary excretion.

A number of dietary factors affect Mg absorption. Minerals have a varying effect on Mg absorption. Evidence from rat studies indicate that minerals such as sodium or potassium[67] do not influence Mg absorption, whereas there is some evidence which suggests that a high calcium and high phosphate diet may inhibit Mg absorption in the intestine[68-69]. Complexing agents are another class of dietary compounds that have been investigated. Of the several complexing agents such as phytic acid, oxalic acid and polyphenols which have been found to chelate with divalent ions such as iron[70-71], zinc[72] and calcium[72], only phytic acid was found to have a significant effect on decreasing Mg absorption[73-76]. Phytic acid is found in all plant cells. It is the main storage form of phosphorus in cereals, legumes, and oilseeds and is found in foods based on wholemeal flour or bran. Oxalic acid is mainly found in the leaves of spinach and rhubarb. Since spinach itself contains a high amount of Mg, the presence of oxalate is not likely to have a significant effect on Mg absorption. Polyphenols are mainly found in fruits and beverages (e.g tannins in tea) and the intake in the western diet was estimated to be 1g/day[77-78]. Mg absorption was found to be inhibited by relatively high concentrations of polyphenols in rats (1g/100g in the diet)[79]. Hence polyphenols may have a significant impact on Mg absorption but this has not yet been proven in humans. Other weak complexing agents such as EDTA has been used to enhance absorption of minerals such as iron by preventing it from being complexed to phytic acid and therefore making iron more bioavailable. However, EDTA was not found to increase the bioavailability of Mg in infants[80], possibly due to the weaker Mg-EDTA complex that can be formed compared to iron-EDTA[81]. It has also been suggested that the Mg-chlorophyll complex may protect Mg and increase its bioavailability[82]. However chlorophyll degrades easily under acidic conditions in the stomach[83]. Hence such a protective action might not exist.

Other dietary components which are present in larger quantities, namely proteins, fats, carbohydrates and dietary fibre, also influence Mg absorption. A number of studies have suggested that proteins increases Mg absorption in humans[84-86]. Studies that showed dietary proteins had no effect on Mg absorption[87-89] appear to suffer from methodological limitations such as a lack of

standardization of Mg content of test meals. Studies looking at the effect of fat intake on Mg absorption were contradictory as there was no standardization of diet and type of fat investigated[90-91]. Dietary fibre can be classified as either fermentable or non-fermentable. The findings for non-fermentable fibre were inconsistent due to its significant content of phytic acid and Mg, the varying nature of the fibre and the study design[92-96]. It was suggested Mg colonic absorption could be facilitated by non-digestible but fermentable carbohydrates (e.g. hemicellulose, pectin, gums, resistant starch) which cause a decrease in pH in the large intestine by increased bacteria degradation.

2.2.3.3 Recommended Dietary Allowances

Dietary Reference Intakes (DRIs) were established in 1997 and comprise of the Estimated Average Intake (EAR), Recommended Dietary Allowance (RDA), Adequate Intakes (AI) and Tolerable Upper (UL) Intake levels. The EAR is the nutrient intake value that is estimated to meet the requirement defined by a specified indicator of adequacy in 50% of the individuals in a life stage and gender group. EAR is used in setting the RDA and is one factor used for assessing the adequacy of intake of groups not individuals. RDA, on the other hand, is applicable to individuals. It is the average daily dietary intake level that is sufficient to meet the nutrient requirements of nearly all (97-98%) individuals in a life stage and gender group. AI is set instead of an RDA if sufficient evidence is not available to calculate an EAR. As seen in the table below, the AI instead of RDA is given for infants. It is estimated from the daily mean nutrient intake supplied by human milk for healthy, full term infants who are exclusively breastfed. UL is the highest level of daily nutrient intake that is likely to pose no risks of adverse health effects in almost all individuals in a general population. We will focus on RDA for the purpose of this literature review.

Methods for estimating Mg RDA are mainly metabolic balance procedures[54, 69, 85, 97] in the past and stable isotope techniques[98-99] in recent years. RDA is determined from the amount of Mg intake in

diet which balances the output in feces, urine and sweat. Table 1 summarizes the Mg RDA[100] for individuals at different life stages.

Table 1. Mg RDA for different life stages[100].

Life stage	Male (mg/d)	Female (mg/d)
Infants		
0 – 6 mths	30*	30*
6 – 12 mths	75*	75*
Children		
1 – 3 y	80	80
4 – 8 y	130	130
Teenagers		
9 – 13 y	240	240
14 – 18 y	410	360
Adults		
19 – 30 y	400	310
>31 y	420	320
Pregnancy	NA	360
Lactation	NA	320

*Adequate intake (AI)

It is important to note that DRI values were developed from the diets of Canadians and Americans and are therefore not generalizable globally, especially where different dietary preferences may result in very different bioavailability of nutrients[101].

2.2.4 Measurement of Mg status

In a clinical setting, serum is the most commonly measured biological fluid to determine Mg deficiency or toxicity. Serum Mg which contains only 0.3% of total body Mg, does not reflect total body Mg level[102]. In subtle chronic Mg deficiency, individuals whose serum Mg levels are within the reference range may have a low Mg status, for instance in the elderly[103]. Age is a risk factor of Mg deficiency as the elderly are known to absorb less in the diet and lose more in the urine.

Twenty-five percent of total body Mg store is found in muscles and it is therefore a significant compartment for the assessment of Mg status. However, because tissue biopsy is an invasive technique, it is generally not preferred. Similarly, bone Mg concentration (60% of total body Mg)

may be an accurate indicator of status. Given the invasiveness of obtaining bone biopsies, research has only been carried out in rats. The results of a study comparing Mg deficient and normal rats showed that bone content is correlated with the amount of Mg consumed in the diet. It also showed that bone Mg data requires cautious interpretation because Mg concentration of bone varies between different bones, at sites within a single bone, and with age and maturity[104]. Even if bone Mg correlates well with Mg status, it is of little use in patient care since it is not clinically available in humans.

The Mg load test is currently the best proxy and standard tool for assessing status due to its non-invasiveness. After a fixed amount of Mg is given orally or intravenously (Mg load), changes in urinary Mg excretion is used to determine the extent of intestinal Mg absorption which is inversely correlated with Mg concentration in bone[105-106]. Urine collection is carried out for 24 hours after administration of the Mg load as urinary Mg excretion fluctuates depending on the time of the day[107]. In normal subjects, 80% of loaded Mg is excreted in urine within 24 h. Individuals with less than 30% of loaded Mg excreted are likely to be Mg deficient. This method of assessment can be done for adults with normal renal and gastrointestinal function, but not for infants and children.

The determination of intracellular Mg is likely to be a more accurate indicator of Mg status since it is present in a much larger proportion (99% of total body Mg) than extracellular Mg. Studies were conducted to determine the correlations between intracellular Mg concentration in blood mononuclear (lymphocyte) cells and serum Mg. In healthy subjects, no correlation was observed between Mg in blood mononuclear cells (intracellular) and that in serum (extracellular)[108]. The Mg content of mononuclear blood cells measured in patients with normal serum Mg levels were found to be low in those with cardiovascular disease[109], parathyroid disease[110] and digitalis-toxic arrhythmias[111] and migraines[112]. Studies conducted on Mg in red blood cells showed conflicting results for individuals with and without disease[113-116].

Thus far the above discussions were based on total Mg content of serum, that is Mg that is bound to anions, proteins and those that exist as free Mg^{2+}. Since it is free Mg^{2+} ions that play the primary biological role of Mg, ionized Mg may be a possible indicator of status. The use of ionized Mg content in serum, plasma and blood cells as an indicator of Mg status has been investigated as they show greater potential as indicator of Mg status than total Mg content. Total Mg content is often measured using flame Atomic Absorption Spectroscopy whereas ionized Mg can be measured using Nuclear Magnetic Resonance[117], zero-point titration[118], ion-selective electrodes[119] and fluorescent probes[112]. There is evidence to show that ionized Mg may be a good indicator of Mg status[112, 119-120]. However, at present, none of the methods based on free ionized Mg measured either in plasma, lymphocytes or red blood cells has been validated with the reference method (Mg loading test). There is also a need to standardize results obtained using different measurement techniques. A good indicator for Mg status in the clinical setting has yet to be found.

2.2.5 Magnesium deficiency and toxicity

When the body is depleted in Mg as indicated by low serum Mg levels (< 0.7 mmol/L), clinical symptoms of deficiency may arise. Clinical symptoms of moderate to severe Mg deficiency include hypocalcemia[121], neuromascular manifestations such as seizures and cardiovascular manifestations such as cardiac arrhythmia[122]. If Mg deficiency is allowed to persist over time (e.g. due to low dietary Mg intake), it may contribute to a number of disease states. Epidemiological studies have shown the association between low dietary Mg intake and diabetes mellitus[123-126], hypertension[127-128] and post-menopausal osteoporosis[129].

Magnesium deficiency can be due to low dietary intake, gastrointestinal and renal disorders. The dietary Mg intake in industrialized countries[130-131] has declined over the years as populations become more affluent and consume more highly processed foods. Gastrointestinal disorders may contribute to Mg depletion via vomiting and nasogastric suction, acute and chronic diarrhoea, regional enteritis, ulcerative colitis Crohn, and intestinal and biliary fistulas[132]. A genetic mutation that affects

the expression of TRPM6/7 involved in active intestinal transport may affect Mg absorption and result in Mg deficiency[133]. Renal disorders may cause excessive excretion of Mg into urine. Factors that decrease renal Mg reabsorption at the TALH, such as hypercalcemia[134] and the use of medications such as diuretic drugs (loop and thiazides)[135], proton pump inhibitors (e.g. omeprazole) and tacrolimus; chemotherapeutic agents such as cisplatin, cyclosporine and cetuximab; and some phosphate-based drugs will result in Mg depletion. Dietary factors such as caffeine, ethanol, protein and sodium, discussed earlier, can cause excessive renal loss of Mg and is a potential cause of deficiency. The elderly is particularly a vulnerable population to Mg deficiency. Coupled with generally low Mg intakes among the elderly[136], gastrointestinal and renal mechanisms weaken with age. A study based on the Mg loading test conducted on healthy Norwegian young and elderly persons showed that the elderly have a lower Mg status than young[137].

On the contrary, Mg intoxication is not a common clinical problem. It is usually due to excessive administration of Mg salts as part of treatment of eclampsia and suspected drug overdose, usually in the presence of impaired renal function. Some of the effects of very high serum Mg levels include lethargy, confusion, muscle weakness and respiratory difficulty.

2.3 Magnesium Isotope Effects in Nature

2.3.1 Geosphere and Hydrosphere

Research exploring Mg isotope efects in nature started about a decade ago following early investigations by Galy et al. using MC-ICP-MS and the standard-sample bracketing method for correction of instrumental mass bias correction[138]. Mg has only three isotopes and cannot be analysed using the double spike technique and, thus, TIMS. Up to now, studies of natural Mg isotope effects have been confined to geology, hydrology and biogeochemistry. Rocks and minerals usually contain a higher proportion of Mg than soils, which reflects the loss of Mg during weathering[139]. In decreasing proportion, rocks such as dolomite contains 20% Mg, igneous rocks 2.33% Mg, shales 1.5%, sandstone 1.1% and limestone 0.3%. Soils generally contain 0.3% Mg. Mg isotopic

fractionation effects have been used to study weathering[140]. So far, $\delta^{26}Mg$ values were investigated in silicate soil, silicate rock, ground water, river water, and limestone. Unless otherwise noted, Mg isotope effects are reported here and in the following relative to DSM-3 as the current consensus reference standard for reporting of Mg isotope effects in nature. Silicate soil (-0.03‰) was found to be heavier than silicate rock (-0.54‰). During silicate weathering, fractionation of Mg isotope ratios was found to occur by retaining heavy Mg in the solid residue, and enriching the companion waters in light Mg isotopes.

In the hydrosphere which has the most abundant Mg in the natural environment (1,350 ppm Mg in sea water, 4.1 ppm in fresh water), it was found that the Mg isotopic composition of river waters is highly heterogeneous. The range of $\delta^{26}Mg$ is 2 ‰ in the rivers near the Himalayas region. It is defined by mixtures of water derived from dissolution of the bedrock (silicate) and the precipitation of Mg bearing mineral in soil from weathering reactions, but does not depend on the type of rock reservoir (limestone, silicate or dolostone) that they are draining from[141-142]. The density of vegetation in the catchment area also does not correlate well with the difference in Mg isotopic composition in bedrock and river water. On the contrary, the Mg isotopic composition of sea water was found to be homogeneous (-0.83 ± 0.11 ‰, n = 49, 2SD) although it is dependent on processes such as the incoming river-water, precipitation of minerals such as carbonate and oceanic hydrothermal interactions[143]. The homogeneous Mg isotopic composition of sea water all over the world suggests that the various processes are in equilibrium and/or that residual times of Mg in seawater is much longer than mixing time of the sea water reservoir.

The earth's history, which involved mantle processes and rock formation, has been investigated using Mg isotope fractionation effects. It has been shown that Mg isotopes are not fractionated during magmatic differentiation[144], which implies that the isotopic composition of terrestrial basalts reflects that of the mantle. Rock formation from minerals which resulted in isotopic fractionation

was first demonstrated using Ca and Li isotopes between molten basalt and rhyolite using laboratory experiments[145]. The kinetic isotopic fractionation measured for chemical diffusion of Mg from basalt into rhyolite was about 10‰, and a larger extent of isotopic fractionation of Mg was associated with thermal diffusion[146].

2.3.2 Biosphere

Investigation of Mg isotope fractionation effects in the biosphere came much later than that of the geosphere and hydrosphere. Magnesium is the central element in chlorophyll which is required for photosynthesis and therefore essential to all life on our planet. Magnesium isotope fractionation in chlorophyll-a biosynthesis showed a depletion of the heavier isotope from the culture medium during the early growth phase[147]. This is an indication that mass dependent isotope fractionation occurred during the enzyme mediated formation of the Mg-porphyrin complex in chlorophyll. Bulk plants are enriched in heavy isotopes of Mg relative to their nutrient source and roots. On the contrary, plant leaves were observed to be isotopically lighter in Mg due to two processes[148]. Firstly, there is a preferential chelation of the lighter Mg isotope during the formation of chlorophyll. Secondly, lighter Mg isotopes are preferentially transported from the roots to the leaves. These phenomena in plants were also observed when investigating the potential of Mg isotopes as tracers in biogeochemical processes in a small forested catchment[149]. On average, $\delta^{26}Mg$ of vegetation samples (roots, leaves, wood, needles) lie in between that of rain water (-0.75 to -0.51‰) and their soil solution (-1.44 to 0.06‰) relative to DSM-3 as the reporting standard.

Magnesium plays a role in the precipitation of biogenic marine calcium carbonate (aragonite, calcite) and carbonate rocks (dolostone, limestone). Hence Mg isotope fractionation effects have been investigated to determine their potential as a proxy for paleo-environmental conditions[150-153]. The $\delta^{26}Mg$ values (Table 2) suggest that biomineralization discriminates against heavy isotopes of Mg as aragonite and calcite have more negative delta values compared to dolostone. Limestones have a

value in between that of aragonite and calcite since it consists of skeletal fragments of both types of biogenic carbonates. In general, $\delta^{26}Mg$ values obtained in bulk plant, organic matter and biogenic rocks are more negative (or isotopically lighter) than geological samples. There is no data available for higher organisms yet in the literature.

Table 2. $\delta^{26}Mg$ (‰) values of different samples relative to DSM-3 as the consensus reference standard for reporting of natural Mg isotope effects

Research Area	**Sample**	$\delta^{26}Mg$ **(‰)**	**Reference**
Geosphere	**Minerals, rocks and soil**		
	Silicate rock	-0.53 to -0.33	[140]
	Silicate soil	-0.11 to 0.02	[140]
	Olivine	-0.22 to -0.45	[144, 154]
	Shale	0.02 to 0.04	[144]
	Orthopyroxene	-0.37 to -0.17	[154]
	Andesite (Guadeloupe)	-0.47	[155]
	Andesite (AGV-2)	-0.21	[156]
	Basalt	-0.31 to -0.19	[156]
		-0.41 to -0.14	[157]
	Granite	-0.28 to -0.22	[156]
		-0.75	[157]
	Marine sediment (MAG-1)	-0.34	[156]
	Bulk soil	-0.49 to -0.19	[155]
	Terrestrial rocks and minerals	-0.26 to 0.06	[158]
	Lunar rocks and olivines	-0.53 to + 0.06	[158]
	Diorite	-0.53 to -0.46	[157]
	Lava lake	-0.42 to -0.29	[144]
	Dolostone (MSR)	-1.085*	[150]
	Limestone (PEK-HOST)	-4.095*	[150]
	Limestone	-4.41 to -4.31	[157]
	Dolomite (Oum6184)	-1.765*	[159]
	Aragonite	-3.10 to -1.50	[152]
	Calcite	-5.57 to -1.04	[152]

Table 2. (cont)

Research Area	Sample	$\delta^{26}Mg$ (‰)	Reference
Hydrosphere	Seawater (North Atlantic)	-0.824*	159
	Seawater	-1.00 to -0.69	157
	Seawater (Gulf of Mexico)	-0.907 to -0.765	143
	Marsyandi river	-1.82 to -1.41	142
	Bhote Kosi (catchment)	-1.39 to -1.18	142
	Himalayan river (LHS mean)	-1.31	142
	Ganges (BGP4)	-1.20	142
	Rain water	-0.75 to -0.51	149
	Soil solutions	-1.44 to 0.06	149
	Stream water	-0.85 to -0.08	149
Biosphere	**Organic matter**		
	Chlorophyll a, Spinach	-1.451*	138
	Chlorophyll a	-3.55 to -2.64	160
	Chlorophyll a, Chlorella	-1.510 to -1.157	147
	Chlorophyll b, Spinach	-2.345*	138
	Chlorophyll b, Chlorella	-1.97	160
	Rye flour (ref material)	-1.10	157
	Sea lettuce (ref material)	-0.90	157
	Hair grass (ref material)	-0.50	157
	Lichen (ref material)	-1.15	157
	Roots (vegetation samples)	0.28 to 0.73	149
	Leaves (vegetation samples)	-0.49	149
	Woods (vegetation samples)	-0.37 to 0.01	149
	Needles (vegetation samples)	-0.93 to -0.44	149

This list is not exhaustive but representative samples have been included. *represent values converted from SRM-980.

2.3.3 Human Body

2.3.3.1 Possible Mg isotope effects in urine

Although Mg isotope effects in the human body have yet to be explored, an isotope effect is likely to be induced by renal reabsorption similar to calcium. The regulation of both calcium and Mg depends on kidney excretion and their homeostasis are tightly coupled[161]. Observed calcium isotope effects in urine are probably induced by renal reabsorption[5, 162].

Calcium and Mg are likely to undergo isotope fractionation because their extents of renal reabsorption (99% and 95% respectively) are high enough to cause a difference in isotopic composition between serum and tubular fluid which passes out from the body as urine. Mass balance dictates that an isotope effect is the stronger the less remains in the source compartment which is the tubular fluid in the case of reabsorption of Mg of calcium from the tubular fluid back to serum. In a Göttingen miniature pig study, it was found that $\delta^{44}Ca$ of faeces (0.42 ‰) was similar to that of diet, and blood $\delta^{44}Ca$ was higher (0.06 to 0.68 ‰) than that of bone (-0.60 to -0.03 ‰) but much lower than for urine (2.05 to 2.68 ‰) which was found to be significantly enriched in the heavier calcium isotopes[162].

In humans, it was found that $\delta^{44}Ca$ values in the urine of a young boy (1.47 ± 0.29 ‰) and an older woman diagnosed with osteoporosis (0.35 ± 0.10 ‰) were higher than that of diet (-1.02 ± 0.10 ‰)[5]. $\delta^{44}Ca$ of diet was assumed to be the same as that of serum/blood which was not measured directly. Physiologically, a difference observed between isotope effects in serum/blood and urine of an individual can only be due to the renal reabsorption process. This lets us hypothesize that isotope effects of calcium and/or Mg in urine may potentially serve as biomarkers of kidney function, of which this thesis chose to focus on Mg.

2.3.3.2 Renal function

The kidneys have several important functions such as maintaining electrolyte and acid-base balance, regulation of the extracellular fluid volume, excretion of metabolic products and foreign substances as well as the production and secretion of hormones. The processes involved in urine production are glomerular filtration, tubular reabsorption and secretion[163].

Glomerular filtration

The circulating blood from the glomerulus is first filtered to form an ultrafiltrate of plasma in the Bowman's space. Filtration is determined principally by the molecular size and shape of the solute and, to a much lesser extent, by its charge. Free ions (Na^+, K^+, Ca^{2+} and Mg^{2+}) and those complexed to anions are able to pass through the negatively charged filtration barrier, but not those complexed to negatively charged proteins such as albumin. However, when this filtration barrier is damaged due to disease, a varying amount of albumin may enter the ultrafiltrate and result in a condition known as proteinuria. The presence of proteinuria is an indication of early stage Chronic Kidney Disease (CKD). The total rate at which fluid is filtered into all the nephrons, known as the glomerular filtration rate (GFR) is typically about 120 ml/min per 1.73 m^2 surface area, but the normal range is wide. The determination of GFR is important for early identification and monitoring of patients with CKD[164].

A measured GFR provides the best index for functioning renal mass. However, because GFR cannot be measured directly in humans, one has to make use of clearance of endogenous or exogenous substances to determine GFR. An ideal substance for the determination of GFR should be one that is freely filtered, not reabsorbed or secreted in the renal tubules and not metabolized or synthesized in the kidney. Several markers have been used for the measurement of GFR. These include exogenous compounds such as inulin, iohexol, non-radiolabled iothalamate and radiolabeled markers e.g. ^{125}I-iothalamate, ^{99m}Tc-diethylenetriamine pentaacetic acid and ^{51}Cr-ethyldiaminetetraacetic acid. However, the use of exogenous compounds for renal function determination are limited by factors

such as cost, difficulty in administration, invasive procedures, restricted availability of these compounds and the need for HPLC assays[165]. As a result, endogenous markers such as serum creatinine and serum cystatin-C are commonly used to estimate renal clearance and function. A number of equations have been derived to estimate GFR from age, gender, ethnicity and serum creatinine values, namely the Cockcroft and Gault equation[166], MDRD equation[167] and the CKD-EPI equation[168]. The Cockcroft and Gault equation was developed from a small pool of 249 healthy subjects with stable renal function, thus limiting its accuracy to determine renal function in individuals with moderate to severe renal dysfunction[169]. Two decades later, the Modification of Diet in Renal Disease (MDRD) Study equation (Eqn. 29) was developed for kidney patients (from 1070 subjects) but it was found to underestimate the GFR from healthy individuals[170] with GFR > 60 ml/min per 1.73m^2. This led to the development of the CKD-EPI equation (Eqn. 30) based on a larger cross-sectional analysis of 5504 participants that gave more precise and accurate GFR measurements than the MDRD equation.

$$GFR = 175 \cdot S_{Cr}^{-1.154} \cdot Age^{-0.203} \cdot 1.212^{\beta} \cdot 0.742^{\theta} \quad (29)$$

$$GFR = 141 \cdot \min(S_{Cr}/\kappa, 1)^{\phi} \cdot \max(S_{Cr}/\kappa, 1)^{-1.209} \cdot 0.993^{Age} \cdot 1.159^{\beta} \cdot 1.018^{\theta} \quad (30)$$

where S_{Cr} refers to serum creatinine concentration (mg/dL); β = 1 if black, 0 if non-black; θ = 1 if female, 0 if male; κ = 0.7 if female, 0.9 if male; ϕ = -0.329 if female, -0.411 if male; min = minimum of S_{Cr} /κ or 1; max = maximum of S_{Cr} /κ or 1;

However, the limitation of using serum creatinine (by-product of muscle breakdown) is that it is dependent on muscle mass and meat ingestion, and it is secreted at variable rates in different individuals[165]. Recently, equations based on serum cystatin-C[171-173] have been compared against those based on serum creatinine but the results are not conclusive. Cystatin-C is a cationic

nonglycosylated low-molecular-weight cysteine proteinase[174] that is freely filtered and not reabsorbed or secreted and does not have the problems associated with serum creatinine measurements. However its measurements may be limited by non-GFR related factors such as inflammation, thyroid disorders and steroid therapy[175]. Models based on both serum creatinine and serum cystatin-C were found to be more accurate than measurements based on individual markers alone[176]. Despite its limitations, eGFR is used widely as the main parameter of kidney function.

Tubular function

In an average adult human, about 150 L to 180 L of largely protein-free plasma is filtered and a large variable volume (0.5 to 1.8 L) of urine is produced each day. The tubular processes of selective reabsorption and secretion are thus important to bring a large amount of water and ions back into the circulatory system. Tubular processes are either passive (reabsorption) or active (secretion). Passive reabsorption involves the movement of ions down a concentration gradient (simple diffusion), with the help of a specific membrane carrier protein (facilitated diffusion) or through a membrane channel. Active secretion involves the movement of ions against a concentration gradient which requires energy, usually through the use of adenosine tri-phosphate (ATP) such as a Na-ATPase pump. Renal tubular segments involved in selective reabsorption/secretion are the Proximal Convoluted Tube (PCT), Loop of Henle, Distal Convoluted Tube (DCT), Connecting Tubule (CT) and the Collecting Duct (CD).

The PCT is responsible for the bulk of Na^+, K^+ and Ca^{2+} reabsorption, and almost complete reabsorption of glucose, amino acids, and low-molecular-weight proteins (e.g., retinol-binding protein, α- and β-microglobulins) that have penetrated the filtration barrier. Most other filtered solutes are also reabsorbed to some extent in the PCT. Reabsorption of cations (Na^+, K^+, Ca^{2+}) continues at the Loop of Henle. The thick ascending loop of Henle (TALH) normally reabsorbs the bulk of filtered Mg^{2+}. The DCT reabsorbs Na^+, Ca^{2+} and Mg^{2+} but not K^+. The CD reabsorbs a small

percentage of Na^+ and secretes K^+. For the reabsorption of water, 67% occurs in the PCT, 15% occurs in the thin ascending loop of Henle and the remaining variable reabsorption occurs in the late DCT (depending on arginine vasopressin, atrial natriuretic peptide, brain natriuretic peptide, uroguanylin, and guanylin levels) and medullary portion of the CD (depending on arginine vasopressin level). Table 3 summarizes the percentage of ultrafilterable, reabsorbed/secreted elements from blood plasma and the filtered load respectively.

Table 3. Summary of approximate % of reabsorption and secretion of Na, K, Ca and Mg at different sites of the renal tubule.

		Sites of tubular reabsorption/secretion (% of filtered load)				
	Ultrafilterable[1] (% of blood plasma)	PCT	TALH	DCT	CD	Urine (% of filtered load)
Na	100%	67% reabsorbed	25% reabsorbed	5% reabsorbed	2% reabsorbed	<1%
K	100%	67% reabsorbed	0	0	0 – 70% secreted	*14%
Ca	60%	50 – 60 % reabsorbed	15% reabsorbed	10 – 15 % reabsorbed	<1% reabsorbed	1%
Mg	80%	15 – 20 % reabsorbed	65 – 75% reabsorbed	5 – 10% reabsorbed	0	5%

Data for Na and K adapted from Koeppen[163] (Appendix C). *Data obtained after calculation from Koeppen[163], rounded off to the nearest whole number. Data for Ca was obtained from Koeppen[163]. Data for Mg was obtained from Quamme[61].

Of the various elements involved in the selective reabsorption process (refer to Table 3), Na is mono-isotopic and cannot undergo isotope fractionation. For K, the extent of reabsorption may not be high enough to induce a significant isotope effect in urine, since it undergoes both reabsorption and variable secretion. Calcium and Mg are thus elements to be further investigated as potential biomarkers of the renal reabsorption process.

PCT reabsorption has been studied using lithium. Lithium was found to be reabsorbed to the same extent as Na and water in the PCT and none reabsorbed in the DCT and CD. It is therefore a suitable

indicator of proximal Na reabsorption[177-179]. This technique requires a single injection of lithium to be administered and the dose has to be high enough to be detected in the plasma and urine after 10 – 12 hr, but not sufficient to cause a change in kidney function. It was used to determine how tubular reabsorption responds to increased GFR in diabetic patients. In diabetic patients, the filtered load is higher than a healthy subject due to the higher amount of glucose present, resulting in an increased GFR. It was found that PCT reabsorption is increased in proportion to GFR so that the overall flux of water and Na to the DCT remains constant[180]. To date, there is no suitable clinical measure of tubular function.

In a clinical setting, physicians make use of the eGFR calculated from serum albumin concentration and the presence of microalbuminuria to determine the onset and severity of kidney disease, although eGFR is only an estimate of one facet of kidney function. When kidney function starts to deteriorate, tubular function will decrease first before GFR. A clinical measure of tubular function will thus be a more sensitive marker of kidney function.

2.4 Measurement of Mg Isotope Fractionation Effects

Galy et al.[138] developed a method for high precision Mg isotope ratio analysis for terrestrial and extraterrestrial samples using MC-ICP-MS and correction of instrumental mass bias by the standard-sample bracketing method. The use of a desolvating nebulizer reduced oxygen, nitrogen, carbon, and hydrogen related interferences to an insignificant level. Long term reproducibility of Mg isotope ratios after mass bias correction was found to be 0.06‰ per amu (1 SD). Since then, there have been several publications (refer to Table 2) on Mg isotope ratio analysis using MC-ICP-MS to study isotope variations in geochemical and biological phenomena which reported measurement precisions of similar order of magnitude. It was found that the presence of calcium, often found in biological samples, resulted in a chemical bias because $^{48}Ca^{2+}$ ions interfered with $^{24}Mg^{+}$ ions when the ratio of

concentrations of Ca to Mg exceeded 0.5. In order to enable accurate correction for mass discrimination, matrix elements e.g. carbon or sodium that may potentially enhance or suppress the ion signal of the element of interest should be removed[34]. Sample preparation which involves microwave digestion and purification by ion-exchange chromatography thus became necessary.

2.4.1 Sample preparation

2.4.1.1 Digestion

Before isotope ratio analysis, the sample matrix has to first be broken down to release the analytes by dissolution for later separation/purification for mass spectrometric analysis. Dissolution techniques include conventional wet-ashing dissolution and microwave assisted acid digestion. Conventional wet-ashing dissolution involves heating the sample in a mixture of acids in an oven or on a hotplate for an extended period of time. It also increases susceptibility to loss of volatile analytes and contamination from the environment. Other disadvantages include the danger of using large amounts of acids or oxidizing agents and incomplete digestion. In contrast, microwave assisted acid digestion can be used for a wide variety of environmental, geological and biological samples that are difficult to break down by conventional techniques[181-184]. By conducting the digestion in a closed vessel at high pressure with the right combination of concentrated acids (HF, HCl, HNO_3) and oxidizing reagents such as hydrogen peroxide and perchloric acid, these difficult matrices can be broken down within a shorter period of time. Concentrated nitric acid is often used in combination with hydrogen peroxide for digestion of biological samples to increase the oxidation potential of the acid and to reduce formation of nitrous oxide fumes. Geological samples that often consist of matrices made up of high melting point silicates and oxides require a significantly higher amount of HF compared to environmental samples. For example, the release of Mg from 50 mg meteorites and terrestrial silicate rocks[185] required a mixture of 0.3 ml concentrated HF and 0.6 ml of 7 M HNO_3 with several drops of concentrated $HClO_4$ (approx. 10 µl), whereas 30 mg of dried, homogenized and powdered barley plant samples[186] could be digested with a mixture of 80 µL HF, 800 µL HNO_3 and

200 µL H_2O_2. Biological samples such as blood, urine and faeces (0.1 – 0.2 g, wet mass) can be digested using 2 ml of $HN0_3$ and 0.5 ml of HCl without the use of HF[187].

2.4.1.2 Ion Exchange Chromatography

After digestion, the presence of other elements may interfere with the analyte of interest during mass spectrometric analysis. Hence there is a need to purify the analyte. There are various methods – precipitation, extraction and ion-exchange chromatography, of which the latter is the most commonly used. In ion-exchange chromatography, ions are separated based on reversible binding to the oppositely charged exchange sites of the resin[188].

An example of an ion exchanger used for the separation of Mg from other trace metals is the Dowex 50WX8-400 resin that has been used in this thesis. It is a strongly acidic, polystyrene, fine-mesh cation-exchange resin. Such a resin is made of a styrene-divinylbenzene copolymer, where linear chains of styrene polymers are cross-linked by divinylbenzene. A higher percentage of cross-linker increases the extent of cross-linking in the resin. The greater the extent of cross-linking, the greater the rigidity and the smaller the pores of the resin. More cross-linking allows for higher selectivity and ion-exchange capacity, as the resin swells less from hydration, and the decreased pore size of the resin provides additional size-based selectivity. However, since the pores are smaller, ions diffuse into and out of the resin more slowly and equilibration takes a longer time.

The ion-exchange properties of a resin are modified by attaching various functional groups to the benzene rings. Dowex 50WX8 is considered strongly acidic as it is modified by attaching sulphonate groups ($–SO_3^-$) to the benzene rings of the polymer, which allows it to remain ionised even in highly acidic solutions. This allows for the use of higher concentrations of acid as solvents and eluents as opposed to carboxyl-modified weakly acidic resins which lose their cation-exchange capacity when they are protonated at lower pH values The negative charges of the sulphonate groups also give the

resin its cation-exchange property, in contrast to anion-exchange resins that have positively charged tertiary or quaternary ammonium groups[189].

Ion exchange works based on the equilibrium that is set up between the exchange sites of the resin and the ions of interest in the solution.

$$x\mathrm{RSO_3^-H^+} + \mathrm{M^{x+}} \rightleftharpoons (\mathrm{RSO_3^-})_x\mathrm{M^{x+}} + x\mathrm{H^+} \qquad (31)$$

Eqn. (31) describes the equilibrium that is set up when a sample solution containing cations is loaded onto a column of resin that is in the protonated form. $\mathrm{RSO_3^-H^+}$ represents a sulphonic acid exchange site on the strongly acidic polystyrene resin, $\mathrm{M^{x+}}$ represents the cations in solution, such as $\mathrm{Mg^{2+}}$, and $(\mathrm{RSO_3^-})_x\mathrm{M^{x+}}$ represents the ions bound to the resin via the exchange sites.

Using $\mathrm{Mg^{2+}}$ as an example, on loading of a sample containing $\mathrm{Mg^{2+}}$, the more tightly bound $\mathrm{Mg^{2+}}$ ions in the sample solution displace $\mathrm{H^+}$ ions such that the $\mathrm{Mg^{2+}}$ ions are now bound to the resin instead. When an acid is used as the eluent, the equilibrium position in Eqn. (31) is shifted to the left because of the higher concentration of $\mathrm{H^+}$ ions present in the acid eluent, and the $\mathrm{Mg^{2+}}$ ions are eluted out. Since the concentration of $\mathrm{H^+}$ influences the equilibrium position (partition coefficient), different concentrations of acid can be used to vary the type of ions that are eluted (e.g. $\mathrm{Na^+}$, $\mathrm{K^+}$, $\mathrm{Ca^{2+}}$, $\mathrm{Mg^{2+}}$), and to adjust the periods of time needed for elution.

2.4.2 Mg isotope ratio measurements

2.4.2.1 Overview

Measurement of isotope fractionation effects requires high precision isotope ratio analysis that is only possible with mass spectrometers (MS) that have a multi-collector (MC) configuration. Multiple collection allows the simultaneous measurement of isotopic components, thereby removing source instability as a limitation on precision. In the event that the total current is drifting, the drift is

cancelled out when two currents that represent a ratio are measured at the same time[190]. Mass spectrometers that are capable of high precision isotope ratio analyses are MC-ICP-MS and MC-TIMS.

The type of mass analyzer affects the resolution and hence the peak shape of the detected ion signal and the achievable precision. A sector field mass analyzer operated at low mass resolution (R=300) produces peaks that are flat-topped[191]. Ion signals are best measured as flat-topped peaks so that any fluctuation in the ion image position in the focal plane does not affect the measured ion current intensity, such as that in MC-TIMS.

Sector field instruments, which are capable of high mass resolution for isotope ratio analysis of heavier elements, were made commercially available in 1988 to overcome the limitations from spectroscopic interferences in ICP-MS. They can either be single focusing or double focusing mass spectrometers. A resolution of R = 3,000 in single focusing MS instruments is basically sufficient to eliminate interferences due to polyatomic ions, with the exception of some ion pairs such as $^{80}Se^{+}$ and $^{40}Ar_2^{+}$ and $^{75}As^{+}$ and $^{40}Ar^{35}Cl^{+}$, for which R > 7,500 are required[192]. As its name suggests, single focusing instruments separate ions by making use of only one magnetic device coupled to a collision or reaction cell for reduction of interferences by molecular ions. On the other hand, double focusing MS are capable of achieving a mass resolution R ≥ 10,000 by combining the use of a magnetic and an electric sector field. A magnetic field separates ions by their mass-to charge-ratio and directs ions on their different trajectories into the detector system. If an ICP source is used, it invariably produces ions with a wide energy spread. Hence, an electric sector field may function as an additional analyser for controlling the energy dispersion of the ions in the magnetic sector field[192]. This can be achieved by the sector fields arranged in the Nier-Johnson[193] or the Mattauch–Herzog geometry[194]. In the Nier-Johnson configuration which consists of two 90° sector fields, both direction and energy are focused in the same direction and only allows a single ion species to be detected at a time. It can be either in the forward (electric field before magnetic field) or reversed (magnetic field before electric

field) configuration. On the contrary, the Mattauch–Herzog geometry is used to focus direction and energy in opposite directions. It makes use of an electric sector field that deflects the ions by 31.82°, followed by a 90° magnetic field whereby all images of the separated ion beams are situated on a straight line. This configuration allows ion species to be detected simultaneously over a wide mass range[194]. Although spectroscopic interferences in ICP-MS can be overcome using a high resolution MS, non-spectroscopic interferences (matrix effects) cannot be eliminated using double-focusing sector field mass analyzers[195].

Ions that have been separated by the mass analyzers are detected by either Faraday cups or Secondary Electron Multipliers for lower ion currents. Faraday Cups are designed to be able to neutralize each incoming positive or negative ion by delivering or accepting exactly one electron per singly charged ion. When a charged ion sputters the inner surface of the Faraday cups, secondary particles may be released but they are prevented from leaving as it would affect the result of the ion current measurement[190]. Faraday cups have high linearity, stability and reproducibility but the high ohmic noise within the amplification circuitry contributes a baseline noise level equivalent to approximately 10,000 ions per second. This is not a problem when large ion beams are measured but is not suitable for measurement of very small ion currents. Secondary Electron Multipliers (SEM) are useful for measuring low ion currents by converting an incoming ion into a cascade of secondary electrons. In current generation instruments, SEMs are used in ion-counting mode to correct for different secondary ion yields depending on the mass of the primary impacting ion. Ion detection using SEMs is commonly less accurate and precise with dead time corrections, linearity, and dark noise as major sources of bias[196].

2.4.2.2 TIMS

In TIMS, sample loading involves electrothermal drying down of a small volume (1 – 10 µL) of aqueous analyte solution (ng to µg amounts of the element) onto a degassed metal filament. The metal filament is made of a material such as rhenium, tungsten or platinum that can withstand high

temperatures. Thermal ionization is best suited for elements with low Ionization Energy (< 7 eV) unless negative ions are produced. In the ion source, the compound is heated in a high vacuum and vaporized from the filament at approx. 1000 – 2500 K. Ionization takes place by electron transfer from the molecule to the metal filament surface (Positive TI) or vice versa (Negative TI). The ionization efficiency depends on factors such as the work function of the filament surface and the ionization potential of the element analyzed. In Positive TI, the ionization efficiency is described by the Saha-Langmuir equation (32) when thermodynamic equilibrium is attained.

$$\alpha = \frac{n^+}{n_0} = \frac{g^+}{g_0} \exp[(W - E_i)/kT] \qquad (32)$$

Where α refers to the ionization yield; n^+ and n_0 refers to the number of emitted ions and neutral atoms respectively; g^+ and g_0 refers to the statistic weights of ion and atom respectively; W refers to the work function of the surface, E_i refers to the first ionization energy of the atom to be ionized; k refers to the Boltzmann constant and T refers to the temperature of the filament (K).

In Positive TI, the ionization efficiency can be increased by ionization agents such as silica gel/phosphoric acid or tantalum oxide which increase the work function of the metal filament surface. On the contrary, the ionization efficiency in negative TI for generation of negatively charged molecular ions is described by a modified Saha-Langmuir equation (33).

$$\alpha = \frac{n^-}{n_0} = \frac{g^-}{g_0} \exp[(E_{ea} - W)/kT] \qquad (33)$$

Where n^- replaced n^+ and E_{ea} refers to the electron affinity of the analyzed element.

In negative TI, the ionization efficiency is increased by reducing the work function which can be done by coating the metal surface with a barium or lanthanum compound. The ionization yield is usually well below 100% and rarely exceeds 20% of the element load on the filament.

As the sample loading and heating procedure is element-specific, TIMS usually allows for single element analysis only. The sample has to be loaded in high purity form which requires sample digestion and extensive analyte purification. The earliest isotope ratio measurements of Mg using a single-collector TIMS was carried out by Daughtry[197]. Precipitation of Mg with ammonium (ethylenedinitrilo)tetraacetate (EDTA) and/or ion-exchange chromatography was necessary to isolate Mg for analysis. The precipitated salt was ignited to obtain magnesium oxide. During ionization, the oxide flaked off from the filament easily, which produced an unstable ion beam. This problem was solved by the addition of beryllium oxide which held the magnesium oxide to the tungsten filament more strongly, and the addition of amorphous carbon which increased the ionization efficiency of Mg^+ at a lower temperature. The Mg loading amount and filament heating procedure were not reported. Catanzaro et al.[198] used uranyl nitrate as a binding agent. Uranyl nitrate forms a homogenous solid solution with magnesium nitrate upon drying[199]. A solid solution is one that consists of two or more types of atoms or molecules that share a crystal lattice, which is less likely to flake off during thermal analysis.Sample preparation involved ammonium EDTA and ignition to convert to magnesium oxide. One hundred micrograms of Mg was deposited on a rhenium filament in the form of solutions containing 5mg Mg/ml, 5mg U/ml and 10% nitric acid. A triple filament ion source was used. Having more than one filaments allowed the evaporation and ionization processes to be controlled and optimized separately. The evaporation filament was not heated. Ionizing filaments were prebaked at 5 A for half hour to remove any Na^+ signal from the rhenium filament. Although there is no spectroscopic interference between ^{23}Na and ^{24}Mg, secondary electrons produced from a high Na beam may affect baseline measurements. The temperature of the ionizing filament was increased to approx. 2,100 °C until Mg^+ ion signals were

about (5 – 7) x 10^{-12} A. The ratio $^{25}Mg/^{24}Mg$ = 0.12663 was used in subsequent publications for internal normalization of $^{26}Mg/^{24}Mg$.

The type of Mg salt (nitrate vs chloride) used for analysis was also investigated[200-201]. Magnesium nitrate first becomes magnesium oxide at 600 K. The oxide would have to be heated to a very high temperature in order to obtain an ion signal as its melting point is 3,073 K. Magnesium chloride, however, has a relatively low melting point and an ion signal can be obtained upon heating to 1,000 K. Aggarwal[202] showed that more reproducible isotope ratio measurements were obtained by heating $MgCl_2$ rather than $Mg(NO_3)_2$.

An ionization enhancement technique involving silica gel/phosphoric acid was used by Schramm[203] and Lee[204] to decrease the loading amount of Mg (100 – 300 ng) onto V-shaped, zone refined Re filaments. Sample loading involved heating a sample with current of 1.5 – 2 A to burn off hydrocarbons, and then fused with silica gel/phosphoric acid and the current was increased until filament glowed a dull red for a few seconds. In the single filament ion source, the filament was baked for 6 – 8h at 960°C to remove most of the $^{23}Na^+$. Then it was slowly heated for 4-5h to a temperature in the range 1,480 – 1,580 °C, where stable ^{24}Mg ion beams of (1 – 2) x 10^{-11} A were obtained. The precision achieved (normalized $^{26}Mg/^{24}Mg$ relative to $^{25}Mg/^{24}Mg$ = 0.12663, 1SD) was 0.01%. The values of normalized $^{26}Mg/^{24}Mg$ were however, not the same for Schramm[203] and Lee[204] who did not carry out Mg separation to reduce total procedural blank. As a result, the measurements were not accurate due to secondary electrons from $^{27}Al^+$ scattered from the wall of the flight tube of the mass spectrometer. The importance of sample purification at the expense of a higher procedural blank for thermal ionization can be seen in this example.

Another ionization enhancement technique was developed which involved silica gel/boric acid. Stegmann[187] attempted the direct loading method for Mg, i.e., only microwave acid digestion without further sample purification. The stability of the ion signal was improved using silica gel/boric

acid compared to silica gel/phosphoric acid. For a loading amount of 50 – 100 ng Mg, the precision achieved was 0.01% using a MC-TIMS at a $^{24}Mg^{+}$ ion signal of > 3 x 10^{-12} A. However, silica gel/phosphoric acid is still the commonly used ionization enhancement technique for various applications using single collector-TIMS[205-207].

Besides generating positively charged atomic ions, the use of molecular ions MgF_3^- ions has been developed for analysis in the negative ion mode[208]. Barium fluoride was first applied onto both the evaporation and ionization filaments to reduce the electron work function of the filament surface and to serve as an additional fluorine source for the formation of MgF_3^- ions. The sample was converted to the MgF_2 form using HF and dried together with boric acid to strengthen the binding of the sample onto the filament. Silver fluoride was finally added to both filaments to act as an additional fluorinating agent. The mass spectrometric measurements were made using the ion-counting mode in single collector-TIMS with a $^{24}Mg^{19}F_3^-$ ion signal of 5 x 10^{-14} A. An advantage of generating molecular ions is the better control of instrumental mass bias to give higher precision in isotope dilution analysis.

The precision attained for Mg isotope ratio measurements thus far using TIMS are at best 0.01% (100 ppm) and have not yet reached the maximum precision achievable (approx. 7 ppm) which is mainly limited by Johnson noise inherent in measurements using Faraday cups[209]. The analytical capability of TIMS has not yet been fully maximized.

2.4.2.3 ICP-MS

In most applications, ICP-MS operates at a high power (1200 – 1300 W) to achieve a plasma temperature of about 8,000 K such that the sample introduced is broken down into atomic ions with a high efficiency. Elements with an ionization energy < 8 eV are ionized with nearly 100 % yield. ICP ionization has a higher efficiency than a thermal ionization source and is applicable for more than 95% of the elements in the periodic table.

The first commercial ICP-MS instruments were made available in 1983, several years after TIMS which was considered the benchmark technique for isotope ratio analysis. It allows sample introduction in solution form or as an aerosol and is suitable for multi-element analysis. The inherent characteristics of the plasma ion source poses a challenge in achieving high accuracy and precision in isotope ratio analysis. There are two types of interferences, namely spectroscopic and non-spectroscopic. Spectroscopic interferences refer to (a) isobaric interferences of two different elements at the same nominal mass e.g. $^{58}Fe^{+}$ and $^{58}Ni^{+}$ (b) polyatomic interferences (MH^{+}, MO^{+}, MOH^{+} etc) due to plasma ionization occuring at atmospheric pressure which allows atomic ions to react with oxygen, water vapour and nitrogen (e.g $^{113}In^{+}$ and $^{96}Ru^{17}O^{+}$)[210], (c) multiply-charged ions and (d) background interferences due to the use of certain acids for sample preparation[211] e.g. $^{75}As^{+}$ and $^{40}Ar^{35}Cl^{+}$ when HCl is used. Such interferences affect mainly elements with atomic weights below 80[212]. Hence Mg is one of the elements affected significantly by isobaric interferences (refer to Table 4). Non-spectroscopic interferences are characterized by a decrease or increase in analyte signal due to factors that affect sample transport, ionization in the plasma, ion extraction, or ion throughput in the ion beam of interest. Sample matrix can have a significant effect on the plasma temperature and hence the atomization, excitation and ionization characteristics of the discharge. Concomitant elements in the sample matrix may also suppress the ion signal, thus requiring sample preparation (e.g. ion-exchange chromatography) that is as extensive and time consuming as that for TIMS. Thus, the nature and concentration of the sample matrix directly affects the extent of non-spectroscopic effects[213].

Different methods have been used to eliminate spectroscopic and non-spectroscopic interferences. Improvements in instrumentation have reduced spectroscopic interferences. A collision cell interface was introduced to break down or prevent the formation of many interfering argon-based molecular ions[214]. High resolution ICP-MS instruments i.e. double focusing magnetic sector mass spectrometers are capable of achieving a resolution of 10,000 but there is a trade off in sensitivity. To eliminate

non-spectroscopic interferences, optimizations of nebulizer and ion transport properties are usually carried out[215].

Table 4. Isobaric interferences for the Mg isotope spectrum in ICP-MS. The required mass resolution to separate the isobaric interferences from the isotope of interest is given in parenthesis in the third column.

Isotope of interest (Abundance)[216]	**Nominal mass (m/z)**	**Isobaric Interferences**
^{24}Mg (78.99%)	24	$^{12}C_2^+$(1,604), $^{23}Na^1H^+$ (1,911), $^{48}Ca^{2+}$(2,732)
^{25}Mg (10.00%)	25	$^{12}C^{13}C^+$(1,426), $^{24}Mg^1H^+$ (3,554), $^{12}C^{12}C^1H^+$ (1,136)
^{26}Mg (11.01%)	26	$^{12}C^{14}N^+$(1,269), $^{13}C^{13}C^+$(1,078), $^{25}Mg^1H^+$ (2,347), $^{12}C^{13}C^1H^+$ (909)

Data was obtained from Wannemacker et al.[217] and Becker et al.[186].

2.4.2.4 Instrumental isotope fractionation (mass bias)

Measurements of isotope ratios using a mass spectrometer will never give us the true isotope ratio of the sample being analyzed. This is because of an inherent problem known as instrumental isotope fractionation or mass discrimination/bias. In a thermal ionization source, the lighter isotopes are commonly evaporated preferentially from the metal filament compared to the heavier isotopes. In consequence, the measured isotope ratios are continuously drifting within and between measurements, which mainly limits the precision and accuracy of the analysis. This effect depends on relative instead of absolute mass differences of the evaporating species. Hence, elements such as Mg, Ca and Fe, which have isotopes that have large relative mass differences between them, can commonly be measured with a lower precision as a result of instrumental mass bias. The exponential mass fractionation law which describes isotope fractionation effects in nature is indistinguishable from the law governing isotope fractionation in the thermal ionization source.

Mass discrimination in a thermal ionization source is relatively small, is time dependent but less matrix dependent compared to ICP-MS[194].

Mass discrimination in ICP-MS occurs due to the space-charge effect. When positively charged ions from the plasma source leave the skimmer cone, the charged ions are repelled, resulting in a loss of transmission through the ion optical lens system because the light ions are deflected more than the heavy ones. Space-charge effects have been described in detail by Douglas and Tanner[218]. As a result of differences in the efficiency of ion extraction, transmission and detection as a function of analyte mass, an isotope ratio measured with ICP-MS may show significant bias with respect to the corresponding true value[219]. Although the induced mass bias is usually much higher in ICP–MS than in TIMS, the repeatability of isotope analysis can be ensured by keeping instrumental conditions constant. For ICP-MS, instrumental mass bias is large and relatively stable, but varies between sample matrices.

Given that both non-spectroscopic interferences and instrumental mass bias are strongly matrix dependent, data generated from ICP-MS have to be critically evaluated. The lack of critical data evaluation may be a reason for the mass-independent fractionation reported in some publications.

2.4.3 Correction of instrumental fractionation effects

2.4.3.1 Internal normalization

The technique of internal normalization assumes that one isotope ratio is known/constant in nature so that all other ratios can be corrected relative to it. However, it corrects for both sample and instrumental mass bias effects if both follow the same or similar laws. Using this law, data can be corrected but can only be used to determine the analytical precision of the mass spectrometric technique as the correction does not distinguish between natural and instrumental isotope fractionation effects.

2.4.3.2 External normalization

In this approach, an element of similar mass – e.g., Tl in Pb isotopic analysis[220] or Zr in Mo isotopic analysis[221] or Cu in Zn isotopic analysis[222] – is added to the sample solution and the bias between the measured $^{203}Tl/^{205}Tl$, $^{90}Zr/^{91}Zr$ or $^{63}Cu/^{65}Cu$ isotope ratio and the corresponding true value is used to determine the mass discrimination per mass unit, which is subsequently used to correct the Pb, Mo or Zn isotope ratio data for mass discrimination. This approach is based on the assumption that the fractionation regularities of two elements are the same which may not always be true depending on the sample matrix. There are also a few limitations. Firstly, isotope fractionation regularities must be firmly established for a given pair of elements such as Tl/Pb, Zr/Mo and Cu/Zn. Secondly, external normalization is limited to ICP-MS with its capability for multi-element analysis.

2.4.3.3 Standard-sample bracketing

In this approach, instrumental mass bias is commonly corrected for by measuring a standard of known isotopic composition in between samples. Such a correction technique can only be carried out using ICP-MS but not using TIMS as it requires fast switching of samples and a relatively constant mass bias between measurements. This technique is sensitive to matrix effects if the samples are not purified before analysis.. Adequate correction for mass discrimination in ICP-MS is still a challenge, as it is affected by both the matrix and the analyte concentration.

2.4.3.4 Double Spiking

Compared to external normalization and the standard-sample bracketing approach, the double spiking technique is the least susceptible to matrix effects. It is therefore the reference technique for both MC-TIMS and MC-ICP-MS measurements. A double spike is a mixture of two highly enriched isotopes of an element which have the least abundance in nature. The spike is first mixed together with the sample to form a blend. The mass bias induced by the mass spectrometer is calculated from the change in the isotope ratio of the double spike after deconvolution of measured isotope ratios. It is then used to correct the ratio of the two most abundant isotopes of the sample in the same blend.

Optimization is usually carried out to determine the best possible spike composition and mixing ratio of spike to sample to minimize measurement uncertainty. Double spike correction is based on the three basic equations shown below.

The first unknown is the sample fractionation index f_{sample} which is the main object of interest.

$$\frac{R_{sample}}{R_{ref}} = M^{\,f_{sample}} \tag{34}$$

with R_{sample} and R_{ref} being the same isotope ratio in the sample and a reference standard used for data reporting which are related to their isotopic mass ratio M according to the exponential law.

The second unknown is the instrumental mass bias which can be represented by the methodological fractionation index f_{method} which is defined in accordance to the exponential law, relating the measured isotope ratio R_m and the true isotope ratio R_t.

$$\frac{R_m}{R_t} = M^{\,f_{method}} \tag{35}$$

The third unknown is the proportion of spike to sample, P. Approximate mixing ratios can be determined by Atomic Absorption Spectroscopy or IDMS but the measurement uncertainty involved is usually so large that it affects the final measurement uncertainty in f_{sample} . Hence it is not recommended to determine P from direct measurement but from calculation instead. The isotope ratio in the blend R_{blend} is related to the isotope ratio of the double spike R_{DS} and of the sample R_{sample} respectively according to the following equation.

$$R_{blend} = P \cdot R_{DS} + (1-P) \cdot R_{sample} \tag{36}$$

Earlier papers on the double spike technique made use of the linear law[11] but over time, different types of mass dependent fractionation laws (e.g. power law, exponential law) have been proposed and used for correction. In principle, Eqs (34) and (35) can be modified to accommodate different

mass dependent laws. Values of f_{sample}, f_{method} and P can be calculated from the isotope ratios of the blend, and the isotope compositions of the double spike and the reference standard. A step-by-step derivation of the equations used in the double spike technique can be found in the publication by Rudge et al.[223]. A geometrical method may be used to solve the equations in the double spike technique as presented by Albarède and Beard[224].

As there are three unknowns, the technique requires measurement of three isotope ratios (with a common reference isotope) which is only possible for elements having at least four stable isotopes such as calcium, iron and zinc. This excludes Mg, a three-isotope element from high precision analysis work using MC-TIMS.

2.4.4 Comparison between MC-TIMS and MC-ICP-MS

In order to determine if MC-TIMS or MC-ICP-MS is suitable for the measurement of Mg isotope ratios, both techniques are evaluated based on precision, accuracy and sensitivity. For Mg isotope ratio analysis, current publications show that MC-ICP-MS (RSD = 0.12‰ for internally normalized $^{26}Mg/^{24}Mg$ isotope ratios)[138] and MC-TIMS (RSD = 0.1‰ for internally normalized $^{26}Mg/^{24}Mg$ isotope ratios)[187] are comparable in terms of precision. Normalization of $^{26}Mg/^{24}Mg$ was based on $^{25}Mg/^{24}Mg$ = 0.12663 from the publication by Catanzaro et al.[198] Mass spectrometric sensitivity can be assessed in terms of the amount of Mg required to produce high precision isotope measurements. The higher the amount required, the lower the sensitivity. In general, isotope ratio analysis by MC-ICP-MS[150, 159] requires a solution concentration that contains a significantly lower amount of Mg compared to the filament loading amount in MC-TIMS[187, 205].

Both MC-TIMS and MC-ICP-MS require extensive sample preparation and are limited by instrumental mass bias effects. The analyte must be separated from the sample matrix so as to reduce non-spectroscopic interferences in MC-ICP-MS and to increase the ionization efficiency in MC-TIMS. In

addition, the precision is limited by mass-dependent fractionation effects that occur during sample evaporation in the thermal ionization source or space-charge effects in an ICP source.

Isobaric interferences may limit precision and accuracy in MC-ICP-MS more than MC-TIMS as they can fluctuate within or between measurements. The list of interfering species is given in Table 4. Unlike MC-ICP-MS, Mg isotope ratio measurements by MC-TIMS are virtually not affected by isobaric interferences.

Thus far, both MC-TIMS and MC-ICP-MS are suitable for Mg isotope ratio analysis. However at present, the only available method to correct for instrumental mass bias in Mg isotope analysis is the standard-sample bracketing technique using MC-ICP-MS. There are two issues to be concerned with. Firstly, if Mg in the sample is not isolated, matrix effects may cause an offset in the measured $\delta^{26}Mg$ in either direction and to a variable degree that depends on the type of instrument, instrument settings and laboratory conditions[225-226]. Secondly, if Mg in the sample is purified by ion-exchange chromatography, great care must be taken to ensure that the recovery is 100%. The ion-exchange process may induce an artificial sample fractionation effect if the recovery is less than 100 %[159]. Recently, it has been found that a mismatch between the acid molarity of the sample and bracketing standard may give rise to artificial mass independent fractionation effects. Even if the molarity was the same at the start, evaporation differences between samples and a single bracketing standard solution used in a sequence that lasts for more than half a day would also cause the calculated $\delta^{26}Mg$ to be inaccurate[227]. The standard-sample bracketing technique using MC-ICP-MS thus has its limitations.

2.4.5 Quality Control

2.4.5.1 Three Isotope Plots

In order to ensure that the isotope ratios generated using MC-ICP-MS or MC-TIMS are not affected by measurement artefacts, stringent quality control protocols are necessary before further

calculations can be carried out. For elements with at least three stable isotopes, two measured isotope ratios can be calculated using a common reference isotope. If the fractionation process is mass dependent and there are no spectroscopic or matrix interferences, the two measured isotope ratios will plot on a straight line corresponding to the theoretical mass fractionation line, as seen in Fig. 6a. The gradient of the line will be consistent with the relative mass differences of the isotopes considered. However, if spectroscopic interferences affect one of the isotope ratios, the plot will fall off the theoretical mass fractionation line (Fig. 6b). If non-spectroscopic interferences (matrix effects) are present due to mismatched analytical conditions between two samples, the data will plot parallel but not on the theoretical mass fractionation line (Fig. 6c)[228].

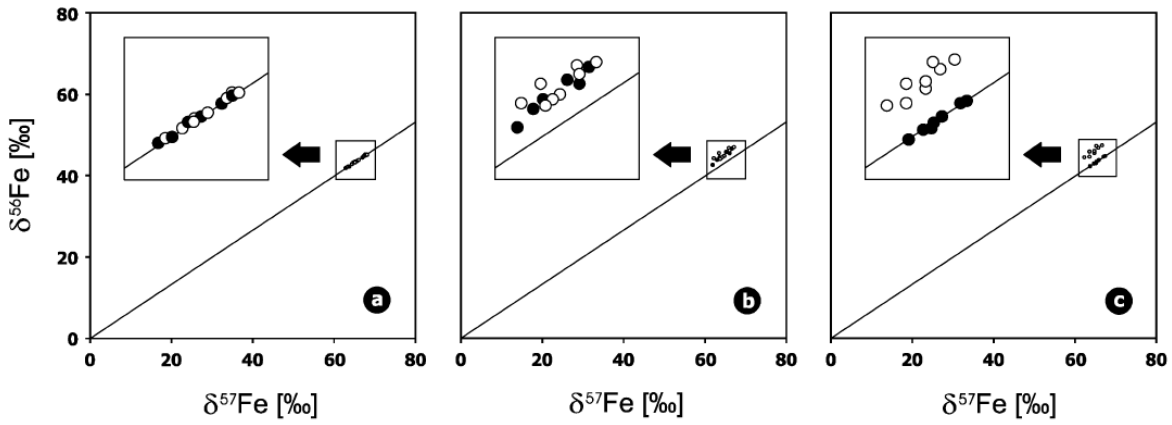

Figure 6. Use of three isotope plots to check for isobaric interferences. Each point represents the mean of an iron isotope ratio measurement of a standard (●) or a sample (○) of natural isotopic composition. Isotope ratios ($^{56}Fe/^{54}Fe$ and $^{57}Fe/^{54}Fe$, respectively) are plotted on a δ-scale ($\delta^{56}Fe$ and $\delta^{57}Fe$, respectively), i.e. as relative deviations in parts per thousand from the known isotope ratio of an isotope reference material of natural isotopic composition (IRMM-014). The diagonal line represents the theoretical fractionation curve as defined by the isotope masses and an exponential fractionation law. (a) Absence of isobaric interferences. Data points from standard and sample plot on the theoretical curve. (b) At least one isotopic signal in the mass spectrum of the standard and the sample is interfered. (c) Matrix differences between standard and sample result in an offset of the sample data points from the theoretical fractionation curve due to isobaric interferences. Adapted from Walczyk (2004).

2.4.5.2 Measurement Uncertainty

The uncertainty of a measurement result needs to be accounted for in order to make measurements comparable across laboratories around the world, yet it is often overlooked. The repeatability or reproducibility of a measurement allows for valid comparisons between samples when measured in the same laboratory but they do not equal its overall measurement uncertainty. Instead, to estimate the combined measurement uncertainty, all sources of random and systematic influences need to be identified and accounted for. Concepts for estimating measurement uncertainties are described in the authoritative Guide to the Expression of Uncertainty in Measurement (GUM)[229], a document that is issued and recognized by major organizations such as IUPAC (International Union of Pure and Applied Chemistry), IUPAP (International Union of Pure and Applied Physics), ISO (International Standardizing Organization) and BIPM (Bureau International des Poids et Mesures).

The most commonly used method to estimate the combined measurement uncertainty is the partial derivative approach. It assumes that all input quantities follow the Gaussian distribution which is not always true. In order to overcome the limitation of the partial derivative method, the use of Monte Carlo simulations can be considered for the evaluation of measurement uncertainty[230]. In contrast to the derivative approach, the Monte Carlo approach is a numerical technique. It is used to simulate measurement results by means of the simulation of random variables[231-232] according to the probability density functions (PDFs) of the input quantities[233] which can be of any type (e.g. triangular, rectangular, Gaussian PDF). The combined measurement uncertainty is calculated from the standard deviation of the simulated measurement results which together form its own PDF.

Monte Carlo simulations have been used to study error propagation in isotope dilution analysis[234-235]. Such analysis enables a user to determine the major contributors of error so as to optimize parameters that will give the lowest combined measurement uncertainty.

2.4.5.3 Outlier Testing

Outlier testing enables a user to remove gross errors before performing calculations on the generated data set. Before outlier testing can be carried out, it is necessary to ensure that the analytical conditions in which isotope ratio measurements were carried out were proper, e.g. ion signal intensities are stable and sufficiently high such that baseline fluctuations are insignificant; peak shape is flat-top and symmetrical and that all peaks coincide; measurement of certified reference materials to check if internally normalized ratios fall within representative ranges given by IUPAC[216]. A three-isotope plot can be used to check for spectroscopic and/or matrix interferences. If the data set follows the mass dependent exponential law, it will plot on the theoretical straight line with a gradient proportional to the relative mass differences of the isotopes.

There are various approaches to outlier testing commonly used in the MS community. The first approach of outlier testing is to identify any cycle that is out by 2σ of the mean value of a particular isotope ratio. The second approach is the use of Dixon's test[236-237] in which a statistical ratio is calculated to determine if an extreme value should be rejected. In both approaches, outliers are identified from a single set of data (one isotope ratio). However, when isotope ratios of an element having three stable isotopes or more are measured, more than one isotope ratio is usually obtained. This means that within the same group of simultaneously measured isotope ratios, one of the isotope ratios may be an outlier whereas the other(s) are not. Rejection of a single value, however, is not reliable because isotope ratio measurements with a common reference isotope are correlated.

The evaluation of correlated isotope ratios for outliers should therefore be based on regression analysis which could be either according to the linear regression or the robust regression method. In the linear regression method, it minimizes the sum of squares of deviation using the mean whereas the robust regression method minimizes the absolute deviation from the median. The former is more sensitive to the presence of extreme values since the differences are squared[238]. However, the robust regression method[239] is preferable because measured ratios that are furthest away from the

mean are not necessarily outliers. Results are reliable only when proper quality control measures have been put in place and it is the cornerstone on which this thesis is based.

REFERENCES

1. Kelly, S.; Heaton, K.; Hoogewerff, J.; *Trends Food Sci. Technol.* **2005,** *16* (12), 555-567.
2. Walczyk, T.; von Blanckenburg, F.; *Science* **2002,** *295* (5562), 2065-2066.
3. Hotz, K.; Augsburger, H.; Walczyk, T.; *J. Anal. At. Spectrom.* **2011,** *26* (7), 1347-1353.
4. Hotz, K.; Krayenbuehl, P. A.; Walczyk, T.; *J. Biol. Inorg. Chem.* **2012,** *17* (2), 301-309.
5. Heuser, A.; Eisenhauer, A.; *Bone* **2010,** *46* (4), 889-896.
6. Jaouen, K.; Pons, M.-L.; Balter, V.; *Earth. Planet. Sci. Lett.* **2013,** *374* (0), 164-172.
7. Balter, V.; Zazzo, A.; Moloney, A. P.; Moynier, F.; Schmidt, O.; Monahan, F. J.; Albarède, F.; *Rapid Commun. Mass Spectrom.* **2010,** *24* (5), 605-612.
8. Johnson, C. M.; Beard, B. L.; *Rev. Mineral. Geochem.* **2004,** *55*, 1-24.
9. Hoefs, J., *Stable isotope geochemistry*. Springer: 2009.
10. Chacko, T.; Cole, D. R.; Horita, J.; *Rev. Mineral. Geochem.* **2001,** *43* (1), 1-81.
11. Dodson, M.; *J. Sci. Instrum.* **1963,** *40*, 289.
12. Allègre, C. J., *Isotope geology*. Cambridge University Press Cambridge: 2008.
13. Rom, W.; Golser, R.; Kutschera, W.; Priller, A.; Steier, P.; Wild, E. M.; *Radiocarbon* **1999,** *41* (2), 183-197.
14. Franke, B. M.; Koslitz, S.; Micaux, F.; Piantini, U.; Maury, V.; Pfammatter, E.; Wunderli, S.; Gremaud, G.; Bosset, J.-O.; Hadorn, R.; *Eur. Food Res. Technol.* **2008,** *226* (4), 761-769.
15. Urey, H. C.; *Journal of the Chemical Society (Resumed)* **1947**, 562-581.
16. Galy, A.; Yoffe, O.; Janney, P. E.; Williams, R. W.; Cloquet, C.; Alard, O.; Halicz, L.; Wadhwa, M.; Hutcheon, I. D.; Ramon, E.; Carignan, J.; *J. Anal. At. Spectrom.* **2003,** *18* (11), 1352-1356.
17. Schauble, E. A.; *Rev. Mineral. Geochem.* **2004,** *55* (1), 65-111.
18. Hart, S. R.; Zindler, A.; *Int. J. Mass Spectrom. Ion Processes* **1989,** *89* (2-3), 287-301.
19. Young, E. D.; Galy, A.; Nagahara, H.; *Geochim. Cosmochim. Acta* **2002,** *66* (6), 1095-1104.
20. Epov, V. N.; Malinovskiy, D.; Vanhaecke, F.; Bégué, D.; Donard, O. F.; *J. Anal. At. Spectrom.* **2011,** *26* (6), 1142-1156.
21. Schauble, E. A.; *Geochim. Cosmochim. Acta* **2007,** *71* (9), 2170-2189.
22. Buchachenko, A. L.; *Pure Appl. Chem.* **2000,** *72* (12), 2243-2258.
23. Bergquist, B. A.; Blum, J. D.; *Science* **2007,** *318* (5849), 417-420.
24. Malinovsky, D.; Latruwe, K.; Moens, L.; Vanhaecke, F.; *J. Anal. At. Spectrom.* **2010,** *25* (7), 950-956.
25. Gehrke, G. E.; Blum, J. D.; Meyers, P. A.; *Geochim. Cosmochim. Acta* **2009,** *73* (6), 1651-1665.
26. Ghosh, S.; Xu, Y.; Humayun, M.; Odom, L.; *Geochem. Geophys. Geosyst.* **2008,** *9*.
27. Carignan, J.; Estrade, N.; Sonke, J. E.; Donard, O. F. X.; *Environ. Sci. Technol.* **2009,** *43* (15), 5660-5664.
28. Moynier, F.; Fujii, T.; Telouk, P.; *Anal. Chim. Acta* **2009,** *632* (2), 234-239.
29. Fujii, T.; Moynier, F.; Telouk, P.; Albarède, F.; *Chem. Geol.* **2009,** *267* (3–4), 157-163.

30. Schmitt, A.-D.; Galer, S. J. G.; Abouchami, W.; *J. Anal. At. Spectrom.* **2009,** *24* (8), 1079-1088.

31. Shibahara, Y.; Yasaka, Y.; Izumi, Y.; Ema, K.; Takeda, S. i.; Nishijima, S.; Fujii, T.; *Solvent Extr. Ion Exch.* **2006,** *24* (6), 915-929.

32. Fujii, T.; Moynier, F.; Uehara, A.; Abe, M.; Yin, Q.-Z.; Nagai, T.; Yamana, H.; *J. Phys. Chem. A* **2009,** *113* (44), 12225-12232.

33. Doucelance, R.; Manhes, G.; *Chem. Geol.* **2001,** *176* (1-4), 361-377.

34. Albarede, F.; Telouk, P.; Blichert-Toft, J.; Boyet, M.; Agranier, A.; Nelson, B.; *Geochim. Cosmochim. Acta* **2004,** *68* (12), 2725-2744.

35. Malinovsky, D.; Vanhaecke, F.; *Anal. Bioanal. Chem.* **2011,** *400* (6), 1619-1624.

36. King, M. M.; Carlson, G. M.; *J. Biol. Chem.* **1981,** *256* (21), 11058-11064.

37. Guynn, R. W.; Webster, L. T.; Veech, R. L.; *J. Biol. Chem.* **1974,** *249* (10), 3248-3254.

38. Carvalho, A. P.; Leo, B.; *J. Gen. Physiol.* **1967,** *50* (5), 1327-1352.

39. Takakuwa, Y.; Kanazawa, T.; *J. Biol. Chem.* **1982,** *257* (18), 10770-10775.

40. Flatman, P. W.; Lew, V. L.; *J. Physiol. (Lond).* **1981,** *315* (1), 421-446.

41. Robinson, J. D.; *Biochim. Biophys. Acta* **1983,** *727* (1), 63-69.

42. Noronha, J. L.; Matuschak, G. M.; *Intensive Care Med.* **2006**, 157-169.

43. Swaminathan, R.; *Clin. Biochem. Rev.* **2003,** *24* (2), 47.

44. Cowan, J. A.; *BioMetals* **2002,** *15*.

45. Elin, R. J.; *Am. J Clin. Pathol.* **1994,** *102* (5), 616-22.

46. Konrad, M.; Schlingmann, K. P.; Gudermann, T.; *Am. J Physiol. Renal.* **2004,** *286* (4), F599-F605.

47. Wallach, S.; *Magnes. Trace Elem.* **1990,** *9* (1), 1-14.

48. Quamme, G. A.; *Kidney Int.* **1997,** *52* (5), 1180.

49. Quamme, G. A.; de Rouffignac, C.; *Front. Biosci.* **2000,** *5* (D694-711), 15.

50. Kalbfleisch, J. M.; Lindeman, R. D.; Ginn, H. E.; Smith, W. O.; *J. Clin. Invest.* **1963,** *42* (9), 1471-1475.

51. Fankushen, D.; Raskin, D.; Dimich, A.; Wallach, S.; *Am. J. Med.* **1964,** *37* (5), 802-812.

52. Abbott, L.; Nadler, J.; Rude, R. K.; *Alcohol. Clin. Exp. Res.* **1994,** *18* (5), 1076-1082.

53. Osswald, H.; Mühlbauer, B.; Schenk, F.; *Kidney Int. Suppl.* **1991,** *32*, S128.

54. Mahalko, J. R.; Sandstead, H. H.; Johnson, L. K.; Milne, D. B.; *Am. J. Clin. Nutr.* **1983,** *37* (1), 8-14.

55. Kesteloot, H.; Joossens, J.; *J. Hum. Hypertens.* **1990,** *4* (5), 527.

56. Quamme, G. A.; Dirks, J. H.; *Kidney Blood Press. Res.* **1986,** *9* (5), 257-269.

57. Schlingmann, K. P.; Waldegger, S.; Konrad, M.; Chubanov, V.; Gudermann, T.; *Biochim. Biophys. Acta* **2007,** *1772* (8), 813-821.

58. Gunzel, D.; Yu, A. S. L.; *Pflugers Arch. EJP* **2009,** *458* (1), 77-88.

59. Quamme, G. A.; *Curr. Opin. Gastroenterol.* **2008,** *24* (2), 230-235.

60. Xi, Q.; Hoenderop, J. G. J.; Bindels, R. J. M.; *Pflugers Arch. EJP* **2009,** *458* (1), 89-98.

61. Quamme, G. A.; *Miner. Electrol. Metab.* **1993,** *19* (4-5), 218-225.

62. Arnaud, M. J.; *Br. J. Nutr.* **2008,** *99* (Suppl 3), S24-36.

63. Ismail, A. A.; Ismail, Y.; Ismail, A., Clinical Assessment of Magnesium Status in the Adult: An Overview. In *Magnesium in Human Health and Disease*, Watson, R. R.; Preedy, V. R.; Zibadi, S., Eds. Humana Press: 2013; pp 3-34.

64. Seelig, M. S.; *Am. J. Clin. Nutr.* **1964,** *14* (6), 342-390.

65. Marier, J. R.; *Magnesium* **1986,** *5* (1), 1-8.

66. Abdulla, M.; Andersson, I.; Asp, N. G.; Berthelsen, K.; Birkhed, D.; Dencker, I.; Johansson, C. G.; Jägerstad, M.; Kolar, K.; Nair, B. M.; Nilsson-Ehle, P.; Nordén, A.; Rassner, S.; Akesson, B.; Ockerman, P. A.; *Am. J. Clin. Nutr.* **1981,** *34* (11), 2464-77.

67. Brink, E. J.; Beynen, A. C.; *Prog. Food Nutr. Sci.* **1992,** *16* (2), 125-162.

68. Heaton, F.; Hodgkinson, A.; Rose, G.; *Clin. Sci.* **1964,** *27*, 31.

69. Greger, J.; Smith, S.; Snedeker, S.; *Nutr. Res.* **1981,** *1* (4), 315-325.

70. Hurrell, R. F.; Juillerat, M.-A.; Reddy, M. B.; Lynch, S. R.; Dassenko, S. A.; Cook, J. D.; *Am. J. Clin. Nutr.* **1992,** *56* (3), 573-578.

71. Zijp, I. M.; Korver, O.; Tijburg, L. B.; *Crit. Rev. Food Sci. Nutr.* **2000,** *40* (5), 371-398.

72. Lide, D. R., *CRC Handbook of Chemistry and Physics 2004-2005: A Ready-Reference Book of Chemical and Physical Data*. CRC press: 2004.

73. McCance, R.; Widdowson, E. M.; *J. Physiol.* **1942,** *101* (1), 44-85.

74. Reinhold, J. G.; Faradji, B.; Abadi, P.; Ismail-Beigi, F.; *J. Nutr.* **1976,** *106* (4), 493.

75. Morris, E. R.; Ellis, R.; Steele, P.; Moser, P. B.; *Nutr. Res.* **1988,** *8* (5), 445-458.

76. Bohn, T.; Davidsson, L.; Walczyk, T.; Hurrell, R. F.; *Am. J. Clin. Nutr.* **2004,** *79* (3), 418-423.

77. Scalbert, A.; Williamson, G.; *J. Nutr.* **2000,** *130* (8), 2073S-2085S.

78. Scalbert, A.; Johnson, I. T.; Saltmarsh, M.; *Am. J. Clin. Nutr.* **2005,** *81* (1), 215S-217S.

79. Mitjavila, S.; Lacombe, C.; Carrera, G.; Derache, R.; *J. Nutr.* **1977,** *107* (12), 2113.

80. Davidsson, L.; Ziegler, E.; Zeder, C.; Walczyk, T.; Hurrell, R.; *Am. J. Clin. Nutr.* **2005,** *81* (1), 104-109.

81. Bothwell, T. H.; Macphail, A. P.; *Int. J. Vitam. Nutr. Res.* **2004,** *74* (6), 421-434.

82. Fairweather-Tait, S.; Hurrell, R. F.; *Nutr. Res. Rev.* **1996,** *9*, 295-324.

83. Siefermann-Harms, D.; Ninnemann, H.; *Photobiochem Photobiophys* **1983,** *6*, 85-91.

84. Schwartz, R.; Woodcock, N. A.; Blakely, J. D.; MacKellar, I.; *Am. J. Clin. Nutr.* **1973,** *26* (5), 519-523.

85. Hunt, S. M.; Schofield, F. A.; *Am. J. Clin. Nutr.* **1969,** *22* (3), 367-373.

86. Lakshmanan, F. L.; Rao, R. B.; Kim, W. W.; Kelsay, J. L.; *Am. J. Clin. Nutr.* **1984,** *40* (6), 1380-1389.

87. Verbeek, M. J.; van den Berg, G. J.; Lemmens, A. G.; Beynen, A. C.; *J. Nutr.* **1993,** *123* (11), 1880-1887.

88. Hunt, J. R.; Gallagher, S. K.; Johnson, L. K.; Lykken, G. I.; *Am. J. Clin. Nutr.* **1995,** *62* (3), 621-32.

89. Dokkum, W. V.; Wesstra, A.; Luyken, R.; Hermus, R.; *Br. J. Nutr.* **1986,** *56* (02), 341-348.

90. Van Dokkum, W.; Cloughley, F.; Hulshof, K.; Oosterveen, L.; *Ann. Nutr. Metab.* **1983,** *27* (5), 361-369.

91. Ricketts, C.; Kies, C.; Garcia, P.; Fox, H. In *Manganese and magnesium utilization of humans as affected by level and kind of dietary-fat*, Fed. Proc., 1985; p 1850.

92. Camire, A.; Clydesdale, F.; *J. Food Sci.* **1981,** *46* (2), 548-551.

93. McHale, M.; Kies, C.; Fox, H.; *J. Food Sci.* **1979,** *44* (5), 1412-1417.

94. Drews, L. M.; Kies, C.; Fox, H. M.; *Am. J Clin. Nutr.* **1979,** *32* (9), 1893.

95. Slavin, J.; Marlett, J.; *Am. J. Clin. Nutr.* **1980,** *33* (9), 1932-1939.

96. Behall, K.; Scholfield, D.; Lee, K.; Powell, A.; Moser, P.; *Am. J. Clin. Nutr.* **1987,** *46* (2), 307-314.

97. Schwartz, R.; Spencer, H.; Welsh, J. J.; *Am. J. Clin. Nutr.* **1984,** *39* (4), 571-6.

98. Bohn, T.; Walczyk, T.; Davidsson, L.; Pritzkow, W.; Klingbeil, P.; Vogl, J.; Hurrell, R. F.; *Br. J. Nutr.* **2004,** *91* (1), 113-120.

99. Coudray, C.; Feillet-Coudray, C.; Rambeau, M.; Mazur, A.; Rayssiguier, Y.; *J. Trace Elem. Med Biol.* **2005,** *19* (1), 97-103.

100. Monsen, E.; *J. Am. Diet. Assoc.* **1989,** *89*.

101. *Dietary reference intakes: for calcium, phosphorus, magnesium, vitamin D, and fluoride*; 0309063507; Institute of Medicine: National Academies Press, 1997.

102. Reinhart, R. A.; *Arch. Intern. Med.* **1988,** *148* (11), 2415-2420.

103. Martin, B.; *Aging (Milan, Italy)* **1990,** *2* (3), 291.

104. Caddell, J.; Scheppner, R.; *J. Forensic Sci.* **1978,** *23* (2), 335.

105. Gullestad, L.; Dolva, L. O.; Waage, A.; Falch, D.; Fagerthun, H.; Kjekshus, J.; *Scand. J. Clin. Lab. Invest.* **1992,** *52* (4), 245-253.

106. Nicar, M.; Pak, C.; *Miner. Electrolyte Metab.* **1982,** *8* (1), 44.

107. Graham, L.; Caesar, J.; Buegen, A.; *Metabolism* **1960,** *9*, 646-659.

108. Elin, R. J.; Hosseini, J. M.; *Clin. Chem.* **1985,** *31* (3), 377-80.

109. Ryzen, E.; Elkayam, U.; Rude, R. K.; *Am. Heart J.* **1986,** *111* (3), 475-480.

110. Elin, R.; Hosseini, J.; Fitzpatrick, L.; Bliziotes, M.; Marx, S.; *Magnes. Trace Elem.* **1990,** *9* (3), 119.

111. Cohen L, K. R.; *JAMA* **1983,** *249* (20), 2808-2810.

112. Thomas, J.; Millot, J. M.; Sebille, S.; Delabroise, A. M.; Thomas, E.; Manfait, M.; Arnaud, M. J.; *Clin. Chim. Acta* **2000,** *295* (1-2), 63-75.

113. Basso, L. E.; Ubbink, J. B.; Delport, R.; *Clin. Chim. Acta* **2000,** *291* (1), 1-8.

114. Ulger, Z.; Ariogul, S.; Cankurtaran, M.; Halil, M.; Yavuz, B. B.; Orhan, B.; Kavas, G. O.; Aribal, P.; Canlar, S.; Dede, D. S.; Ozkayar, N.; Akyol, O.; *J. Nutr. Health Aging* **2010,** *14* (10), 810-814.

115. Gürlek, A.; Bayraktar, M.; Özaltin, N.; *Horm. Metab. Res.* **1998,** *30* (02), 99-102.

116. Simsek, E.; Karabay, M.; Kocabay, K.; *Turkish J. Pediatr* **2005,** *47* (2), 132-137.

117. Rude, R. K.; Stephen, A.; Nadler, J.; *Magnes. Trace Elem.* **1991,** *10* (2-4), 117-121.

118. Malon, A.; Wagner, B.; Bulska, E.; Maj-Zurawska, M.; *Anal. Biochem.* **2002,** *302* (2), 220-223.

119. Malon, A.; Brockmann, C.; Fijalkowska-Morawska, J.; Rob, P.; Maj-Zurawska, M.; *Clin. Chim. Acta* **2004,** *349* (1–2), 67-73.

120. Nadler, J. L.; Malayan, S.; Luong, H.; Shaw, S.; Natarajan, R. D.; Rude, R. K.; *Diabetes Care* **1992,** *15* (7), 835-841.

121. Vetter, T.; Lohse, M.; *Curr. Opin. Nephrol. Hy.* **2002,** *11* (4), 403-410.

122. Rude, R. K.; Oldham, S. B., *Disorders of magnesium metabolism*. Bailliere Tindall: London, 1990; p 1124-1148.

123. Bo, S.; Durazzo, M.; Guidi, S.; Carello, M.; Sacerdote, C.; Silli, B.; Rosato, R.; Cassader, M.; Gentile, L.; Pagano, G.; *Am. J. Clin. Nutr.* **2006,** *84* (5), 1062-1069.

124. He, K.; Liu, K.; Daviglus, M. L.; Morris, S. J.; Loria, C. M.; Van Horn, L.; Jacobs, D. R.; Savage, P. J.; *Circulation* **2006,** *113* (13), 1675-1682.

125. Ford, E. S.; Li, C. Y.; McGuire, L. C.; Mokdad, A. H.; Liu, S. M.; *Obesity* **2007,** *15* (5), 1139-1146.

126. McKeown, N. M.; Jacques, P. F.; Zhang, X. L. L.; Juan, W. Y.; Sahyoun, N. R.; *Eur. J. Nutr.* **2008,** *47* (4), 210-216.

127. Jee, S. H. a.; Miller Iii, E. R.; Guallar, E.; Singh, V. K.; Appel, L. J.; Klag, M. J.; *Am. J. Hypertens.* **2002,** *15* (8), 691-696.

128. Touyz, R. M.; *Mol. Aspects Med.* **2003,** *24* (1–3), 107-136.

129. Reginster, J. Y.; Strause, L.; Deroisy, R.; Lecart, M. P.; Saltman, P.; Franchimont, P.; *Magnesium* **1989,** *8* (2), 106-109.

130. Ford, E. S.; Mokdad, A. H.; *J. Nutr.* **2003,** *133* (9), 2879-2882.

131. Galan, P.; Preziosi, P.; Durlach, V.; Ribas, L.; Bouzid, D.; Fieux, B.; Favier, A.; Hercberg, S., Dietary Magnesium Intake in French Adult Population. In *Magnesium: Current Status and New Developments*, Theophanides, T.; Anastassopoulou, J., Eds. Springer Netherlands: 1997; pp 147-149.

132. Rude, R. K.; Shils, M. E., Magnesium. In *Modern nutrition in health and disease*, Maurice, E. S., Ed. Lippincott Williams & Wilkins: Philadelphia, 2006; pp 224-247.

133. Schlingmann, K. P.; Weber, S.; Peters, M.; Niemann Nejsum, L.; Vitzthum, H.; Klingel, K.; Kratz, M.; Haddad, E.; Ristoff, E.; Dinour, D.; Syrrou, M.; Nielsen, S.; Sassen, M.; Waldegger, S.; Seyberth, H. W.; Konrad, M.; *Nat. Genet.* **2002,** *31* (2), 166-170.

134. Quamme, G. A.; *Am. J Physiol. Renal.* **1989,** *256* (2), F197.

135. Quamme, G. A.; *Am. J Physiol* **1981,** *241* (4), F340-7.

136. Costello, R.; Moser-Veillon, P.; *Magnes. Res.* **1992,** *5* (1), 61.

137. Gullestad, L.; Nes, M.; Rønneberg, R.; Midtvedt, K.; Falch, D.; Kjekshus, J.; *J. Am. Coll. Nutr.* **1994,** *13* (1), 45-50.

138. Galy, A.; Belshaw, N. S.; Halicz, L.; O'Nions, R. K.; *Int. J. Mass spectrom.* **2001,** *208* (1), 89-98.

139. Bowen, H. J. M., *Trace elements in biochemistry*. 1966.

140. Tipper, E. T.; Galy, A.; Bickle, M. J.; *Earth. Planet. Sci. Lett.* **2006,** *247* (3-4), 267-279.

141. Tipper, E.; Galy, A.; Gaillardet, J.; Bickle, M.; Elderfield, H.; Carder, E.; *Earth Planet. Sci. Lett.* **2006,** *250* (1-2), 241-253.

142. Tipper, E. T.; Galy, A.; Bickle, M. J.; *Geochim. Cosmochim. Acta* **2008,** *72* (4), 1057-1075.

143. Ling, M. X.; Sedaghatpour, F.; Teng, F. Z.; Hays, P. D.; Strauss, J.; Sun, W.; *Rapid Commun. Mass Spectrom.* **2011,** *25* (19), 2828-2836.

144. Teng, F. Z.; Wadhwa, M.; Helz, R. T.; *Earth. Planet. Sci. Lett.* **2007,** *261* (1), 84-92.

145. Richter, F. M.; Davis, A. M.; DePaolo, D. J.; Watson, E. B.; *Geochim. Cosmochim. Acta* **2003,** *67* (20), 3905-3923.

146. Richter, F. M.; Watson, E. B.; Mendybaev, R. A.; Teng, F.-Z.; Janney, P. E.; *Geochim. Cosmochim. Acta* **2008,** *72* (1), 206-220.

147. Black, J. R.; Yin, Q. Z.; Casey, W. H.; *Geochim. Cosmochim. Acta* **2006,** *70* (16), 4072-4079.

148. Bolou-Bi, E. B.; Poszwa, A.; Leyval, C.; Vigier, N.; *Geochim. Cosmochim. Acta* **2010,** *74* (9), 2523-2537.

149. Bolou-Bi, E. B.; Vigier, N.; Poszwa, A.; Boudot, J. P.; Dambrine, E.; *Geochim. Cosmochim. Acta* **2012**.

150. Galy, A.; Bar-Matthews, M.; Halicz, L.; O'Nions, R. K.; *Earth Planet. Sci. Lett.* **2002,** *201* (1), 105-115.

151. Chang, V. T. C.; Williams, R. J. P.; Makishima, A.; Belshawl, N. S.; O'Nions, R. K.; *Biochem. Biophys. Res. Commun.* **2004,** *323* (1), 79-85.

152. Wombacher, F.; Eisenhauer, A.; Bohm, F.; Gussone, N.; Regenberg, M.; Dullo, W. C.; Ruggeberg, A.; *Geochim. Cosmochim. Acta* **2011,** *75* (19), 5797-5818.

153. Hippler, D.; Buhl, D.; Witbaard, R.; Richter, D. K.; Immenhauser, A.; *Geochim. Cosmochim. Acta* **2009,** *73* (20), 6134-6146.

154. Huang, F.; Zhang, Z. F.; Lundstrom, C. C.; Zhi, X. C.; *Geochim. Cosmochim. Acta* **2011,** *75* (12), 3318-3334.

155. Opfergelt, S.; Georg, R.; Delvaux, B.; Cabidoche, Y. M.; Burton, K.; Halliday, A.; *Earth. Planet. Sci. Lett.* **2012,** *341*, 176-185.

156. Choi, M. S.; Ryu, J.-S.; Lee, S.-W.; Shin, H. S.; Lee, K.-S.; *J. Anal. At. Spectrom.* **2012,** *27* (11), 1955-1959.

157. Bolou-Bi, E. B.; Vigier, N.; Brenot, A.; Poszwa, A.; *Geostand. Geoanal. Res.* **2009,** *33* (1), 95-109.

158. Wiechert, U.; Halliday, A. N.; *Earth. Planet. Sci. Lett.* **2007,** *256* (3–4), 360-371.

159. Chang, V. T. C.; Makishima, A.; Belshaw, N. S.; O'Nions, R. K.; *J. Anal. At. Spectrom.* **2003,** *18* (4), 296-301.

160. Ra, K.; Kitagawa, H.; *J. Anal. At. Spectrom.* **2007,** *22* (7), 817-821.

161. Ferre, S.; Hoenderop, J. G. J.; Bindels, R. J. M.; *Kidney Int.* **2012,** *82* (11), 1157-1166.

162. Heuser, A.; Eisenhauer, A.; Scholz-Ahrens, K. E.; Schrezenmeir, J.; *Geochim. Cosmochim. Acta* **2007,** *71* (15), A402-A402.

163. Koeppen, B. M.; Stanton, B. A., *Renal physiology*. Mosby Inc: 2007.

164. Levey, A. S.; Coresh, J.; Balk, E.; Kausz, A. T.; Levin, A.; Steffes, M. W.; Hogg, R. J.; Perrone, R. D.; Lau, J.; Eknoyan, G.; *Ann. Intern. Med.* **2003,** *139* (2), 137-147.

165. Ferguson, M. A.; Waikar, S. S.; *Clin. Chem.* **2012,** *58* (4), 680-689.

166. Cockcroft, D. W.; Gault, M. H.; *Nephron* **1976,** *16* (1), 31-41.

167. Levey, A. S.; Bosch, J. P.; Lewis, J. B.; Greene, T.; Rogers, N.; Roth, D.; *Ann. Intern. Med.* **1999,** *130* (6), 461-470.

168. Levey, A. S.; Stevens, L. A.; *Am. J. Kidney Dis.* **2010,** *55* (4), 622.

169. Nyman, H. A.; Dowling, T. C.; Hudson, J. Q.; Peter, W. L. S.; Joy, M. S.; Nolin, T. D.; *Pharmacotherapy* **2011,** *31* (11), 1130-1144.

170. Eknoyan, G.; Levin, N. W.; *Am. J. Kidney Dis.* **2002,** *39* (2 Suppl 1), S1-266.

171. Dharnidharka, V. R.; Kwon, C.; Stevens, G.; *Am. J. Kidney Dis.* **2002,** *40* (2), 221-226.

172. Pei, X.; Liu, Q.; He, J.; Bao, L.; Yan, C.; Wu, J.; Zhao, W.; *Int. Urol. Nephrol.* **2012,** *44* (6), 1877-1884.

173. Taal, M. W.; *Curr. Opin. Nephrol. Hypertens.* **2012,** *21* (6), 607-611.

174. Grubb, A. O.; *Adv. Clin. Chem.* **2001,** *35*, 63-99.

175. Stevens, L. A.; Schmid, C. H.; Greene, T.; Li, L.; Beck, G. J.; Joffe, M. M.; Froissart, M.; Kusek, J. W.; Zhang, Y. L.; Coresh, J.; *Kidney Int.* **2008,** *75* (6), 652-660.

176. Inker, L. A.; Schmid, C. H.; Tighiouart, H.; Eckfeldt, J. H.; Feldman, H. I.; Greene, T.; Kusek, J. W.; Manzi, J.; Van Lente, F.; Zhang, Y. L.; Coresh, J.; Levey, A. S.; *New Engl. J. Med.* **2012,** *367* (1), 20-29.

177. Thomsen, K.; Schou, M.; Steiness, I.; Hansen, H. E.; *Pflugers Arch. EJP* **1969,** *308* (2), 180-&.

178. Hayslett, J.; Kashgarian, M.; *Pflügers Archiv* **1979,** *380* (2), 159-163.

179. Thomsen, K.; *Nephron* **1984,** *37* (4), 217-223.

180. Brøchner-Mortensen, J.; Støckel, M.; Sørensen, P. J.; Nielsen, A. H.; Ditzel, J.; *Diab tologia* **1984,** *27* (2), 189-192.

181. Kingston, H. M.; Jassie, L. B., *Introduction to microwave sample preparation: theory and practice*. American Chemical Society: 1988.

182. Kuss, H. M.; *Fresenius J. Anal. Chem.* **1992,** *343* (9-10), 788-793.

183. Quevauviller, P.; Imbert, J.-L.; Ollé, M.; *Microchimica Acta* **1993,** *112* (1-4), 147-154.

184. Smith, F. E.; Arsenault, E. A.; *Talanta* **1996,** *43* (8), 1207-1268.

185. Wang, G.; Lin, Y.; Liang, X.; Liu, Y.; Xie, L.; Yang, Y.; Tu, X.; *J. Anal. At. Spectrom.* **2011,** *26* (9), 1878-1886.

186. Becker, J. S.; Fullner, K.; Seeling, U. D.; Fornalczyk, G.; Kuhn, A. J.; *Anal. Bioanal. Chem.* **2008,** *390* (2), 571-578.

187. Stegmann, W.; Goldstein, S. L.; Georgieff, M.; *Analyst* **1996,** *121* (7), 901-904.

188. Helfferich, F., *Ion exchange*. McGraw-Hill Book Company: New York, 1962.

189. Zagorodni, A. A., Ion exchangers, their structure and major properties. In *Ion exchange materials : properties and applications*, Elsevier: Amsterdam, 2007.

190. Platzner, I. T.; Habfast, K.; Walder, A.; Goetz, A., *Modern isotope ratio mass spectrometry*. J. Wiley: 1997.

191. Vanhaecke, F.; Balcaen, L.; Malinovsky, D.; *J. Anal. At. Spectrom.* **2009,** *24* (7), 863-886.

192. Moens, L.; Jakubowski, N.; *Anal. Chem.* **1998,** *70* (7), 251A-256A.

193. Johnson, E. G.; Nier, A. O.; *Physical Review* **1953,** *91* (1), 10-17.

194. Becker, J. S., *Inorganic mass spectrometry*. Springer: Berlin/Heidelberg, 2007.

195. Vanhaecke, F.; Riondato, J.; Moens, L.; Dams, R.; *Fresenius J. Anal. Chem.* **1996,** *355* (3-4), 397-400.

196. Richter, S.; Goldberg, S. A.; Mason, P. B.; Traina, A. J.; Schwieters, J. B.; *Int. J. Mass spectrom.* **2001,** *206* (1–2), 105-127.

197. Daughtry, A. C.; Perry, D.; Williams, M.; *Geochim. Cosmochim. Acta* **1962,** *26* (8), 857-866.

198. Catanzaro, E. J.; Murphy, T. J.; Garner, E. L.; Shields, W. R.; *J. Res. Nat. Bur. Stand* **1966**, 453-458.

199. Fujino, T.; Hoshi, Y.; Sato, N.; Yamada, K.; *J. Nucl. Mater.* **1999,** *275* (1), 19-27.

200. Touloukian, Y. S., *Thermophysical Properties of High Temperature Materials*. Plenum Press: New York, 1973.

201. Barin, I.; Knacke, D., *Thermochemical Properties of Inorganic Substances*. Springer-Verlag: Heidelberg,, 1973.

202. Aggarwal, S. K.; Kavimandan, V. D.; Jain, H. C.; Mathews, C. K.; *Talanta* **1977,** *24* (11), 701-703.

203. Schramm, D. N.; Tera, F.; Wasserburg, G. J.; *Earth. Planet. Sci. Lett.* **1970,** *10* (1), 44-59.

204. Lee, T.; Papanastassiou, D. A.; Wasserburg, G. J.; *Geochim. Cosmochim. Acta* **1977,** *41* (10), 1473-1485.

205. Vieira, N. E.; Yergey, A. L.; Abrams, S. A.; *Anal. Biochem.* **1994,** *218* (1), 92-97.

206. Abrams, S. A.; Grusak, M. A.; Stuff, J.; O'Brien, K. O.; *Am. J. Clin. Nutr.* **1997,** *66* (5), 1172-7.

207. Midwood, A. J.; Proe, M. F.; Harthill, J. J.; *Analyst* **2000,** *125* (3), 487-492.

208. Richter, S.; Berglund, M.; Hennessy, C.; *Fresenius J. Anal. Chem.* **1999,** *364* (5), 478-481.

209. Wieser, M. E.; Schwieters, J. B.; *Int. J. Mass spectrom.* **2005,** *242* (2-3), 97-115.

210. May, T. W.; Wiedmeyer, R. H.; *At. Spectrosc.* **1998,** *19* (5), 150-155.

211. Tan, S. H.; Horlick, G.; *Appl. Spectrosc.* **1986,** *40* (4), 445-460.

212. Beauchemin, D.; McLaren, J. W.; Herman, S. S.; *Spectrochimica Acta Part B: Atomic Spectroscopy* **1987,** *42* (3), 467-490.

213. Evans, E. H.; Giglio, J. J.; *J. Anal. At. Spectrom.* **1993,** *8* (1), 1-18.

214. Becker, J. S.; Dietze, H.-J.; *Fresenius J. Anal. Chem.* **2000,** *368* (1), 23-30.

215. Bjorn, E.; Frech, W.; *J. Anal. At. Spectrom.* **2001,** *16* (1), 4-11.

216. Berglund, M.; Wieser, M. E.; *Pure Appl. Chem* **2011,** *83* (2), 397-410.

217. De Wannemacker, G.; Ronderos, A.; Moens, L.; Vanhaecke, F.; Bijvelds, M. J. C.; Kolar, Z. I.; *J. Anal. At. Spectrom.* **2001,** *16* (6), 581-586.

218. Douglas, D.; Tanner, S., Inductively Couple Plasma Mass Spectrometry. Montaser, A., Ed. Wiley: New York, 1998; p 656.

219. Vanhaecke, F.; Moens, L.; *Fresenius J. Anal. Chem.* **1999,** *364* (5), 440-451.

220. Ketterer, M. E.; Peters, M. J.; Tisdale, P. J.; *J. Anal. At. Spectrom.* **1991,** *6* (6), 439-443.

221. Pietruszka, A. J.; Walker, R. J.; Candela, P. A.; *Chem. Geol.* **2006,** *225* (1–2), 121-136.

222. Marechal, C. N.; Telouk, P.; Albarede, F.; *Chem. Geol.* **1999,** *156* (1-4), 251-273.

223. Rudge, J. F.; Reynolds, B. C.; Bourdon, B.; *Chem. Geol.* **2009,** *265* (3-4), 420-431.

224. Albarède, F.; Beard, B.; *Rev. Mineral. Geochem.* **2004,** *55* (1), 113-152.

225. Huang, F.; Glessner, J.; Ianno, A.; Lundstrom, C.; Zhang, Z.; *Chem. Geol.* **2009,** *268* (1–2), 15-23.

226. Teng, F.-Z.; Li, W.-Y.; Ke, S.; Marty, B.; Dauphas, N.; Huang, S.; Wu, F.-Y.; Pourmand, A.; *Geochim. Cosmochim. Acta* **2010,** *74* (14), 4150-4166.

227. Teng, F. Z.; Yang, W.; *Rapid Commun. Mass Spectrom.* **2014,** *28* (1), 19-24.

228. Walczyk, T.; *Anal. Bioanal. Chem.* **2004,** *378* (2), 229-231.

229. JCGM 100:2008. Evaluation of measurement data - Guide to the expression of uncertainty in measurement. Joint Committee for Guides in Metrology.

230. Dobney, A.; Klinkenberg, H.; Souren, F.; Van Borm, W.; *Anal. Chim. Acta* **2000,** *420* (1), 89-94.

231. Ferguson, D. M.; Siepmann, J. I.; Truhlar, D. G., *Advances in Chemical Physics, Monte Carlo Methods in Chemical Physics*. John Wiley & Sons: 2009; Vol. 105.

232. Rubinstein, R. Y.; Kroese, D. P., *Simulation and the Monte Carlo method*. Wiley. com: 2011; Vol. 707.

233. Cox, M.; Harris, P.; Siebert, B.-L.; *Measurement Techniques* **2003,** *46* (9), 824-833.

234. Patterson, K. Y.; Veillon, C.; O'Haver, T. C.; *Anal. Chem.* **1994,** *66* (18), 2829-2834.

235. Wolff Briche, C. S.; Harrington, C.; Catterick, T.; Fairman, B.; *Anal. Chim. Acta* **2001,** *437* (1), 1-10.

236. Dixon, W. J.; *The Annals of Mathematical Statistics* **1951,** *22* (1), 68-78.

237. Dixon, W. J.; *Biometrics* **1953,** *9* (1), 74-89.

238. Chernick, M. R., *The essentials of biostatistics for physicians, nurses, and clinicians*. Wiley: 2011.

239. Iglewicz, B.; Hoaglin, D. C., *How to detect and handle outliers*. ASQC Quality Press Milwaukee, WI, 1993.

3. EXPERIMENTAL SECTION

In Manuscript 1, we will demonstrate how Monte Carlo Simulations can be carried out using standard spreadsheet software. Monte Carlo Simulations is a computerized mathematical technique that performs random sampling from probability distributions of the input quantities. Hence there is no need to compute first-order derivatives which is tedious to perform when the mathematical model is complex. It can also be performed using technical computing software such as MATLAB, which allows different combinations of input variables to be used to calculate the measurement uncertainty of the output variable. This allows the user to determine the optimal combination of input variables that will give the lowest measurement uncertainty in the output variable.

Manuscript 2 describes a novel mass bias correction technique suitable for elements with three or more isotopes (Gravimetric Spiking-Isotope Dilution Analysis, GS-IDA) which has been developed within this thesis. Measured $^{25}Mg/^{24}Mg$ and $^{26}Mg/^{24}Mg$ ratios do not reflect the true Mg isotope ratios of the sample as they may have been shifted by isotope fractionation during sample preparation or mass spectrometric analysis. The sample fractionation index, f_{sample} as the parameter of interest is determined from the measured Mg isotope ratios and the mass ratios of sample and spike solution of the two blends using spreadsheet software. The GS-IDA method is based on the principle that calculated molar ratios of spike to sample must be the same using either the $^{25}Mg/^{24}Mg$ or the $^{26}Mg/^{24}Mg$ isotope ratio in the absence of a methodological isotope fraction effect (f_{sample} =0) and that spike-to-sample ratios must plot on a straight line passing through the origin when plotted against the mass ratio of spike to sample solution in the blends. The successful application of the GS-IDA technique depends critically on the spike composition and mass ratios of spike-to-sample. Optimization of these parameters was carried out using Monte Carlo Simulations as described in Manuscript 1. Our mathematical model for GS-IDA is a complex one involving three non-linear equations with three unknowns. Calculating measurement uncertainties using the partial derivative method would have been very tedious to carry out.

We finally applied our validated technique to explore Mg isotope fractionation effects in human urine for which we have recruited twenty healthy Chinese males of a wide age range (24 – 69 years old), see Manuscript 3. A standard meal was provided in the evening followed by a timed urine collection from evening until next day morning when blood was withdrawn at the hospital. Several kidney-related serum and urine parameters were analysed together with the measurement of $\delta^{26}Mg$ in urine to assess how $\delta^{26}Mg$ in urine correlates with eGFR and other parameters of kidney function.

Manuscript 1

A Monte Carlo approach for estimating measurement uncertainty using standard spreadsheet software

Published in Analytical and Bioanalytical Chemistry, 2012, 402 (7), 2463-2469.

Gina Chew[1] and Thomas Walczyk[1,2,3*]

[1]NUS Graduate School for Integrative Sciences and Engineering,
National University of Singapore (NUS), Singapore

[2]NutriTrace@NUS, Department of Chemistry, Faculty of Science (NUS)

[3]Department of Biochemistry, Yong Loo Lin School of Medicine (NUS)

*corresponding author: NutriTrace@NUS
Department of Chemistry
National University of Singapore (NUS)
Science Drive 4
Singapore 117543

walczyk@nus.edu.sg

ABSTRACT

Despite the importance of stating the measurement uncertainty in chemical analysis, concepts are still not widely applied by the broader scientific community. The Guide to the Expression of Uncertainty in Measurement (GUM) approves the use of both the partial derivative approach and the Monte Carlo approach. There are two limitations to the partial derivative approach. Firstly, it involves the computation of first-order derivatives of each component of the output quantity. This requires some mathematical skills and can be tedious if the mathematical model is complex. Secondly, it is not able to predict the probability distribution of the output quantity accurately if the input quantities are not normally distributed. Knowledge of the probability distribution is essential to determine the coverage interval.

The Monte Carlo approach performs random sampling from probability distributions of the input quantities. Hence there is no need to compute first-order derivatives. In addition, it gives the probability density function of the output quantity as the end result, from which the coverage interval can be determined. Here we demonstrate how the Monte Carlo approach can easily be implemented to calculate measurement uncertainty using standard spreadsheet software such as Microsoft EXCEL. It is our aim to provide the analytical community with a tool to calculate measurement uncertainty using software that is already widely available and that is so simple to apply that it can be even used by students with basic computer skills and minimal mathematical knowledge.

Keywords: Metrology, Monte Carlo, measurement uncertainty, spreadsheet

INTRODUCTION

Any measurement, be it physical or chemical in nature, is associated with an uncertainty. The uncertainty of a measurement value is a numerical value that states “the dispersion of the quantity values being attributed to a measurand based on the information used”[1]. If the measurement uncertainty is known, it is possible to make a reliable judgement if an analytical result exceeds a certain threshold limit or if two random samples belong to the same entity or not. Such judgements may result in fines and economic loss and may have an impact on decisions regarding the future life of an individual or even society as a whole. In environmental analysis[2], clinical chemistry[3], food safety[4] as well as forensic and regulatory legislation[5], a statement on measurement uncertainty is now regarded as an indispensable requirement. Taking measurement uncertainty into account, economic resources and manpower can also be used more effectively in basic and applied research. If the measurement uncertainty is known, it is possible to judge if the chosen method or analytical technique is (or was) fit for the purpose of the investigation[6].

It is a common misconception among students and even scientists that the repeatability or reproducibility of a measurement equals its overall measurement uncertainty. To estimate the combined uncertainty of a measurement, all sources of random and systematic influences in a measurement must be known and the contribution of each individual component to the measurement uncertainty assessed. Concepts for estimating measurement uncertainties are laid out in the authoritative Guide to the Expression of Uncertainty in Measurement[6] (GUM), a document that is issued and recognized by major organizations such as IUPAC (International Union of Pure and Applied Chemistry), IUPAP (International Union of Pure and Applied Physics), ISO (International Standardizing Organization) and BIPM (Bureau International des Poids et Mesures).

Considering the clarity and consistency of GUM concepts and its weight as an internationally recognized consensus document, it is remarkable that GUM still lacks the impact and recognition by the wider scientific community that it deserves. Technically, it is not too difficult to identify major

sources of uncertainty and their magnitude in a chemical measurement such as sample weight, the volume of a measurement flask or the uncertainty in the concentration of a commercial standard used for instrument calibration, to name just a few. Practically, it becomes a challenge to most chemists to assess the contribution of each source of uncertainty to the overall measurement uncertainty. In the conventional approach, this is done by partial differentiation of the mathematical equation that relates the output quantity to its input quantities following basic laws of uncertainty propagation. Metrology software packages such as *Evaluator, Predictor, MetroCom*, *MetroVal* or *GUM Workbench* are available but at costs that are often forbiddingly high for potential users outside the metrological community (USD 500 - 1000). Furthermore, they are intended for the professional user which makes them less useful as an educational tool.

In this note we will demonstrate that such evaluations can be done much easier with minimal mathematical background by Monte Carlo simulations in full accordance with GUM and no other tool than standard spreadsheet software.

Assessment of measurement uncertainty by the partial derivative approach

In the partial derivative approach according to GUM, the first step in estimating measurement uncertainty involves formulating the mathematical model or equation that relates the output quantity Y with the input quantities X_i where *i* = 1,2, …, N .

$$Y = f(X_1, X_2, ..., X_N) \quad (1)$$

The partial derivative approach requires the computation of partial derivatives of the first order of Y with respect to X_i , the so called sensitivity factor. The combined standard uncertainty $u_c(y)$ is the square root of the combined variance $u_c^2(y)$, which is given by:

$$u_c^2(y) = \sum_{i=1}^{N} \left(\frac{\partial f}{\partial x_i} \right)^2 u^2(x_i) \quad (2)$$

Where f is the function given in Eqn. (1). x_i is the mean of the quantity X_i and $u(x_i)$ is the standard uncertainty associated with x_i. Following GUM, values of $u(x_i)$ can be either derived from a "Type A" or "Type B" evaluation. Type A evaluations are based on the statistical analysis of a series of observations such as measurement repeatability. Type B evaluations are from sources other than the measurment such as the consideration of the stated uncertainty for the reference weights used for balance calibration.

Monte Carlo simulations: an alternative approach for estimating measurement uncertainty

In contrast to the derivative approach, the Monte Carlo approach is a purely numerical technique. It is used to predict/simulate measurement results based on probability density functions (PDFs) of the input quantities. The PDF of an input quantity, such as a Gaussian distribution for normally distributed data, determines the probability by which a certain value of this quantity is observed in a random measurement. With the known PDFs of the quantities in the measurements, which can be obtained by Type A or Type B evaluation, it is possible to simulate an unlimited number of unique measurements based on random sampling. Taken together, the distribution of the simulated measurement results reflects not only the PDF of the output quantity but also its measurement uncertainty. In order for this principle to work, the random number generator (RNG) needs to be adequate. An initial consideration for any RNG is that its period, or the cycle before numbers start repeating, has to be sufficiently long [7]. Since we intend to implement the Monte Carlo approach using standard spreadsheet software such as MICROSOFT EXCEL, an evaluation of its RNG is necessary. It was found that earlier versions of EXCEL (97, 2000 and XP) generated random numbers with an unacceptably short period of about one million [8,9]. Although MICROSOFT issued a patch for EXCEL 2003 using the Wichmann and Hill (1982) RNG [10] to remedy this problem, it was still found to be inadequate [11]. We therefore do not recommend using EXCEL's in-built RNG. Instead,

we suggest to use the Mersenne Twister RNG that is available online (http://www.ntrand.com) as an EXCEL Add-in. The Mersenne Twister algorithm provides a super-astronomical period of 2^{19937} -1 [12] which is adequate for Monte Carlo Simulations.

To begin, the mathematical model that links the output quantity (measurand) with the input quantities has to be known. Sometimes, the build-up of the model for the measurand may not be straight-forward. However, in this paper, we assume that the formulation of the mathematical model is not an issue. Guidelines published by the Joint Committee for Guides in Metrology [13] are closely followed in this paper. For illustration purpose, we have chosen a simple mathematical model that links the output quantity Y with the input quantities X_1, X_2 and X_3 :

$$Y = \frac{X_1.X_2}{X_3} \tag{3}$$

For estimating the combined measurement uncertainty of the output quantity $u_c(y)$ from the measurement uncertainty of the input quantities $u(x_1)$, $u(x_2)$ and $u(x_3)$, we set up a simple spreadsheet as illustrated in Fig. (1). A column is allocated to each of the input quantities X_1, X_2 and X_3 as well as the output quantity *Y*. The parameters that determine the PDF of each of the input quantities are entered in the first few rows of the spreadsheet (see Fig. 1, Step 1). For a Gaussian PDF, the mean and its standard deviation are required. For a rectangular or triangular distribution, the lower and upper limits a and b are needed.

The generation of random data for each of the input quantities that are in close agreement with its PDF requires two steps (see Fig. 1, Step 2). First, an array (R) of uniformly-distributed random numbers (0,1) is generated for each input quantity using the Mersenne Twister RNG and the formula '{=NTRAND(M)}'. M is the number of Monte Carlo trials and will be explained in greater detail in

the following paragraph. Next, the EXCEL standard built-in function, 'NORMINV(R_r, mean, standard deviation)' , where R_r is the r^{th} row in the array generated, is invoked. The NORMINV function ensures that the generated data in the respective columns are normally distributed with a mean and standard deviation as entered earlier. In a similar fashion, the random values for a rectangular and triangular PDF can be generated using the formulae 'a + (b – a) * R_r' and 'a + ((b-a)/2) * ($R_{r,1}$ + $R_{r,2}$)', respectively where a and b refer to the lower and upper limits of the distribution. For the triangular distribution, $R_{r,1}$ and $R_{r,2}$ refer to two different random numbers generated from separate arrays of random numbers. The relevant EXCEL function for a given quantity is copied in each cell of the column assigned to this quantity (see Fig. 1, Step 2).

As each column in the spreadsheet represents a random sampling of the PDF of a given quantity, each row in Fig. 1 (Step 3) represents one Monte Carlo Trial $(x_{i,r})$ where r = 1, … , M . A set of M trials represents one Monte Carl Simulation. For each trial, the output quantity y_r is computed according to Eqn. (3), giving M results (see Fig. 1, Step 3). The distribution of the M results determines the PDF of the output quantity *Y* (see Fig. 1, Step 4). The standard deviation calculated for the M values of y_r gives the estimate of the combined standard uncertainty of the output quantity, i.e. $u_c(y)$. The coverage interval can be determined from the built-in EXCEL function 'PERCENTILE(array, nth_percentile)'. The 2.5th and 97.5th percentiles of the set y_r are the limits for a coverage interval having a level of confidence of approximately 95%. In EXCEL, the 'array' refers to the set y_r and the nth_percentile refers to 0.025 and 0.975 for the 2.5th and the 97.5th percentiles respectively.

Step 1		Input quantities								Output quantity
		X_1			X_2			X_3		Y
Mean		16			8			21		6.1
Standard deviation		0.2			-			-		
									2.5th percentile	5.3
Lower Limit, a		-			7			20.7	97.5th percentile	6.9
Upper Limit, b		-			9			21.3		
	Step 2	↓			↓			↓	**Estimate of $u_c(y)$**	*0.45*
Trial #	R			R		R	R		*Step 3* $Y = \frac{X_1 . X_2}{X_3}$	↑ *Step 4*
1	0.5951289	16.0481517		0.4082304	7.8164608	0.9365797	0.3857695	21.0967048	→	5.945940394
2	0.9301352	16.2953597		0.6341869	8.2683739	0.8216910	0.7563123	21.1734010	→	6.363461719
3	0.7577666	16.1398273		0.8926104	8.7852208	0.0783340	0.6139960	20.9076990	→	6.781805378
4	0.0958926	15.7389368		0.5968310	8.1936621	0.1396491	0.0080404	20.7443069	→	6.216622724
5	0.0553860	15.6810534		0.0945892	7.1891784	0.7251624	0.4465629	21.0515176	→	5.355143138
6	0.3413470	15.9182421		0.3509564	7.7019127	0.2971322	0.0338621	20.7992983	→	5.894473438
7	0.1344238	15.7788560		0.9086253	8.8172507	0.3922105	0.3390564	20.9193801	→	6.650585624
8	0.0389011	15.6472834		0.4804955	7.9609910	0.7182656	0.2097281	20.9783981	→	5.937911996
9	0.7203099	16.1167525		0.4239636	7.8479272	0.1768817	0.8176036	20.9983456	→	6.023479314
⋮	⋮	⋮		⋮	⋮	⋮	⋮	⋮	→	⋮
M	0.2318140	15.8534228		0.2056900	7.4113800	0.1773628	0.3107016	20.8464193	→	5.636255255

Figure 1. (Caption on next page)

Figure 1. Spreadsheet for estimating the combined measurement uncertainty $u_c(y)$ using the Monte Carlo approach and standard spreadsheet software (EXCEL). X_1, X_2 and X_3 are the input quantities and Y is the output quantity. In Step 1, parameters are entered that describe the probability density function (PDF) for each input quantity. Input quantity X_1 is supposed to have a Gaussian PDF with a mean of 16 and standard deviation 0.2, X_2 has a rectangular PDF with 7 and 9 as the lower and upper limits [a, b] and X_3 has a triangular PDF with 20.7 and 21.3 as the lower and upper limits [a, b]. In Step 2, an array of uniformly-distributed random numbers, R is generated for each input quantity. Each array is then used to generate a set of random numbers that reflect the PDF of each of these quantities. For a Gaussian distribution (X_1), the built-in EXCEL function 'NORMINV(R_r, mean, standard deviation)' is used, where R_r is the r^{th} random number in the array generated; for a rectangular distribution (X_2), the formula 'a + (b - a)* R_r' is used; for a triangular distribution (X_3), the function 'a + ((b-a) / 2) * ($R_{r,1}$ + $R_{r,2}$)' is used where $R_{r,1}$ and $R_{r,2}$ refers to two different random numbers In Step 3, y_r , where r = 1,…, M , is computed for each row according to the mathematical function that links the input quantities to the output quantity. Each row represents one Monte Carlo trial, i.e. a single simulated measurement/experiment. In Step 4, the mean of Y is calculated directly from the mean of X_1, X_2 and X_3 according to the mathematical function. The standard deviation calculated from all generated values of y_r gives an estimate of the combined standard uncertainty $u_c(y)$. The 95% coverage interval can be assessed by using the built-in function 'PERCENTILE()'. Only 9 rows (trials) are shown in this figure. The number of trials can be easily expanded by copying the content of one row to the rows below it

Validation of the Monte Carlo Approach

It lies in the nature of Monte Carlo simulations that each simulation triggered by a new cell entry or by pressing the F9 key delivers a different estimate of $u_c(y)$. Estimates are considered reasonably accurate when repeated simulations deliver values of $u_c(y)$ that do not differ from each other in the second significant digit, i.e. within 1%. This threshold can be determined by computing the estimate of $u_c(y)$ ten times for M = 10^2, 10^3, 10^4, 10^5 and 10^6 trials.

Let us assume that the input quantities in Eqn. (3), $X_i = \mu \pm \sigma$ follow a Gaussian PDF with mean μ and standard deviation σ : X_1 = 16 ± 0.2, X_2= 8 ± 1 and X_3 = 21 ± 0.3. Fig. (2) shows the values of the combined uncertainty $u_c(y)$ for 10 repeated simulations consisting of 10^2, 10^3, 10^4, 10^5 and 10^6 trials each, respectively. Repeated estimates of $u_c(y)$ are deemed to give repeatable outputs from M = 10^4 trials onwards. This makes 10^4 trials or rows in the spreadsheet a reasonable number for routine applications if computation time is a limiting factor. It should be noted that M is not known a priori and has to be determined for each mathematical function.

For validating the described Monte Carlo approach we have calculated the combined standard uncertainty by the partial derivative method using Eqns. (2) and (3):

$$u_c(y) = \sqrt{(\frac{x_2}{x_3}.u(x_1))^2 + (\frac{x_1}{x_3}.u(x_2))^2 + (-\frac{x_1 x_2}{x_3^2}.u(x_3))^2} \qquad (4)$$

In the above example, the partial derivative method gives $u_c(y)$ = 0.77 for *y* = 6.1. To obtain the 95% coverage interval for a Gaussian distribution, the expanded uncertainty $U = ku_c(y)$ is obtained by applying a coverage factor of k = 2. Since the partial derivative method always assumes that the output quantity has a Gaussian distribution, Y can be reported as 6.1 ± 1.5 (k =2) with a 95% coverage interval of [4.6, 7.6]. In comparison, the Monte Carlo approach with 10^4 trials gives an

estimate of $u_c(y)$ as 0.77 and a 95% coverage interval of [4.6, 7.6]. To confirm that the PDF of Y determined by Monte Carlo simulation follows the PDF of the partial derivative approach, we plotted the calculated Gaussian distribution curve together with the PDF as determined by Monte Carlo simulation in the same diagram (see Fig. 3a). As can be seen from Fig. 3a, both distributions are very similar. To plot simulation results as a relative frequency histogram, ≥ 10^6 trials are recommended. As an alternative tool to EXCEL, the MATLAB code for Monte Carlo simulations following the described principles has been posted online. This code has been used at numerous occasions by the authors to assess the accuracy of the PDFs that are derived by EXCEL calculations including the examples presented in this article.

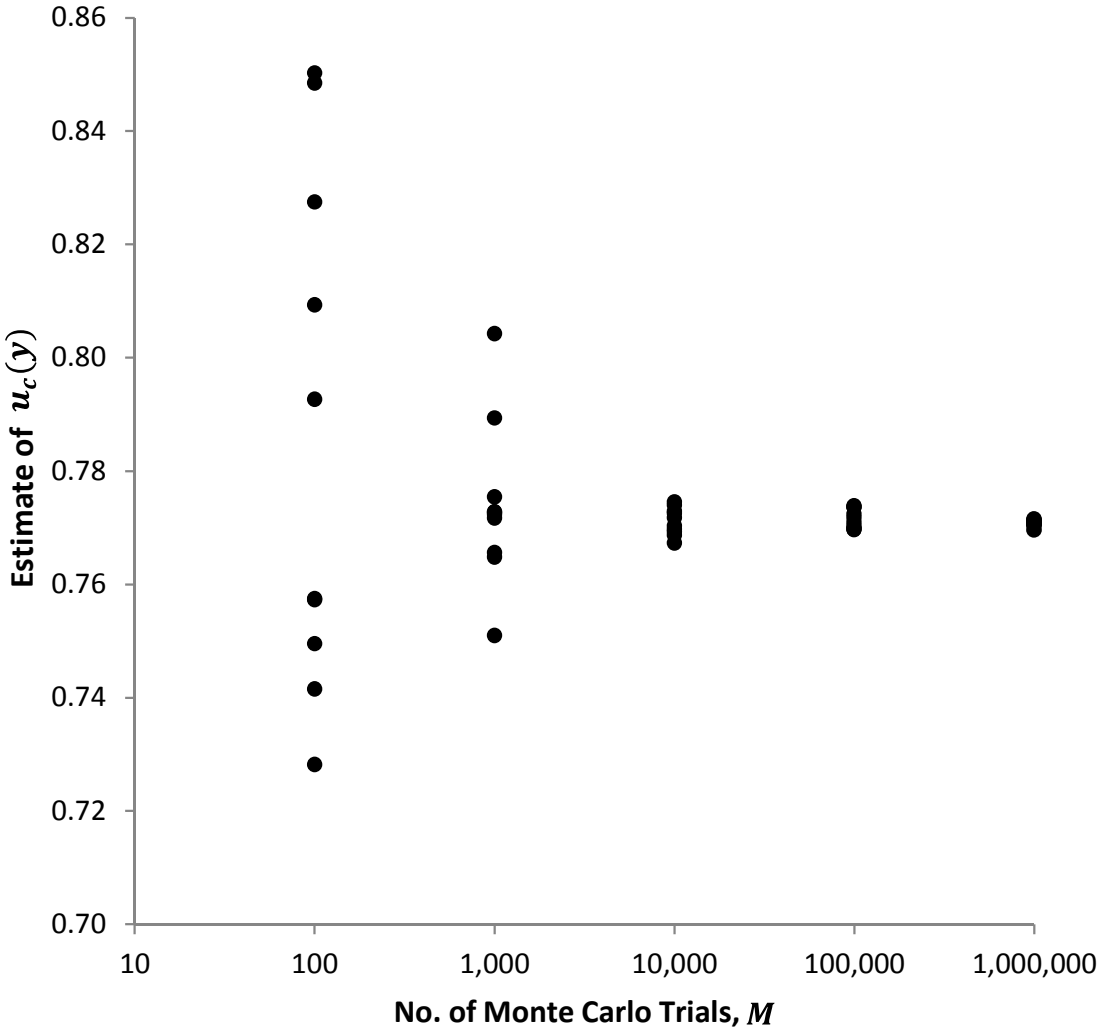

Figure 2. Statistical variations in estimates of $u_c(y)$ for different number of Monte Carlo trials M per simulation. Calculations are based on input quantities X_1, X_2 and X_3 and Eqn. (3) as given in the text. We performed 10 independent simulations with the stipulated number of trials M per simulation with each simulation delivering a different value for $u_c(y)$, as indicated by the symbol (•). As can be expected, the variability between estimates of $u_c(y)$ decreases with increasing M. At 10^4 trials per simulation or more, the variability in $u_c(y)$ is less than 1% of its nominal value which is deemed appropriate for standard applications. The x-axis is plotted on a log scale.

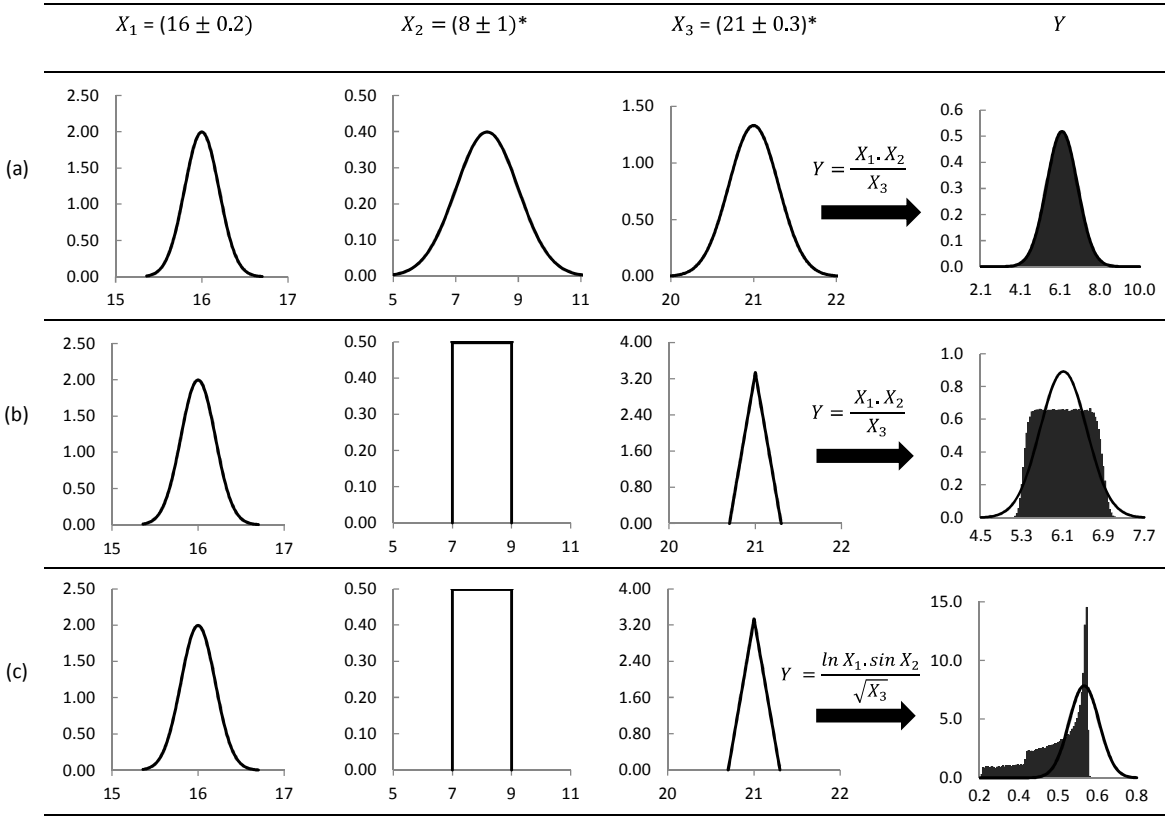

Figure 3. Comparison of PDFs for the combined measurement uncertainty $u_c(y)$ obtained for Y by applying both the partial derivative approach (plotted as a Gaussian curve) and the Monte Carlo approach (plotted as a relative frequency histogram). (a) The mathematical function that links the input quantities to the output quantity is Eqn. (3). All input quantities are normally distributed. X_1 = 16 ± 0.2, X_2 = 8 ± 1 and X_3 = 21 ± 0.3. PDFs for the partial derivative approach and the Monte Carlo approach are approximately the same. (b) The mathematical function is the same as (a). The PDFs of input quantities are different. X_1 = 16 ± 0.2 (Gaussian PDF), X_2 = 8 ± 1 (Rectangular PDF) and X_3 = 21 ± 0.3 (Triangular PDF). PDFs for the partial derivative approach and the Monte Carlo approach are appreciably different. The coverage interval determined using the partial derivative approach is a slight over-estimate compared to the Monte Carlo approach. (c) The input quantities are the same as (b). The mathematical function that links the input quantities to the output quantity is Eqn. (5). For more complex mathematical models and input quantities that are not normally distributed, the Monte Carlo approach is preferred over the partial derivative approach which poorly reflects the actual PDF and, thus, may give wrong estimates of measurement uncertainty and coverage intervals.

Critical Comparison of the Derivative Approach and the Monte Carlo Approach

The derivative approach requires that uncertainties in all input quantities X_i follow a Gaussian (normal) distribution. In turn, the combined uncertainty also follows a Gaussian distribution. This is put to the test using the same equation as before (Eqn. 3), but assigning a different PDF to X_2 and X_3. Like the previous example, X_1 is assigned a Gaussian PDF with a mean of 16 and a standard deviation of 0.2. X_2 is assigned a rectangular PDF with a mean of 8 and a half width of 1. X_3 is assigned a triangular PDF with a mean of 21 and a half width of 0.3. X_2 and X_3 are symmetrical distributions with half widths defined as (b-a)/2.

Following GUM guidelines, rectangular and triangular distributions must be converted first to be compatible with the derivative approach which requires normally distributed input quantities and their standard deviations. In accordance with GUM, this is achieved by dividing half widths by $\sqrt{3}$ and $\sqrt{6}$, respectively. Hence, X_2 will have a mean of 8 and a standard deviation of $\frac{1}{\sqrt{3}}$ while X_3 will have a mean of 21 and a standard deviation of $\frac{0.3}{\sqrt{6}}$. Following Eqn. (4), the partial derivative method gives Y = 6.1 ± 0.9 (k =2) and a 95% coverage interval of [5.2, 7.0]. The Monte Carlo approach with 10^4 trials gives the estimate of $u_c(y)$ as 0.45 and a 95% coverage interval of [5.3, 6.9].

In this example, the obtained value for $u_c(y)$ is the same for both approaches with a slight overestimate of the coverage interval for the partial derivative method (see Fig. 3b). However, the histogram of the actual PDF delivered by the Monte Carlo method differs significantly from the idealized normal distribution that is obtained by the derivative approach. This is of significance when PDFs are being used for the prediction of measurement values, for outlier testing or evaluation of

statistical differences between samples or measurement runs. In all these situations, the actual PDF must be known for accurate assessments.

There are occasions, however, when the derivative approach can fail in estimating measurement uncertainty. This is illustrated for the more complex mathematical model linking the input quantities X_1, X_2 and X_3 with the output quantity Y:

$$Y = \frac{\ln X_1 . \sin X_2}{\sqrt{X_3}} \tag{5}$$

According to the partial derivative method,

$$u_c(y) = \sqrt{(\frac{1}{x_1}.\frac{\sin x_2}{\sqrt{x_3}}.u(x_1))^2 + (\cos x_2.\frac{\ln x_1}{\sqrt{x_3}}.u(x_2))^2 + (-\frac{1}{2}x_3^{-\frac{3}{2}}.\ln x_1.\sin x_2.u(x_3))^2} \tag{6}$$

As in the earlier example, X_1 is assigned a Gaussian PDF with a mean of 16 and a standard deviation of 0.2. X_2 is assigned a rectangular PDF with a mean of 8 and a half width of 1. X_3 is assigned a triangular PDF with a mean of 21 and a half width of 0.3. X_2 and X_3 are symmetrical distributions with half widths defined as (b-a)/2. Non-Gaussian distributed input quantities were converted by dividing the half width with the factors $\sqrt{3}$ and $\sqrt{6}$ respectively. Using Eqn. (6), the partial derivative approach gives a combined standard uncertainty of $u_c(y)$ = 0.051 and a 95% coverage interval (k =2) of [0.50, 0.70]. On the other hand, the Monte Carlo approach with 10^5 trials gives the estimate of $u_c(y)$ as 0.095 with a 95% coverage interval of [0.28, 0.61]. This example requires M = 10^5 trials for estimates of $u_c(y)$ to give repeatable outputs that do not change in the second significant figure. Figure (3c) shows that the Gaussian PDF for Y resulting from the partial derivative approach and the relative frequency histogram obtained by the Monte Carlo approach are

appreciably different and result in a wrong estimate of both measurement uncertainty and the coverage interval.

CONCLUSION

We have demonstrated how the Monte Carlo approach for estimating combined measurement uncertainties can be easily implemented with widely available spreadsheet software such as Microsoft EXCEL. Because of the numerical nature of this approach, Monte Carlo simulations can be easily performed with minimal mathematical knowledge and no expertise in writing computer codes. This makes it an ideal tool to familiarize students with uncertainty concepts and to apply basic GUM concepts in daily laboratory practice.

We could also illustrate major shortcomings of the partial derivative method which does not take into account that the PDF of the input quantities affects the PDF of the output quantity. This is irrelevant when input quantities are normally distributed but can result in the wrong assessment of measurement uncertainties when measurement data do not follow a normal distribution and when the mathematical model is complex.

REFERENCES

1. JCGM 100:2008. Evaluation of measurement data - Guide to the expression of uncertainty in measurement. Joint Committee for Guides in Metrology.
2. Linsinger TPJ, Fuhrer M, Kandler W, Schuhmacher R (2001) Determination of measurement uncertainty for the determination of triazines in groundwater from validation data. Analyst 126 (2):211-216. doi:10.1039/b008618p
3. Fuentes-Arderiu X (2000) Uncertainty of measurement in clinical laboratory sciences. Clin Chem 46 (9):1437-1438
4. Alder L, Korth W, Patey AL, van der Schee HA, Schoeneweiss S (2001) Estimation of measurement uncertainty in pesticide residue analysis. Journal of Aoac International 84 (5):1569-1578
5. King B, Lawn R (1999) International interlaboratory study of forensic ethanol standards. Analyst 124 (7):1123-1130. doi:10.1039/a900487d
6. Evaluation of measurement data - Guide to the Expression of Uncertainty in Measurement. JCGM 100:2008.
7. Gentle JE (2003) Random number generation and Monte Carlo methods. Springer Verlag,
8. McCullough BD, Wilson B (1999) On the accuracy of statistical procedures in Microsoft Excel 97. Comput Stat Data Anal 31 (1):27-37. doi:10.1016/s0167-9473(99)00004-3
9. McCullough BD, Wilson B (2002) On the accuracy of statistical procedures in Microsoft Excel 2000 and Excel XP. Comput Stat Data Anal 40 (4):713-721
10. Wichmann BA, Hill ID (1982) Algorithm AS 183: An Efficient and Portable Pseudo-Random Number Generator. Journal of the Royal Statistical Society Series C (Applied Statistics) 31 (2):188-190
11. McCullough BD (2008) Microsoft Excel's 'Not the Wichmann-Hill' random number generators. Comput Stat Data Anal 52 (10):4587-4593. doi:10.1016/j.csda.2008.03.006
12. Matsumoto M, Nishimura T (1998) Mersenne twister: a 623-dimensionally equidistributed uniform pseudo-random number generator. ACM Trans Model Comput Simul 8 (1):3-30. doi:10.1145/272991.272995
13. JCGM 101:2008. Evaluation of measurement data - Supplement 1 to the "Guide to the expression of uncertainty in measurement" - Propagation of distributions using a Monte Carlo method. Joint Committee for Guides in Metrology.

Manuscript 2

Measurement of Isotope Abundance Variations in Nature by Gravimetric Spiking Isotope Dilution Analysis (GS-IDA)

Published in Analytical Chemistry, 2013, 85 (7), 3667-3673.

Gina Chew[1] and Thomas Walczyk[1,2,3*]

[1]NUS Graduate School for Integrative Sciences and Engineering,
National University of Singapore (NUS), Singapore

[2]NutriTrace@NUS, Department of Chemistry, Faculty of Science (NUS)

[3]Department of Biochemistry, Yong Loo Lin School of Medicine (NUS)

*corresponding author: NutriTrace@NUS
Department of Chemistry
National University of Singapore (NUS)
Science Drive 4
Singapore 117543

walczyk@nus.edu.sg

ABSTRACT

Subtle variations in the isotopic composition of elements carry unique information about physical and chemical processes in nature and are now exploited widely in diverse areas of research. Reliable measurement of natural isotope abundance variations is among the biggest challenges in inorganic mass spectrometry as they are highly sensitive to methodological bias. For decades, double spiking of the sample with a mix of two stable isotopes has been considered the reference technique for measuring such variations both by multi-collector inductively coupled plasma mass spectrometry (MC-ICP-MS) and multi-collector thermal ionization mass spectrometry (MC-TIMS). However, this technique can only be applied to elements having at least four stable isotopes. Here we present a novel approach that requires measurement of three isotope signals only and which is more robust than the conventional Double Spiking technique. This became possible by gravimetric mixing of the sample with an isotopic spike in different proportions and by applying principles of isotope dilution for data analysis (GS-IDA). The potential and principle use of the technique is demonstrated for Mg in human urine using MC-TIMS for isotopic analysis. Mg is an element inaccessible to Double Spiking methods as it consists of three stable isotopes only and shows great potential for metabolically induced isotope effects waiting to be explored.

KEYWORDS

isotope fractionation, isotope dilution, MC-TIMS, MC-ICP-MS, magnesium, urine

INTRODUCTION

With the exception of mono-isotopic elements, the abundances of the stable isotopes of a chemical element are highly constant but not invariant in nature. Variations in the isotopic abundances of an element can arise both from radioactive decay as well as isotope fractionation processes. Reaction or transfer rates can differ between isotopes or isotopologues. Isotope effects are now exploited widely across scientific disciplines for tracing element transport and sample history. Isotope effects, however, can also be also induced during sample preparation or in the mass spectrometer. The latter makes the accurate measurement of isotope variations one of the biggest challenges in inorganic mass spectrometry. Natural isotope fractionation and instrumental fractionation follow mostly similar regularities.

Although still being subject of scientific debate, it is widely agreed that the empirically derived "exponential law"[1] describes the mass dependency of isotope fractionation processes best as long as biasing factors in the measurement including uncorrected isobaric interferences, gain/amplifier instabilities or peak shape are under control[2]. This law relates the measured/observed isotope ratio R_m in a fractionated sample with its true/original isotope ratios R_t:

$$R_m = R_t \cdot M^f \quad (1)$$

where R_m and R_t refer to the mole ratio of the two isotopes $n_{(isotope\ B)}/n_{(isotope\ A)}$ or measured ion currents $I_{(isotope\ B)}/I_{(isotope\ A)}$, M refers to the ratio of the nuclide masses $m_{(isotope\ B)}/m_{(isotope\ A)}$ and f refers to the fractionation index which describes the degree of isotope fractionation. Eqn. (1) shows that fractionation is not determined by the absolute differences in the isotope's masses but their ratio. This entails that fractionation effects for elements of low atomic weight such as hydrogen, carbon or oxygen are usually stronger. Isotope effects for the heavier elements have long been assumed to

exist but as they are much smaller they became routinely measurable more recently with the advent of new analytical techniques[3].

Availability of Multi-Collector Inductively Coupled Plasma Mass Spectrometry (MC-ICP-MS) and, to a lesser extent, Multi-Collector Thermal Ionization Mass Spectrometry (MC-TIMS) turned exploration of isotope abundance variations of the heavier elements quickly into a research area of its own. Possible applications under scrutiny are now countless and reach from the Earth and Planetary Sciences[4], as traditional domains of stable isotope based research, to environmental[5] and even biomedical research[6]. In such measurements, instrumental mass bias is commonly corrected for by measuring intermittently a standard of known isotopic composition (standard sample bracketing) or by normalizing measurements to the known isotope ratios of a reference standard of another element spiked to the sample (external normalization)[7]. These techniques, however, can only be used in MC-ICP-MS which permits easy switch between samples and shows a high but relatively constant mass bias during a measurement sequence[3].

The above correction techniques have become the method of choice in MC-ICP-MS for practical reasons and for reaching experimental limits of measurement repeatability. But these advantages come with a not so insignificant risk of producing measurement artifacts. This makes implementation of stringent quality control protocols an indispensable requirement[8]. The alternative "Double Spiking" approach is certainly more challenging to use but less sensitive to bias as it is less sensitive to matrix effects. As such, it remains the undisputed reference technique in MC-ICP-MS and the only way to measure isotope effects reliably by MC-TIMS[8]. Introduced merely 50 years ago[9] and widely used since then, this technique is limited to elements having at least four stable isotopes such as iron, calcium or zinc. A less sophisticated single spiking approach has been suggested by Hirata et al. for osmium isotope ratio measurements[10]. Here we describe a new concept of using an isotopic spike for mass bias correction based on gravimetric spiking (GS) and isotope dilution analysis (IDA) of the blends (GS-IDA). This novel and fresh take on isotope spiking is applicable to elements

with three stable isotopes only, which we demonstrate here for magnesium as a typical candidate element and by employing a refined MC-TIMS technique for isotopic analysis.

Correction of instrumental mass bias by double spiking

Many excellent articles exist on double spiking theories and their application[9, 11-15] which allows us to describe classical double spiking concepts only briefly. The double spike is prepared by mixing two stable isotopes of the element of interest in highly enriched form. Choice of isotopes and mixing proportions are tailored to minimize measurement uncertainty. The resulting double spike is characterized for isotopic composition and added to the sample in a predetermined proportion to minimize impact of uncertainties in measured isotope ratios. As the isotope composition of the double spike is known, it can be used to monitor and correct for mass bias using iterative algorithms laid out elsewhere[16-18].

Correction techniques aim at determination of the sample fractionation index f_{sample}

$$\frac{R_{sample}}{R_{ref}} = M^{\,f_{sample}} \qquad (2)$$

with R_{sample} and R_{ref} being the same isotope ratio in the sample and a reference standard. While the fractionation index f_{sample} is the same for all isotope ratios in the sample, the ratio R_{sample} to R_{ref} differs between isotope ratios and is dependent on M, based on the exponential law. Isotope abundance variations are commonly expressed on a relative δ-scale using the isotope ratio of the reference sample R_{ref} as the anchoring point (δ_{ref} = 0) in units of parts per thousand (per mil).

$$\delta = \frac{R_{sample} - R_{ref}}{R_{ref}} = \frac{R_{sample}}{R_{ref}} - 1 = M^{\,f_{sample}} - 1 \qquad (3)$$

To determine f_{sample}, and thus its δ-value by Double Spiking, the proportion P of added spike to the amount of element in the sample (in moles) together with the methodological fractionation index f_{method} must be known which is defined in accordance to the exponential law.

$$\frac{R_m}{R_t} = M^{\,f_{method}} \tag{4}$$

In conventional double spiking experiments, iterative procedures permit calculation of f_{sample}, f_{method} and P from the isotope ratios of the spiked sample, the isotope composition of the double spike and the reference standard. As there are three unknowns, the technique requires measurement of three isotope ratios which is only possible for elements having at least four stable isotopes.

Measurement of isotope variations by gravimetric spiking and isotope dilution mass spectrometry (GS-IDA)

Isotope dilution mass spectrometry (IDMS) is widely used for measuring the amount of element in a sample by spiking the element with a highly enriched isotope of the same element[19].

$$P = \frac{n_{spike}}{n_{sample}} = \frac{(R_{blend} - R_{sample})}{(R_{spike} - R_{blend})} \cdot \frac{\sum_i {}^i R_{spike} + 1}{\sum_i {}^i R_{sample} + 1} = A \cdot B \tag{5}$$

In Eqn. (5), n_{sample} and n_{spike} are the number of moles of sample and spike in the blend, respectively, R_{spike} is the isotope ratio of the pure spike, R_{blend} is the isotope ratio of the blend (mix of spike and sample) and R_{sample} is the original isotope ratio of the sample before spiking. Term *A* in Eqn. (5) is multiplied with term *B* which is the sum of all isotope ratios in the sample and the pure spike. All isotope ratios in Eqn. (5) have the same reference isotope in common.

In the classical double-spike approach, P must be known to obtain f_{sample} and f_{method}. In GS-IDA, P is eliminated by gravimetric mixing of the sample with different amounts of spike in solution. It can be shown that P is linearly correlated with the mixing ratio Ψ (see Supporting Information for step-by-step derivation of equations), which is proportional to the mass ratio of spike and sample solution and which can be determined at high accuracy and minimal uncertainty using a calibrated analytical balance. For elements with three stable isotopes, P can then be calculated from two different isotope ratios ${}^x R_{blend}$ and ${}^y R_{blend}$. As fractionation affects isotope ratios differently, calculated values

for ${}^{x}P$ and ${}^{y}P$ equal each other only in absence of methodological bias (see Fig. 1). Because *B* in Eqn. (5) is the same irrespective which ratio is used for calculation of P, we can define this restriction as

$$
\begin{aligned}
{}^{x}A &= \frac{{}^{x}R_{blend,m}\cdot{}^{x}M^{-F_{method}} - {}^{x}\overline{R}_{ref,m}\cdot{}^{x}M^{f_{sample}}}{{}^{x}\overline{R}_{spike,m}\cdot{}^{x}M^{-F_{spike}} - {}^{x}R_{blend,m}\cdot{}^{x}M^{-F_{method}}} \\
&= \frac{{}^{y}R_{blend,m}\cdot{}^{y}M^{-F_{method}} - {}^{y}\overline{R}_{ref,m}\cdot{}^{y}M^{f_{sample}}}{{}^{y}\overline{R}_{spike,m}\cdot{}^{y}M^{-F_{spike}} - {}^{y}R_{blend,m}\cdot{}^{y}M^{-F_{method}}} = {}^{y}A
\end{aligned}
\tag{6}
$$

with the true isotope ratios being expressed as measured isotope ratios following Eqns. (1 and 2). Only measured average isotope ratios of the reference standard $\overline{R}_{ref,m}$ and the spike $\overline{R}_{spike,m}$ and not their true values are needed when measurements are made relative to the reference standard on a δ-scale using normalized fraction indices F. By definition, the δ-value of the reference standard is zero absolute.

$$F_{spike} = f_{spike} - f_{ref} \tag{7}$$

$$F_{method} = f_{method} - f_{ref} \tag{8}$$

When no spike is added to the sample, the trendline in Fig. 1 must pass through the origin in absence of instrumental bias (${}^{x}A_n = {}^{y}A_n = A_n$). This allows us to define an additional restriction for the intercept of the trendline

$$\sum_n A_n \cdot \sum_n \Psi_n^{\,2} - \sum_n \Psi_n \cdot \left(\sum_n A_n \cdot \Psi_n \right) = 0 \tag{9}$$

Together with the two restriction for the blends, a definite solution for the three unknowns (f_{sample}, $F_{method,blend1}$ and $F_{method,blend2}$) can thus be obtained. Calibration of the spike against the reference standard by gravimetric spiking delivers F_{spike}. As can be seen from Eqns. (6 and 9), the GS-IDA approach requires measurement of two isotope ratios only (${}^{x}R$ and ${}^{y}R$). For elements having more than 3 stable isotopes, all other isotope ratios can be neglected. Techniques for computing f_{sample} using commercial software (Microsoft Excel, MATLAB) are accessible online (see Supporting Information).

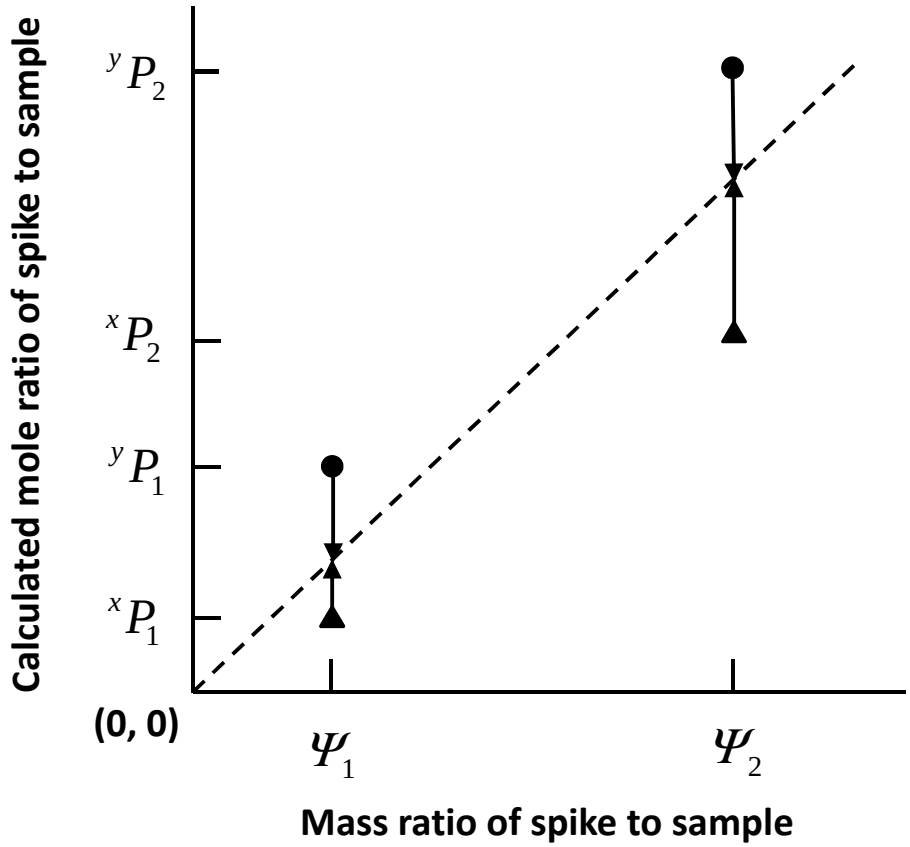

Figure 1. Plot of calculated mole ratio of spike to sample P against mass ratio of spike to sample Ψ. In the absence of instrument mass bias, both are linearly correlated with the trend line (---) passing through the origin. When no spike is added to the sample, both Ψ and P equal zero. Instrumental mass bias affects the two isotope ratios in each blend differently. Accordingly, calculation of *P* following isotope dilution principles yields different values when using the measured isotope ratio ^{x}R (▲) or the measured isotope ratio ^{y}R (●) of the blend. Instrument mass bias is corrected for when (a) calculations yield the same value for P irrespective of the isotope ratio in the blend used for calculation and (b) both points fall on a straight line that passes through the origin.

EXPERIMENTAL SECTION

For experimental verification of GS-IDA we have chosen Mg, an element having three stable isotopes only (^{24}Mg, ^{25}Mg and ^{26}Mg) which renders conventional Double Spiking techniques inapplicable. The same principles can be applied to elements having more than three stable isotopes for which any three isotopes can be selected for isotopic analysis while ignoring all other isotopes in the mass spectrum.

Magnesium isotopic analysis

All isotopic analysis was carried out with a thermal ionisation mass spectrometer (Triton, Thermofisher Scientific, Bremen, Germany) using a rhenium double filament ion source. Tantalum oxide was used to enhance formation of positive Mg^+ ions which were analyzed using an array of nine Faraday Cups for simultaneous ion beam collection after *m/z* separation in a magnetic sector field. For technical details the interested reader is referred to the Supporting Information. Measurement quality was assessed by plotting ^{25}Mg/^{24}Mg and ^{26}Mg/^{24}Mg isotope ratios of a measurement against each other after logarithmic transformation. A measurement was rejected when the coefficient of determination r^2 was less than 0.999.

External measurement precision (1 SD) for 7 independent runs of a commercial Mg standard of natural isotopic composition (Titrisol, Merck, Germany) was 0.0018% for the ^{26}Mg/^{24}Mg isotope ratio (0.1394366 ± 0.0000025) when normalized to the natural ^{25}Mg/^{24}Mg isotope ratio[20] (0.12663) and 0.00091% for the ^{25}Mg/^{24}Mg isotope ratio (0.1265759 ± 0.0000012) when normalized to the natural ^{26}Mg/^{24}Mg isotope ratio[20] (0.13932) using the exponential law[21]. Optimization of the MC-TIMS measurement technique allowed us to approach the instrumental limits of precision in Mg isotope ratio analysis but this came clearly at the cost of losing analytical sensitivity. Sample loadings for Mg isotopic analysis using MC-TIMS and Faraday cups for ion detection are usually of the order of 0.5-2 µg using a mixture of silica gel and phosphoric acid to enhance formation of Mg^+ ions[22-23] or by

making use of MgF_2^- ions[24]. Reported precisions in Mg isotopic analysis ($^{26}Mg/^{24}Mg$, 1SD) using these techniques are of the order of 0.01% to 0.05% for independent runs of the same sample after correction of instrumental mass bias by internal normalization. Such levels of repeatability are clearly inferior to the 0.0018 % for normalized data sets that we are reporting here. This became possible by using tantalum oxide as the activator which permitted sample loadings of 30-40 µg Mg per run which yielded Mg^+ ion emissions that were sufficiently high and stable to generate data of the desired quality. This compares unfavorably to sample requirements of the order of < 1 µg Mg per analytical run using MC-ICP-MS. It must be noted, however, that we have not attempted to improve measurement sensitivity in this study. At a Mg concentration of approximately 80 mg/L in human urine[25], required amounts can be easily obtained from mL volumes of collected urine.

Optimization of GS-IDA method

Spike composition and mass ratios Ψ_1 and Ψ_2 for the mixtures of spike and sample solution were optimized using an iterative procedure with minimization of combined standard uncertainty in the sample fractionation index f_{sample} as the target. The combined standard uncertainty for a given set of variables was determined by Monte Carlo Simulation as described earlier[26] and as laid out in the Supporting Information.

The fractionation indices, F_{spike}, F_{method} and f_{sample}, were set to zero as their actual values do not affect the combined standard uncertainty of f_{sample} after solving. Natural Mg isotope ratios as reported by Catanzaro et al. (1966) as the current best measurement recognized by IUPAC[27] were used for $^{x}\overline{R}_{ref,m}$ and $^{y}\overline{R}_{ref,m}$,while spike ratios $^{x}\overline{R}_{spike,m}$ and $^{y}\overline{R}_{spike,m}$ were set as variables for optimization. Known inhomogenities in the reference material SRM980 used by Catanzaro et al.[28] did not affect our optimization process as we only needed an approximate isotopic composition of natural Mg in order to begin our optimization. Blend ratios were simulated based on the isotopic abundances of the reference and the spike for different mass ratios of spike to sample solution Ψ_1 and Ψ_2.

Measurement uncertainty for the isotope ratios of reference and spike were set to 0.00091% and 0.0018% for $^{25}Mg/^{24}Mg$ and $^{26}Mg/^{24}Mg$ as experimental measurement precision for normalized data. Measurement uncertainty for the mass ratios Ψ_1 and Ψ_2 was set to zero as its contribution to the combined standard uncertainty is negligible when a calibrated, high precision analytical balance is used.

Results of the optimization are shown in Fig. 2 for spike composition and in Fig. 3 for the mass ratios Ψ_1 and Ψ_2 in the blend. There is no single isotopic composition but a wide range of optimal spike ratios that will give a low combined standard uncertainty of f_{sample} (blue colour region in Fig. 2). The same is given for the optimal mass ratios of spike to sample solution which can range from 0.01 to 1 for Ψ_1 and 1 to 10 for Ψ_2 (see Fig. 3). The latter demonstrates the robustness of the technique in terms of concentration matching of spike and sample solution when preparing the blends. Adjustments in Ψ are unnecessary if concentrations of spike solution and sample solution are similar within one order of magnitude.

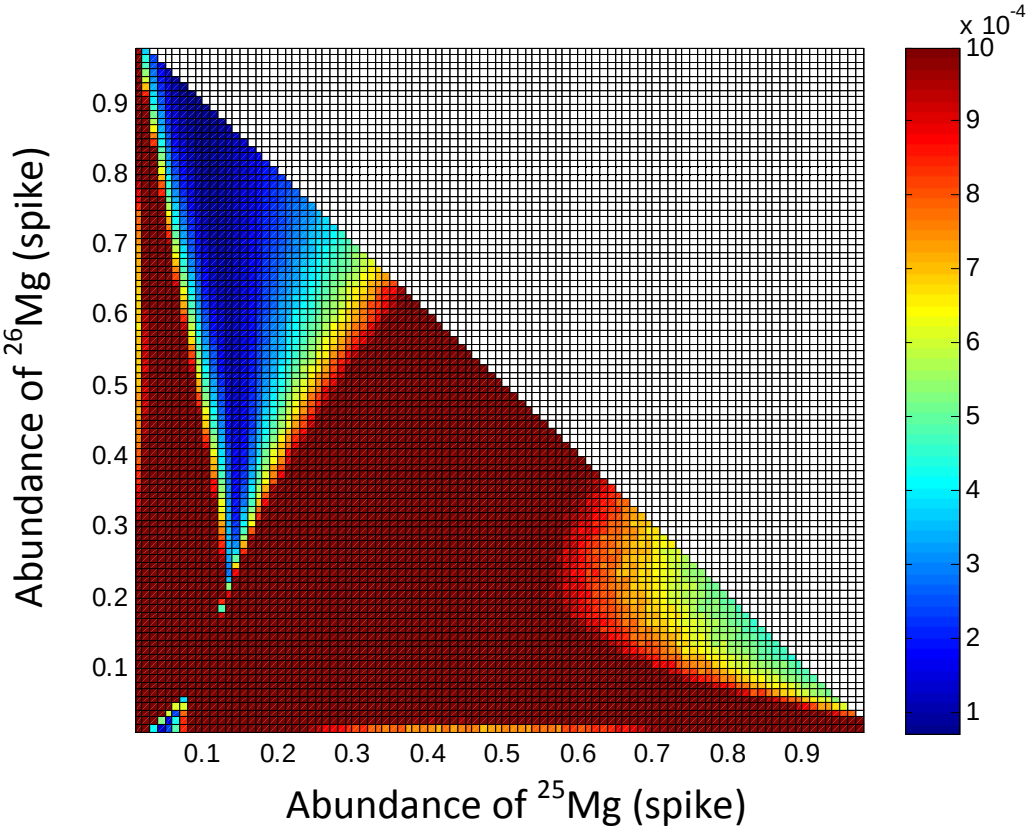

Figure 2. Pseudo color plot of the calculated combined standard uncertainty in f_{sample} for various spike compositions as obtained by Monte Carlo simulation. Abundance of ^{24}Mg is determined by the plotted abundances of ^{25}Mg and ^{26}Mg in the spike. Colors represent the magnitude of the combined standard uncertainty (k=1) on the given color scale. Combined standard uncertainties greater than 10^{-3} were truncated (dark red area) so as to better illustrate uncertainty distributions. Blue areas represent spike compositions which yield the lowest combined standard uncertainty in f_{sample}.

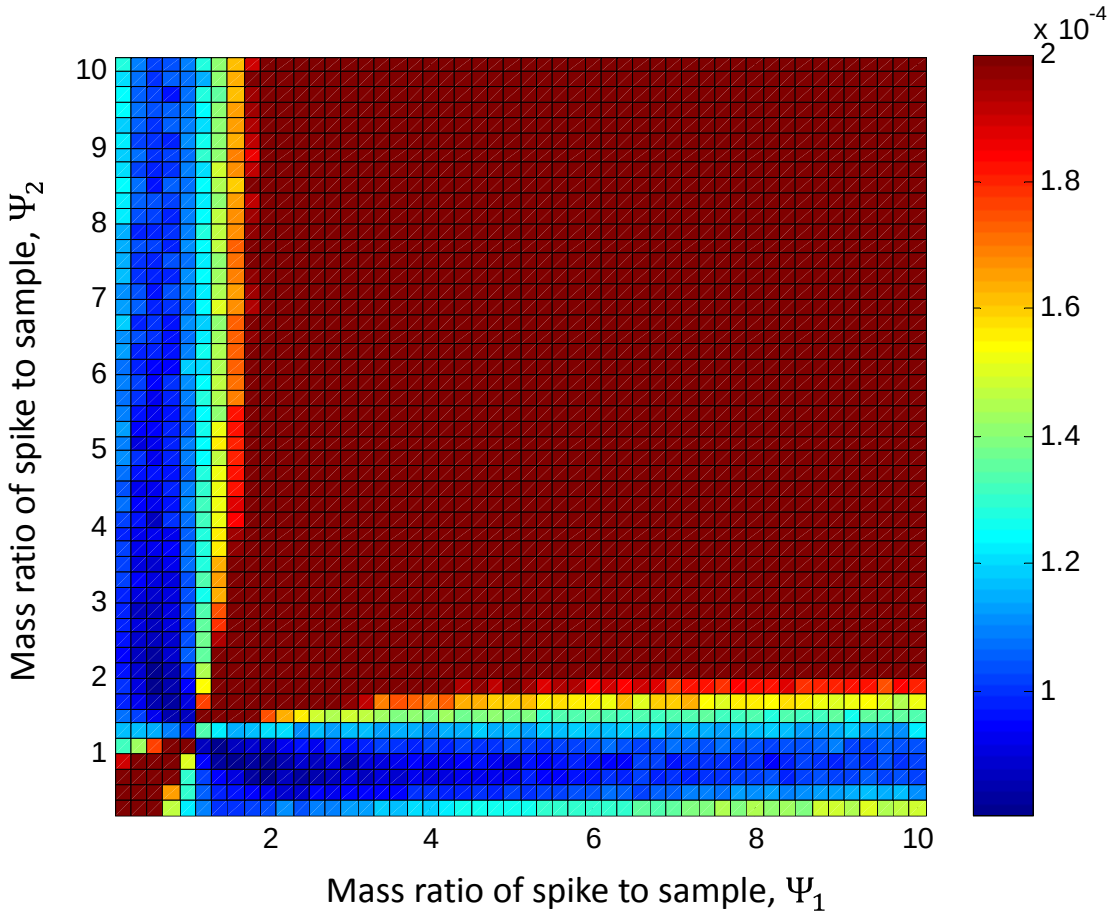

Figure 3. Pseudo color plot of the calculated combined standard uncertainty in f_{sample} for different mass ratios of spike to sample Ψ_1 and Ψ_2 in the blend as obtained by Monte Carlo simulation. Simulations were based on a fixed spike composition (10% ^{24}Mg, 10% ^{25}Mg and 80% ^{26}Mg) in accordance with Fig. 2. Combined standard uncertainties greater than 2 x 10^{-4} were truncated (dark red area) so as to better illustrate uncertainty distributions. Blue areas represent values for Ψ_1 and Ψ_2 which yield the lowest combined standard uncertainty in f_{sample}.

Spike characterization

A spike consisting of approximately 10% ^{24}Mg, 10% ^{25}Mg and 80% ^{26}Mg was prepared from isotopically enriched [^{25}Mg]-MgO, [^{26}Mg]-MgO (Chemgas, France) and elemental Mg (99.999% purity, Alfa Aesar). Materials were dissolved separately in 1 ml of 6 M HCl and solutions were made up to 50 g with Milli-Q water. Aliquots were mixed gravimetrically to yield a spike of the desired composition at an approximate Mg concentration of 20 µg/g. Because we were refused a sample of DSM 3 as the common anchoring material for the Mg δ-scale from its owner (Albert Galy,

Cambridge), we decided to prepare our own anchoring material from a commercially available aqueous Mg standard (Titrisol, Merck, Germany). Both standard (n = 7) and spike (n = 5) were analyzed for Mg isotopic composition and average Mg isotope ratios $\overline{R}_{ref,m}$ and $\overline{R}_{spike,m}$ were calculated without normalization or correction for instrumental mass bias. Measured isotope ratios of the reference standard (±1SD) were 0.12653 ± 0.00021 ($^{25/24}\overline{R}_{ref,m}$) and 0.13922 ± 0.00044 ($^{26/24}\overline{R}_{ref,m}$). Measured isotope ratios of the spike (±1SD) were 1.0173 ± 0.0046 ($^{25/24}\overline{R}_{spike,m}$) and 8.570 ± 0.076 ($^{26/24}\overline{R}_{spike,m}$), see Supporting Information (Table S-1). The spike was calibrated by analyzing 5 sets of 2 mixtures of spike and standard solution each (Ψ_1 = 0.5, Ψ_2 = 5.0) with both being similar in Mg concentration. Mixing ratios but not element concentrations of spike and sample solution must be known accurately in GS-IDA, i.e. the spike does not have to be highly characterized or recalibrated when being diluted. Mixtures were prepared using a micro-analytical balance (> 0.5 g per weighing aliquot) at a measurement uncertainty of 0.0005 g (k=1) and dried down in Teflon cups in a Class 10 laminar flow hood in a Class 10,000 clean-room environment before filament loading. Measurements were repeated, in general, if they did not fulfill the following criteria: (1) ion signal intensity of the least abundant Mg isotope ≥ 1 V; (2) The RSD of the ion signal intensity should be less than 10% among blocks; and (3) coefficient of determination (r^2) for the correlation between logarithmically transformed ratios (three-isotope plot) ≥ 0.999 for a single measurement. Removal of raw data showing a residual greater than 10^{-4} in correlation analysis usually improves the r^2 value to close to 0.9999. Measured isotope ratios for the blends were used to calculate the normalized spike fractionation index F_{spike} (0.0160 ± 0.0015) following the procedures described in the Supporting Information.

Method validation

As the only available certified isotopic reference material for Mg (SRM 980) was found to be isotopically inhomogeneous[28], we decided to validate our technique by treating the referencing

standard as a sample and analyze the referencing standard using the calibrated spike. From a metrological perspective, the GS-IDA technique can be considered validated if GS-IDA analysis of the reference standard (with an assigned δ-value of zero) yields experimentally a δ-value of zero when using the F_{spike} value resulting from spike calibration (circular validation strategy). Cross validation against samples analyzed by MC-ICP-MS were not considered as an alternative as standard sample bracketing techniques or external normalization are sensitive to artifacts and were considered secondary to our first principle approach. For method validation, we prepared five mixtures of referencing standard and spike at mass ratios of Ψ_1 = 0.5 and Ψ_2 = 5.0 as described earlier, analyzed the mixtures and calculated the δ-value of the reference material using the normalized spike fractionation index F_{spike}. The measured δ-value of the reference standard for the $^{26}Mg/^{24}Mg$ isotope ratio was 0.00 ± 0.12 ‰ (1 SD), see Supporting Information, Table S-2.

Sample analysis

To demonstrate the applicability of the technique and evaluate performance characteristics, we analyzed a human urine sample for Mg isotopic composition. Urine and spike solution were mixed at mass ratios of Ψ_1 = 0.5 and Ψ_2 = 5.0 with both being similar in Mg concentration (ca. 20 µg/g) followed by microwave acid digestion and ion-exchange separation using standard protocols (Details in Supporting Information). Mg recovery was 100.1 ± 0.8 % (1SD) at a total procedural blank of 5 - 11 ng as determined by processing aliquots of a pure ^{25}Mg spike solution. Modeling of data revealed that procedural blanks were low enough to have a negligible effect on measured isotope ratios within the repeatability of the measurement. Five aliquots of the same urine sample were analyzed independently using the described procedures. The analyzed δ-value of the urine sample for the $^{26}Mg/^{24}Mg$ isotope ratio was 1.36 ± 0.10 ‰ (1 SD) relative to the used Mg standard (see Supporting Information, Table S-2).

DISCUSSION

GS-IDA versus Double Spiking Technique

Double spiking techniques have been used for decades as the undisputed reference technique for measuring natural isotope abundance variations. While GS-IDA also involves addition of an isotopically enriched spike to the sample, the conceptual approach we are presenting here is actually different. Double spiking requires preparation of a blend of two different spikes which permits, technically, normalization of measured isotope ratios to the isotopic composition of the added double spike. GS-IDA does not require a double spike. Because the technique follows IDMS concepts, a single 100% pure isotopic spike could also be used. This entails that optimization of spike composition is less crucial compared to double spiking experiments. Spike composition has some effect on measurement uncertainty but the optimal range is rather wide (see Fig. 2). This makes method optimization for different sets of spikes with different isotopic enrichments unnecessary once they have been determined for a given element. The method is also relatively robust when it comes to the choice of the optimal mixing ratios of spike to sample (see Fig. 3). In addition, element concentration of spike and sample solution need not be known accurately as long as their mole ratio in the blend is of the same order as the mass ratio of the solutions. This can be ensured by semi-quantitative analysis of the sample and spike solution.

A major advantage of the GS-IDA approach, and the key motivation for developing the GS-IDA technique, is the possibility to study natural isotope abundance variations by measuring only two isotope ratios of a given element as opposed to three isotope ratios for the conventional double-spiking technique. In this paper we demonstrated that isotope abundance variations can be measured by GS-IDA for elements having three stable isotopes only such as Mg. For elements having more than three stable isotopes, isotope ratio measurements can be restricted to the three most abundant isotopes or those three isotopes for which measurements are least affected by isobaric interferences in the mass spectrum. This can be of particular advantage when adopting the GS-IDA

technique for MC-ICP-MS where isobaric interferences are much more common than in MC-TIMS. As shown earlier, all other isotopes can be safely ignored and do not have to be measured. This is of significant advantage for elements such as Ca for which all isotopes can be hardly measured simultaneously because of the limited mass dispersion of multi-collector most instruments and the massive interference of $^{40}Ar^{+}$ ions with $^{40}Ca^{+}$ which renders measurement of the $^{40}Ca^{+}$ signal practically impossible. In addition, matrix effects are also minimized as in the conventional double spiking approach. In all mixtures, the spike amount varies while the amount of sample inclusive of all impurities is kept constant. Likewise, isotopic fractionation due to incomplete analyte recovery during sample purification is accounted for as the spike is added before sample digestion and separation.

Measurement Accuracy

Isotope abundance variations in nature are small for the heavier elements and rarely exceed a few parts per thousand (per mil) in a given isotope ratio. To decipher the information that is coded in these variations, measurements have not only be extremely precise but also highly accurate to avoid misinterpretation or over-interpretation of data. This becomes a challenge when using MC-ICP-MS for analysis. For iron, as an example, the range of natural isotope abundance variations in the $^{56}Fe/^{54}Fe$ ratio is of the order of 0.3% with the ratio being shifted further by 5-8% at the moment that the sample is transferred from the plasma to the mass analyzer[29]. In addition, iron isotope ratios of the sample can be altered during sample preparation[30]. Techniques employing standard-sample bracketing, external normalization or a combination of both have been developed to correct for such adulterations and are now employed widely but they have their well-known limitations. They cannot correct for hidden isobaric interferences, differences in fractionation behaviour between standard and sample because of matrix effects, or unexpected deviations in the fractionation behaviour of the analyte element and the spiking element when using external normalization techniques. Control of these effects makes chemical separation of the analyte element indispensable for generation of

meaningful data. Close to 100% recovery is also necessary to prevent isotope fractionation during ion-exchange separation[31], thus ensuring high accuracy. Quality control protocols have been developed for MC-ICP-MS[29] and are valuable to identify and reject measurement artifacts but they are not perfect. Spiking techniques will therefore remain the reference method and benchmark for assessing measurement accuracy.

Similar to double-spiking, GS-IDA allows a better control of several sources of measurement bias. Spiking of the sample before isolation of the element for analysis automatically corrects for fractionation effects induced during sample preparation. Differences in sample matrix between standard and sample are also of minor concern as the GS-IDA approach involves addition of a high purity spike to the sample. As for the standard addition method, blends to be analyzed differ only in the amount of analyte present and not in matrix composition. At the same time, GS-IDA does not require knowledge of the true isotope ratios of the spike and the referencing standard. This becomes possible by calibration of the spike using a circular approach in which the referencing standard is used to determine the normalized spike fractionation index F_{spike} using the very same algorithms that are used for sample analysis. For spike calibration, F_{spike} is the unknown while the δ-value of the referencing standard is known (zero by definition). In reverse, the δ-value of the sample can be determined using the F_{spike} value from spike calibration. In essence, the concept of calibrating the spike against the reference material in the GS-IDA approach follows closely the concept of reversed IDMS analysis in which the spike is characterized against a standard of known element concentration[19]. In both cases, the spike functions as the messenger that bridges quantitative information contained in the calibrant/reference with the quantitative information in the sample material.

Restrictions of GS-IDA

While the GS-IDA is robust in terms of chosen spike composition, blend composition and matrix effects, measurement uncertainty is strongly influenced by the quality of the isotope ratio measurements. Similar to IDMS, uncertainties in isotope ratio measurements are magnified significantly when the amount ratio of spike to sample is calculated from measured isotope ratios. In the case of Mg, we found that the coefficient of determination (r^2) for the correlation between logarithmically transformed Mg isotope ratios (three-isotope plots) must be 0.999 or better for a given analysis to reach a target measurement uncertainty of ±0.1 in the δ-value (1 SD). To reach this target we identified criteria that measurements had to fulfill strictly for inclusion in data analysis such as the minimum required signal intensities, stability of the ion current during the measurement and correlation analysis of measured data after logarithmic transformation. By applying these criteria strictly, external precision for independent measurements could be lowered to 0.0018% ($^{26}Mg/^{24}Mg$, 1 SD) for internally normalized data. Approximately two out of three loadings of sample or standard fulfilled all inclusion criteria. Even if analysis of two different blends of the sample may be considered as analytical replicates, although not strictly independent, sample analysis by GS-IDA is probably more time-consuming as compared to double spiking analysis, standard-sample bracketing and external normalization, in descending order.

As for the double spiking technique, isotope fractionation in nature and during analysis must follow strictly a unifying fractionation law. For the GS-IDA approach presented here we have chosen the exponential law but any law can be used, in principle, as long as it describes the mass dependence of the fractionation process both in nature and the ion source accurately.

Based on first principles, this disqualifies GS-IDA and double spiking techniques from analysis of samples affected by mass independent isotope fractionation (MIF) either in nature or during sample analysis. MIFs are known for the lighter elements and have recently been reported also for heavier

elements[32]. However, based on our current state of knowledge they appear to be rare in nature for the heavier elements and it still remains unclear to what extent they are actually measurement artifacts induced during isotopic analysis, namely when using MC-ICP-MS[2, 33]. As an example, isotope fractionation becomes largely irreproducible and dependent on signal intensities when baseline signal intensities are measured incorrectly. Other sources of bias include over- or under-correction of isobaric interferences in the mass spectrum or offsets between detectors in the used multi-collector array. This points to the undisputed strength of MC-TIMS for reliable measurement of isotope abundance variations. Firstly, isobaric interferences are less common. Secondly, there are only a few exceptional cases for MC-TIMS in which a deviation from conventional mass dependent fractionation laws, namely the common exponential law, was reported[34-36]. Finally, instrumental fractionation in MC-TIMS is much smaller but less stable as compared to MC-ICP-MS. Progressive alteration of isotope composition of the sample during a MC-TIMS measurement caused by mass sensitive evaporation of the sample from the filaments results usually in a continuous drift of measured isotope ratios. This drift makes it easier to identify measurement artifacts using three-isotope-plots for technique optimization and to tightly control measurement quality when samples are being analyzed.

Magnesium isotope variations in urine

We have applied the developed GS-IDA technique successfully to Mg isotopic analysis of a human urine sample after validating the technique by independent analysis of the calibration standard using a circular validation approach. The urine sample was found to be enriched in the heavier Mg isotopes relative to the referencing standard. Urine is a likely candidate for Mg isotope variations similar to Ca for which isotope variations have already been reported[37-38]. Both Ca and Mg are bone forming minerals and Mg homeostasis is likewise controlled by tubular reabsorption in the kidneys with less than 5% of the filtered Mg load being excreted in urine[39]. Mg isotope variations in nature have been studied so far only by MC-ICP-MS in the areas of geology and geochemistry[31, 40-49]. We are

the first to study Mg isotope variations in a human biological sample. Repeatability of ± 0.1 ‰ for the presented GS-IDA technique using MC-TIMS compare well to reported measurement repeatabilities for MC-ICP-MS (ca. ± 0.1 ‰).

CONCLUSIONS

By combining gravimetric spiking and standard addition principles, we were able to develop a fundamentally new concept for measurement of natural isotope variations of heavier elements. In contrast to established protocols for double spiking, the described GS-IDA approach requires measurement of three isotope signals only which makes it also applicable to elements such as Mg. Similar to the double spiking technique, GS-IDA is not restricted to a specific measurement platform and can be used both in MC-TIMS and MC-ICP-MS. In MC-ICP-MS, GS-IDA can become an alternative to standard-sample bracketing and external normalization which are more susceptible to measurement artifacts from first principles. While these techniques will remain the only choice for elements having two stable isotopes only, adoption of GS-IDA principles in MC-ICP-MS as well as MC-TIMS opens up a new avenue to improve the accuracy of isotopic analysis in the measurement of natural isotope abundance variations in this rapidly developing area of interdisciplinary research.

SUPPORTING INFORMATION. A step-by-step derivation of equations and detailed information on the optimization procedure and the calculation of F_{spike} and f_{sample} using the GS-IDA technique are supplied in the Supporting Information. In addition, technical details on how Mg isotopic analysis was carried out are provided together with procedures for data analysis by robust simple regression and data from all analytical runs. This material is available free of charge via the Internet at http://pubs.acs.org.

ACKNOWLEDGMENT

The authors would like to acknowledge the contribution of Ms Lim Li Yan Clare who helped to develop the protocol for the digestion and ion-exchange separation of Mg in urine samples. We also want to thank Mr Go Jun Hong for his contributions in optimizing the MC-TIMS technique for high precision Mg isotope ratio analysis.

REFERENCES

1. Russell, W.; Papanastassiou, D.; Tombrello, T., *Geochim. Cosmochim. Acta* **1978,** *42* (8), 1075-1090.
2. Albarede, F.; Telouk, P.; Blichert-Toft, J.; Boyet, M.; Agranier, A.; Nelson, B., *Geochim. Cosmochim. Acta* **2004,** *68* (12), 2725-2744.
3. Albarède, F.; Beard, B., *Rev. Mineral. Geochem.* **2004,** *55* (1), 113-152.
4. Elburg, M. A., Geochronological Dating. In *Isotopic Analysis: Fundamentals and Applications Using ICP-MS*, Vanhaecke, F.; Degryse, P., Eds. Wiley-VCH: Weinheim, Germany, 2012; pp 235-274.
5. Rehkamper, M. S., M.; Andreasen, R., Application of Multiple-Collector Inductively Coupled Plasma Mass Spectrometry to Isotopic Analysis in Cosmochemistry. In *Isotopic Analysis: Fundamentals and Applications Using ICP-MS*, Vanhaecke, F.; Degryse, P., Eds. Wiley-VCH: Weinheim, Germany, 2012; pp 275-315.
6. Walczyk, T., The Use of Stable Isotope Techniques for Studying Mineral and Trace Element Metabolism in Humans. In *Isotopic Analysis: Fundamentals and Applications Using ICP-MS*, Vanhaecke, F.; Degryse, P., Eds. Wiley-VCH: Weinheim, Germany, 2012; pp 435-494.
7. Marechal, C. N.; Telouk, P.; Albarede, F., *Chem. Geol.* **1999,** *156* (1-4), 251-273.
8. Walczyk, T., *Anal. Bioanal. Chem.* **2004,** *378* (2), 229-231.
9. Dodson, M., *J. Sci. Instrum.* **1963,** *40*, 289.
10. Hirata, T.; Shimizu, H.; Akagi, T.; Masuda, A., *ICP Inf. Newslett* **1988,** *13*, 731-735.
11. Compston, W.; Oversby, V. M., *J. Geophys. Res.* **1969,** *74* (17), 4338-&.
12. Eugster, O.; Tera, F.; Wasserbu, G., *J. Geophys. Res.* **1969,** *74* (15).
13. Gale, N., *Chem. Geol.* **1970,** *6*, 305-310.
14. Hamelin, B.; Manhes, G.; Albarede, F.; Allegre, C., *Geochim. Cosmochim. Acta* **1985,** *49* (1), 173-182.
15. Galer, S. J. G., *Chem. Geol.* **1999,** *157* (3), 255-274.
16. Heuser, A.; Eisenhauer, A.; Gussone, N.; Bock, B.; Hansen, B.; Nägler, T. F., *Int. J. Mass Spectrom.* **2002,** *220* (3), 385-397.
17. Amelin, Y.; Davis, W., *J. Anal. At. Spectrom.* **2006,** *21* (10), 1053-1061.
18. Gopalan, K.; Macdougall, D.; Macisaac, C., *Int. J. Mass Spectrom.* **2006,** *248* (1), 9-16.
19. Sargent, M.; Harte, R.; Harrington, C., *Guidelines for achieving high accuracy in isotope dilution mass spectrometry (IDMS)*. Royal Society of Chemistry: Cambridge, U.K., 2002.
20. Catanzaro, E. J.; Murphy, T. J.; Garner, E. L.; Shields, W. R., *J. Res. Nat. Bur. Stand* **1966**, 453-458.
21. Go, J. H. Development of techniques for measuring natural isotope abundance variations of Mg in biological samples. Honours Thesis, National University of Singapore, April 2012.
22. Vieira, N. E.; Yergey, A. L.; Abrams, S. A., *Anal. Biochem.* **1994,** *218* (1), 92-97.
23. Stegmann, W.; Goldstein, S. L.; Georgieff, M., *Analyst* **1996,** *121* (7), 901-904.
24. Richter, S.; Berglund, M.; Hennessy, C., *Fresenius. J. Anal. Chem.* **1999,** *364* (5), 478-481.
25. Dlugaszek, M.; Kaszczuk, M.; Mularczyk-Oliwa, M., *Biol. Trace Elem. Res.* **2011,** *142* (1), 1-10.
26. Chew, G.; Walczyk, T., *Anal. Bioanal. Chem.* **2012**, 1-7.
27. Berglund, M.; Wieser, M. E., *Pure Appl. Chem.* **2011,** *83* (2), 397.
28. Galy, A.; Yoffe, O.; Janney, P. E.; Williams, R. W.; Cloquet, C.; Alard, O.; Halicz, L.; Wadhwa, M.; Hutcheon, I. D.; Ramon, E.; Carignan, J., *J. Anal. At. Spectrom.* **2003,** *18* (11), 1352-1356.
29. Schoenberg, R.; von Blanckenburg, F., *Int. J. Mass Spectrom.* **2005,** *242* (2–3), 257-272.
30. Anbar, A.; Roe, J.; Barling, J.; Nealson, K., *Science* **2000,** *288* (5463), 126-128.
31. Chang, V. T. C.; Makishima, A.; Belshaw, N. S.; O'Nions, R. K., *J. Anal. At. Spectrom.* **2003,** *18* (4), 296-301.

32. Epov, V. N.; Malinovskiy, D.; Vanhaecke, F.; Begue, D.; Donard, O. F. X., *J. Anal. At. Spectrom.* **2011,** *26* (6), 1142-1156.
33. Malinovsky, D.; Vanhaecke, F., *Anal. Bioanal. Chem.* **2011,** *400* (6), 1619-1624.
34. Doucelance, R.; Manhes, G., *Chem. Geol.* **2001,** *176* (1-4), 361-377.
35. Schmitt, A.-D.; Galer, S. J. G.; Abouchami, W., *J. Anal. At. Spectrom.* **2009,** *24* (8), 1079-1088.
36. Thirlwall, M. F., *Chem. Geol.* **2000,** *163* (1-4), 299-322.
37. Skulan, J.; Bullen, T.; Anbar, A. D.; Puzas, J. E.; Shackelford, L.; LeBlanc, A.; Smith, S. M., *Clin. Chem.* **2007,** *53* (6), 1155-1158.
38. Heuser, A.; Eisenhauer, A., *Bone* **2010,** *46* (4), 889-896.
39. Quamme, G. A., *Miner. Electrol. Metab.* **1993,** *19* (4-5), 218-225.
40. Galy, A.; Belshaw, N. S.; Halicz, L.; O'Nions, R. K., *Int. J. Mass Spectrom.* **2001,** *208* (1), 89-98.
41. Galy, A.; Bar-Matthews, M.; Halicz, L.; O'Nions, R. K., *Earth Planet. Sci. Lett.* **2002,** *201* (1), 105-115.
42. Young, E. D.; Galy, A., *Rev. Mineral. Geochem.* **2004,** *55* (1), 197-230.
43. Tipper, E.; Galy, A.; Gaillardet, J.; Bickle, M.; Elderfield, H.; Carder, E., *Earth Planet. Sci. Lett.* **2006,** *250* (1-2), 241-253.
44. Teng, F. Z.; Wadhwa, M.; Helz, R. T., *Earth Planet. Sci. Lett.* **2007,** *261* (1), 84-92.
45. Bolou Bi, E. B.; Vigier, N.; Brenot, A.; Poszwa, A., *Geostand. Geoanal. Res.* **2009,** *33* (1), 95-109.
46. Wombacher, F.; Eisenhauer, A.; Heuser, A.; Weyer, S., *J. Anal. At. Spectrom.* **2009,** *24* (5), 627-636.
47. Opfergelt, S.; Georg, R.; Delvaux, B.; Cabidoche, Y. M.; Burton, K.; Halliday, A., *Earth Planet. Sci. Lett.* **2012,** *341*, 176-185.
48. Huang, F.; Zhang, Z. F.; Lundstrom, C. C.; Zhi, X. C., *Geochim. Cosmochim. Acta* **2011,** *75* (12), 3318-3334.
49. Bolou-Bi, E. B.; Vigier, N.; Poszwa, A.; Boudot, J. P.; Dambrine, E., *Geochim. Cosmochim. Acta* **2012**.

Manuscript 2

Measurement of Isotope Abundance Variations in Nature by Gravimetric Spiking Isotope Dilution Analysis (GS-IDA)

(Supporting Information)

Gina Chew[1] and Thomas Walczyk[1,2,3*]

[1]NUS Graduate School for Integrative Sciences and Engineering,
National University of Singapore (NUS), Singapore

[2]Nutritrace@NUS, Department of Chemistry, Faculty of Science (NUS)

[3]Department of Biochemistry, Yong Loo Lin School of Medicine (NUS)

*corresponding author: NutriTrace@NUS
Department of Chemistry
National University of Singapore (NUS)
Science Drive 4
Singapore 117543

walczyk@nus.edu.sg

ABSTRACT

The Supporting Information contains details of the procedures presented in the main text, namely derivations of equations presented in the text (Part A), the algorithm and computational techniques used to identify the optimal composition of the spike as well as optimal mixing ratios of spike and sample solution (Part B), the algorithms used for computation of F_{spike} and f_{sample} (Part C) and the techniques used for Mg isotopic analysis (Part D). In addition, we present results of the individual magnesium isotope ratio measurements of the reference standard, human urine and spike in Part E (Table S-1) together with calculated δ-values for the reference standard and the human urine sample as determined in five fully independent analytical runs (Table S-2).

PART A: Derivation of Equations for Isotopic Analysis by GS-IDA

To extend the double spike technique to elements that have only three naturally occurring stable isotopes, we combined gravimetric spiking (GS) with isotope dilution analysis (IDA). In the classical double-spike approach, the proportion P or mole ratio of added spike to sample must be known to obtain the fractionation indices f_{sample} and f_{method}. In GS-IDA, the unknown P is eliminated by mixing of the sample with different amounts of spike in solution. When adding a certain mass of spike solution m_{spike} to a certain mass of sample solution m_{sample}, the mole ratio of spike to sample is given as:

$$P_1 = \left(\frac{n_{spike}}{n_{sample}}\right)_1 = \left(\frac{m_{spike}}{m_{sample}}\right)_1 \cdot \left(\frac{c_{spike}}{c_{sample}}\right) \cdot \left(\frac{A_{r,sample}}{A_{r,spike}}\right) = \Psi_1 \cdot \left(\frac{c_{spike}}{c_{sample}}\right) \cdot \left(\frac{A_{r,sample}}{A_{r,spike}}\right) \quad \text{(S-1)}$$

with c being the element concentration in the spike and sample solution, respectively, in units of µg/g and A_r being the atomic weight of the element in the spike and sample, respectively, expressed in grams per mole. Atomic weights of the element in the sample and spike are not identical as they differ in isotopic composition. Ψ refers to the mixing ratio of spike to sample solution (g/g) in the blend. For a second blend, in which we add exactly twice as much spike solution to the same mass of sample solution as in Eqn. (S-1), we obtain

$$P_2 = \left(\frac{n_{spike}}{n_{sample}}\right)_2 = \left(2 \cdot \Psi_1\right) \cdot \left(\frac{c_{spike}}{c_{sample}}\right) \cdot \left(\frac{A_{r,sample}}{A_{r,spike}}\right) = 2 \cdot P_1 \quad \text{(S-2)}$$

As concentrations and atomic weights are invariant in Eqn. (S-1) and (S-2), the proportion P or mole ratio of spike to sample in the two blends is linearly correlated with the mass ratio Ψ of spike to sample solution in the blend as shown in Fig. 1. The resulting line passes through the origin as P equals zero when no spike is added to the sample. The proportions P of spike to sample can be obtained from the isotope ratios in the two blends following isotope dilution principles following Eqn. (5). The mixing ratio of spike and sample solution Ψ can be determined at high accuracy and very small measurement uncertainty using a conventional analytical precision balance. Within measurement uncertainty, the mass ratio of spike to sample solution equals their weight ratio. The latter is directly measurable by weighing and does not require buoyancy corrections. Element

concentrations and atomic weights of sample and spike solution, which carry a much higher analytical uncertainty, need not be known.

Mixing of the sample with different amounts of spike allows us to differentiate natural isotope fractionation in the sample (f_{sample}) from fractionation of isotopes during the measurement (f_{method}). Let us assume first that we know the absolute isotope ratios of the reference sample and the used spike, i.e. their true values free from instrumental mass bias. As f_{sample} is an intrinsic property of the sample and thus invariant for all mixtures, blends can only plot on a straight line if isotopic analysis of the blends is free of any methodological mass bias. At the moment that the measurement is affected by isotope fractionation, the isotope ratio R_{blend} is altered which results inevitably in a biased measurement of P according to Eqn. (5). The magnitude of the effect is obviously different for the first blend and the second blend as both measurements carry their own methodological fractionation index f_{method}. However, while f_{method} varies between measurements, it characterizes the individual measurement. This brings us to the fundamental fractionation law introduced earlier (Eqn. 1). Instrumental mass bias is always different between two isotope ratios of the same element with the effect being stronger with increasing mass difference between the isotopes. This entails that the absolute/relative bias in the calculated proportion P in the blend according to Eqn. (5) is always different when either one or the other isotope ratio in the blend is used for calculation. This is illustrated in Fig. 1. Only when the methodological fractionation index f_{method} becomes zero, i. e. in absence of fractionation effects induced during analysis, the calculated proportion P of spike to sample in the blend is the same irrespective of the isotope ratio that was chosen for the calculations.

Assuming that isotope fractionation in nature and during analysis follows the well established exponential law (Eqn. 1), any isotope ratio of the sample ${}^{x}R_{sample}$ can be expressed using the true (absolute) isotope ratio ${}^{x}R_{ref}$ of the reference material and the sample fractionation index f_{sample}

$$ {}^{x}R_{sample} = {}^{x}R_{ref} \cdot {}^{x}M^{\,f_{sample}} \qquad \text{(S-3)} $$

with ${}^{x}R$ being the mole ratio x or $n_{(isotope\ B)}/n_{(isotope\ A)}$ of the sample and reference standard, respectively. In a similar fashion, the measured isotope ratio in the blend ${}^{x}R_{blend,m}$ is related to its true value ${}^{x}R_{blend,t}$ via the ratio of the isotope's masses ${}^{x}M$ and the methodological fractionation index f_{method}

$$ {}^{x}R_{blend,m} = {}^{x}R_{blend,t} \cdot {}^{x}M^{\,f_{method}} \tag{S-4} $$

If f_{method} is known, the true isotope of the blend ${}^{x}R_{blend,t}$ can be expressed using the measured ratio ${}^{x}R_{blend,m}$:

$$ {}^{x}R_{blend,t} = {}^{x}R_{blend,m} \cdot {}^{x}M^{-f_{method}} \tag{S-5} $$

For a sample carrying an isotope effect defined by f_{sample} and using the isotope ratio ${}^{x}R$ for isotope dilution analysis, Eqn. (5) can be rewritten using Eqn. (S-3)

$$ {}^{x}P = {}^{x}\left(\frac{n_{spike}}{n_{sample}}\right) = \frac{{}^{x}R_{blend,t} - {}^{x}R_{ref,t} \cdot {}^{x}M^{\,f_{sample}}}{{}^{x}R_{spike,t} - {}^{x}R_{blend,t}} \cdot \frac{\sum_{i} {}^{i}R_{spike,t} + 1}{\sum_{i} {}^{i}R_{ref,t} \cdot {}^{i}M^{\,f_{sample}} + 1} = {}^{x}A \cdot B \tag{S-6} $$

and further modified using Eqn. (S-5) to calculate ${}^{x}P$ from the measured isotope ratio of the blend ${}^{x}R_{blend,m}$

$$ {}^{x}P = {}^{x}\left(\frac{n_{spike}}{n_{sample}}\right) = \frac{{}^{x}R_{blend,m} \cdot {}^{x}M^{-f_{method}} - {}^{x}R_{ref,t} \cdot {}^{x}M^{\,f_{sample}}}{{}^{x}R_{spike,t} - {}^{x}R_{blend,m} \cdot {}^{x}M^{-f_{method}}} \cdot \frac{\sum_{i} {}^{i}R_{spike,t} + 1}{\sum_{i} {}^{i}R_{ref,t} \cdot {}^{i}M^{\,f_{sample}} + 1} \tag{S-7} $$

In an identical fashion, the mole ratio of spike to standard P can be calculated using a different isotope ratio ${}^{y}R$, i.e. the mole ratio $n_{(isotope\ C)}/n_{(isotope\ A)}$ in the sample, spike and blend

$$ {}^{y}P = {}^{y}\left(\frac{n_{spike}}{n_{sample}}\right) = \frac{{}^{y}R_{blend,m} \cdot {}^{y}M^{-f_{method}} - {}^{y}R_{ref,t} \cdot {}^{y}M^{\,f_{sample}}}{{}^{y}R_{spike,t} - {}^{y}R_{blend,m} \cdot {}^{y}M^{-f_{method}}} \cdot \frac{\sum_{i} {}^{i}R_{spike,t} + 1}{\sum_{i} {}^{i}R_{ref,t} \cdot {}^{i}M^{\,f_{sample}} + 1} \tag{S-8} $$

As the mole ratio of spike to sample is invariant, ${}^{x}P$ must equal ${}^{y}P$. Eqn. (S-7) and (S-8) can thus be combined. This eliminates the multiplier B in both equations:

$$
\begin{aligned}
{}^{x}A &= \frac{{}^{x}R_{blend,m} \cdot {}^{x}M^{-f_{method}} - {}^{x}R_{ref,t} \cdot {}^{x}M^{f_{sample}}}{{}^{x}R_{spike,t} - {}^{x}R_{blend,m} \cdot {}^{x}M^{-f_{method}}} \\
&= \frac{{}^{y}R_{blend,m} \cdot {}^{y}M^{-f_{method}} - {}^{y}R_{ref,t} \cdot {}^{y}M^{f_{sample}}}{{}^{y}R_{spike,t} - {}^{y}R_{blend,m} \cdot {}^{y}M^{-f_{method}}} = {}^{y}A
\end{aligned}
\tag{S-9}
$$

We have assumed that the true (absolute) isotope ratios ${}^{x}R$ and ${}^{y}R$ of the spike and reference material are known. As we will see in the following, this information becomes redundant when relative differences in an isotope ratio between a sample and a reference are measured on a δ-scale. But even then there are two unknowns in Eqn. (S-9), namely the sample fractionation index f_{sample} and the methodological fractionation index f_{method}. By preparing and analyzing a second mixture with a known mass ratio of spike to sample solution, as illustrated in Fig. 1, we obtain a second equation similar to Eqn. (S-9). However, while f_{sample} is an intrinsic property of the sample and therefore the same for each mixture, analysis of a second mixture comes with a second method fractionation index f_{method}. Thus, there will be always *n+1* unknowns for n mixtures and equations, i.e. n method fractionation indices in addition to the sample fractionation index f_{sample} as the information of interest.

To solve the set of equations for the different gravimetric mixtures definitely, an additional equation is needed. Based on first principles (see Fig. 1), the proportion P, as the mole ratio of spike to sample in a given blend, becomes zero when no spike is added to the sample. Accordingly, the line obtained by plotting proportions P against their mass ratios Ψ of spike solution to sample solution in the blend (in g/g) must pass through the origin. For n different mixtures, the intercept I of the line is defined as

$$
I = \frac{\sum_n P_n \cdot \sum_n \Psi_n^{\,2} - \sum_n \Psi_n \cdot \left(\sum_n P_n \cdot \Psi_n \right)}{n \sum_n \Psi_n^{\,2} - \left(\sum_n \Psi_n \right)^2}
\tag{S-10}
$$

For I=0, Eqn. (S-10) can be simplified by multiplication with the denominator and by substituting proportions P_n with $A_n \cdot B$. As B is a constant for all n blends, division of Eqn. (S-10) by B yields Eqn. (9) in the main text:

$$\sum_n A_n \cdot \sum_n \Psi_n^{\,2} - \sum_n \Psi_n \cdot \left(\sum_n A_n \cdot \Psi_n \right) = 0 \qquad \text{(S-11)}$$

We have assumed so far that the true (absolute) isotope ratios of the spike $R_{spike,t}$ and the reference material of natural isotopic composition $R_{ref,t}$ are known. The absolute numerical value of an isotope ratio, however, can never be determined experimentally as every measurement comes naturally with a measurement uncertainty. What can be determined with substantial experimental efforts is only the "best estimate for the true value"[1] of an isotope ratio and the probability at which the true isotope ratio, which is a single value that carries an uncertainty of zero by definition, lies within the boundaries of the stated uncertainty interval[2]. Following Eqn. (S-9), determination of the absolute isotope ratios of the sample requires not only knowledge of the fractionation indices f_{sample} and f_{method} but also knowledge of the absolute isotope ratios of spike and reference material. They become redundant, however, when the isotope ratio of the sample is expressed relative to the reference material on a δ-scale (see Eqn. 3) and when the spike is directly calibrated against the very same reference material.

For spike calibration, we determine first the relevant isotope ratios of the spike solution R_{spike} and that of the reference material R_{ref}. Calculated mean values of the measured isotope ratios $\overline{R}_{spike,m}$ and $\overline{R}_{ref,m}$ are obviously not their true values as both the spike and the reference material undergo isotope fractionation in the ion source. According to Eqn. (S-5), the measured isotope ratios of the spike $\overline{R}_{spike,m}$ can be converted into their true isotope ratios $R_{spike,t}$ if the spike fractionation index f_{spike} is known.

$$R_{spike,t} = \overline{R}_{spike,m} \cdot M^{-f_{spike}} \quad \text{(S-12)}$$

The same holds true for the reference material and its associated fractionation index f_{ref} arising from isotopic analysis.

$$R_{ref,t} = \overline{R}_{ref,m} \cdot M^{-f_{ref}} \quad \text{(S-13)}$$

Both together permit us to rewrite Eqn. (S-9) by replacing the true ratios of the reference material and spike with Eqns. (S-12 and S-13). Use of the reference material for spike calibration removes $M^{f_{sample}}$ from Eqn. (S-9) as the reference material defines the δ-scale and carries, by definition, a sample fractionation index of zero.

$$\frac{{}^{x}R_{blend,m} \cdot {}^{x}M^{-f_{method}} - {}^{x}\overline{R}_{ref,m} \cdot {}^{x}M^{-f_{ref}}}{{}^{x}\overline{R}_{spike,m} \cdot {}^{x}M^{-f_{spike}} - {}^{x}R_{blend,m} \cdot {}^{x}M^{-f_{method}}} = \frac{{}^{y}R_{blend,m} \cdot {}^{y}M^{-f_{method}} - {}^{y}\overline{R}_{ref,m} \cdot {}^{y}M^{-f_{ref}}}{{}^{y}\overline{R}_{spike,m} \cdot {}^{y}M^{-f_{spike}} - {}^{y}R_{blend,m} \cdot {}^{y}M^{-f_{method}}} \quad \text{(S-14)}$$

According to Eqn. (S-14), calibration of the spike by determination of the fractionation index f_{spike} requires determination of four unknowns, namely f_{ref}, f_{sample} and the two fractionation indices f_{method} for the two mixtures that are analyzed. This is obviously not possible using the algorithm outlined before. In a second step, we further divide each side of the equation by the term describing the mass bias in the isotope ratios of the reference material $M^{-f_{ref}}$. This yields Eqn. (S-15)

$$\frac{{}^{x}R_{blend,m} \cdot {}^{x}M^{-F_{method}} - {}^{x}\overline{R}_{ref,m}}{{}^{x}\overline{R}_{spike,m} \cdot {}^{x}M^{-F_{spike}} - {}^{x}R_{blend,m} \cdot {}^{x}M^{-F_{method}}} = \frac{{}^{y}R_{blend,m} \cdot {}^{y}M^{-F_{method}} - {}^{y}\overline{R}_{ref,m}}{{}^{y}\overline{R}_{spike,m} \cdot {}^{y}M^{-F_{spike}} - {}^{y}R_{blend,m} \cdot {}^{y}M^{-F_{method}}} \quad \text{(S-15)}$$

with the normalized fractionation indices F_{spike} and F_{method} as defined in in the main text (Eqns. 7 and 8):

$$F_{spike} = f_{spike} - f_{ref} \quad \text{(S-16)}$$

$$F_{method} = f_{method} - f_{ref} \quad \text{(S-17)}$$

With only three unknowns remaining, F_{spike} and the two fractionation indices of F_{method} can be determined by the gravimetric mixing approach introduced earlier for sample analysis. Normalization of fractionation indices following Eqns. (S-16 and S-17) permits us also to rewrite Eqn. (S-9) for the mixtures of spike and sample which yields Eqn. (6) in the main text:

$$ {}^{x}A = \frac{{}^{x}R_{blend,m} \cdot {}^{x}M^{-F_{method}} - {}^{x}\overline{R}_{ref,m} \cdot {}^{x}M^{f_{sample}}}{{}^{x}\overline{R}_{spike,m} \cdot {}^{x}M^{-F_{spike}} - {}^{x}R_{blend,m} \cdot {}^{x}M^{-F_{method}}} = \frac{{}^{y}R_{blend,m} \cdot {}^{y}M^{-F_{method}} - {}^{y}\overline{R}_{ref,m} \cdot {}^{y}M^{f_{sample}}}{{}^{y}\overline{R}_{spike,m} \cdot {}^{y}M^{-F_{spike}} - {}^{y}R_{blend,m} \cdot {}^{y}M^{-F_{method}}} = {}^{y}A \quad \text{(S-18)} $$

As stated earlier, the sample fractionation index f_{sample} can be obtained from the measured isotope ratios of the spike, the reference material and the blend using Eqns. (S-11 and S-18) without knowledge of their absolute isotope ratios.

PART B: Algorithm and Computational Techniques used for Method Optimization

Optimal mixing ratios of sample and spike and optimal spike isotope composition were identified with minimization of the measurement uncertainty of f_{sample} as the target. Starting values for spike isotope composition (10% ^{24}Mg, 10% ^{25}Mg, 80% ^{26}Mg) were obtained first by random testing of a combination of mass ratios Ψ covering a range from 0.1 to 10. For the first iteration, the spike composition was kept constant whereas the spike-to-sample mass ratios Ψ were varied systematically from 0.1 to 10. Measurement uncertainty for each combination of Ψ_1 and Ψ_2 was calculated and the combination yielding the lowest measurement uncertainty was identified. For the second iteration, the optimum Ψ values from the first iteration were set as constants and the abundances of ^{25}Mg and ^{26}Mg in the spike were varied systematically from 0-100%. Optimal mass ratios Ψ_1 and Ψ_2 were reassessed in the final step for the spike composition that yields the lowest measurement uncertainty in f_{sample} by systematic variation of Ψ values.

Measurement uncertainties for a given set of variables were estimated using Microsoft Excel (Version 2007). We showed recently that Monte Carlo Simulations and standard spreadsheet software can be used for this purpose as an alternative to the partial derivative approach [3]. The used spreadsheet is accessible online. In Step 1 (see Fig. S-1), the mean and standard deviation of the two isotope ratios of each of the two blends ${}^{x}R_{blend}$ and ${}^{y}R_{blend}$ are calculated/simulated for a given mass of sample solution m_{sample} and spike solution ms_{pike} using Eqns. (S-19 and S-20). Division of every term

in the equation by $c_{sample} \cdot m_{sample}$ yields equations dependent on C as the concentration ratio of spike to sample and Ψ. Concentrations c of the sample and spike were assumed to be equal (1 mole/g) for method optimization. In this particular case (C=1) the mole ratio of spike to sample equals the mass ratio Ψ of spike (m_{spike}) to sample (m_{sample}).

$$
\begin{aligned}
{}^{x}R_{blend} &= \frac{{}^{iso2}a_{sample} \cdot c_{sample} \cdot m_{sample} + {}^{iso2}a_{spike} \cdot c_{spike} \cdot m_{spike}}{{}^{iso1}a_{sample} \cdot c_{sample} \cdot m_{sample} + {}^{iso1}a_{spike} \cdot c_{spike} \cdot m_{spike}} \\
&= \frac{{}^{iso2}a_{sample} + {}^{iso2}a_{spike} \cdot C \cdot \Psi}{{}^{iso1}a_{sample} + {}^{iso1}a_{spike} \cdot C \cdot \Psi}
\end{aligned}
\qquad \text{(S-19)}
$$

$$
\begin{aligned}
{}^{y}R_{blend} &= \frac{{}^{iso3}a_{sample} \cdot c_{sample} \cdot m_{sample} + {}^{iso3}a_{spike} \cdot c_{spike} \cdot m_{spike}}{{}^{iso1}a_{sample} \cdot c_{sample} \cdot m_{sample} + {}^{iso1}a_{spike} \cdot c_{spike} \cdot m_{spike}} \\
&= \frac{{}^{iso3}a_{sample} + {}^{iso3}a_{spike} \cdot C \cdot \Psi}{{}^{iso1}a_{sample} + {}^{iso1}a_{spike} \cdot C \cdot \Psi}
\end{aligned}
\qquad \text{(S-20)}
$$

For a given mass ratio Ψ of spike to sample in the blend, mean isotope ratios ${}^{x}R_{blend}$ and ${}^{y}R_{blend}$ were calculated using the isotopic abundances of the composed spike under evaluation (a_{spike}) and the magnesium isotopic abundances of natural magnesium (a_{sample}) as reported by Catanzarro[4]. Uncertainties in isotopic composition of spike and sample can be set to zero as they cancel out when data are reported on a δ-scale (circular spike calibration approach, see main text). The uncertainty in the measurement of the mass of sample and spike solution and of the corresponding mass ratio Ψ of the blend can be safely neglected when determined by a calibrated micro-analytical balance. This leaves instrumental precision as the only source of uncertainty for the estimated isotope ratios in the blend ${}^{x}R_{blend}$ and ${}^{y}R_{blend}$. Measurement uncertainty for these ratios were set to 0.00091% and 0.0018% for $^{25}Mg/^{24}Mg$ and $^{26}Mg/^{24}Mg$, respectively, which reflect the achievable experimental measurement precision for independent measurements after internal normalization of collected data, i.e. in absence of instrumental fractionation effects (F_{spike} = 0, F_{method} = 0, see Fig. S-1).

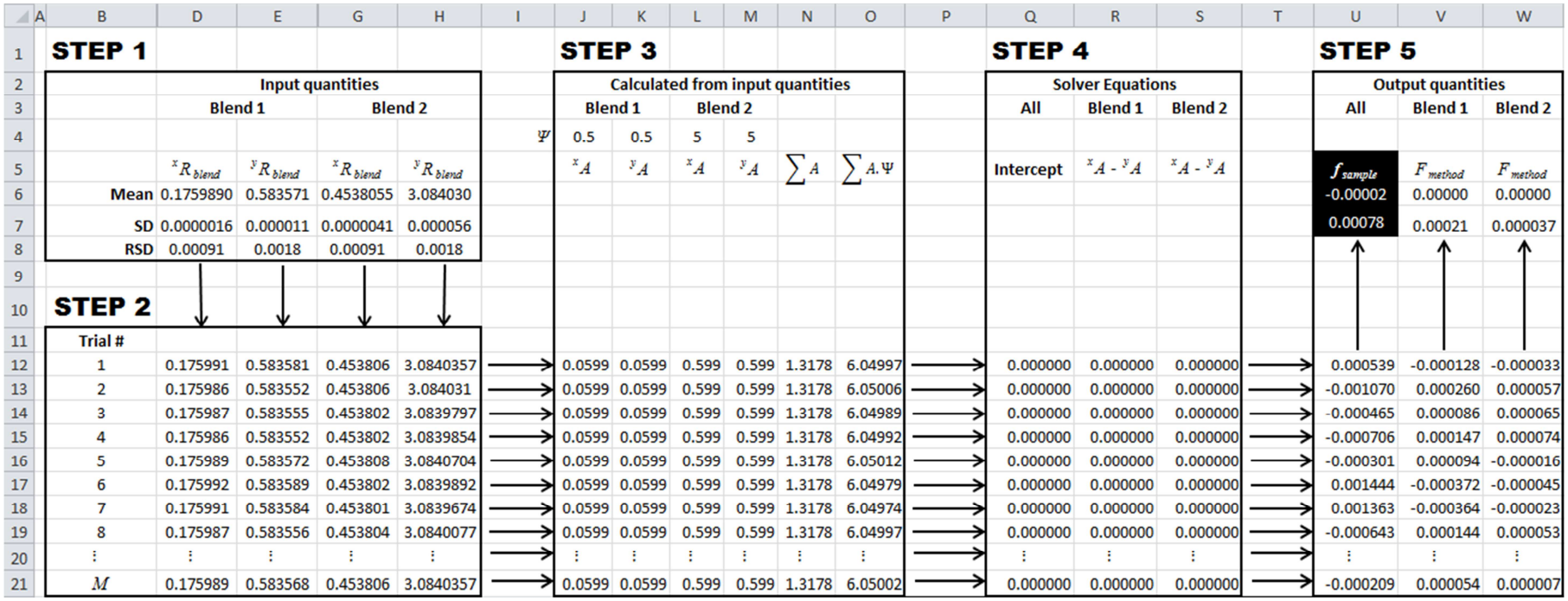

	STEP 1						**STEP 3**							**STEP 4**				**STEP 5**		
		Input quantities					**Calculated from input quantities**							**Solver Equations**				**Output quantities**		
		Blend 1		**Blend 2**			**Blend 1**		**Blend 2**					**All**	**Blend 1**	**Blend 2**		**All**	**Blend 1**	**Blend 2**
						Ψ	0.5	0.5	5	5										
		$^{x}R_{blend}$	$^{y}R_{blend}$	$^{x}R_{blend}$	$^{y}R_{blend}$		^{x}A	^{y}A	^{x}A	^{y}A	$\sum A$	$\sum A.\Psi$		**Intercept**	^{x}A - ^{y}A	^{x}A - ^{y}A		f_{sample}	F_{method}	F_{method}
	Mean	0.1759890	0.583571	0.4538055	3.084030													-0.00002	0.00000	0.00000
	SD	0.0000016	0.000011	0.0000041	0.000056													0.00078	0.00021	0.000037
	RSD	0.00091	0.0018	0.00091	0.0018															
	STEP 2																			
	Trial #																			
	1	0.175991	0.583581	0.453806	3.0840357		0.0599	0.0599	0.599	0.599	1.3178	6.04997		0.000000	0.000000	0.000000		0.000539	-0.000128	-0.000033
	2	0.175986	0.583552	0.453806	3.084031		0.0599	0.0599	0.599	0.599	1.3178	6.05006		0.000000	0.000000	0.000000		-0.001070	0.000260	0.000057
	3	0.175987	0.583555	0.453802	3.0839797		0.0599	0.0599	0.599	0.599	1.3178	6.04989		0.000000	0.000000	0.000000		-0.000465	0.000086	0.000065
	4	0.175986	0.583552	0.453802	3.0839854		0.0599	0.0599	0.599	0.599	1.3178	6.04992		0.000000	0.000000	0.000000		-0.000706	0.000147	0.000074
	5	0.175989	0.583572	0.453808	3.0840704		0.0599	0.0599	0.599	0.599	1.3178	6.05012		0.000000	0.000000	0.000000		-0.000301	0.000094	-0.000016
	6	0.175992	0.583589	0.453802	3.0839892		0.0599	0.0599	0.599	0.599	1.3178	6.04979		0.000000	0.000000	0.000000		0.001444	-0.000372	-0.000045
	7	0.175991	0.583584	0.453801	3.0839674		0.0599	0.0599	0.599	0.599	1.3178	6.04974		0.000000	0.000000	0.000000		0.001363	-0.000364	-0.000023
	8	0.175987	0.583556	0.453804	3.0840077		0.0599	0.0599	0.599	0.599	1.3178	6.04997		0.000000	0.000000	0.000000		-0.000643	0.000144	0.000053
	⋮	⋮	⋮	⋮	⋮		⋮	⋮	⋮	⋮	⋮	⋮		⋮	⋮	⋮		⋮	⋮	⋮
	M	0.175989	0.583568	0.453806	3.0840357		0.0599	0.0599	0.599	0.599	1.3178	6.05002		0.000000	0.000000	0.000000		-0.000209	0.000054	0.000007

Figure S-1. Spreadsheet for calculating the combined standard uncertainty for a GS-IDA experiment. Symbols/calculations in the spreadsheet refer to the equations/symbols in the publication. Measured average isotope ratios of the reference standard and the spike are entered in a separate worksheet. Fixed values were used for optimization of spike and blend composition as described in the main text.

In Step 2, a set of M random numbers was generated for each of the two isotope ratios and both blends (Fig. S-1, Columns D, E, G and H). Data frequency distribution in each column followed a Gaussian probability density function with a mean and standard deviation approximating the values set in Step 1. This was achieved by using the built-in Excel function '= NORMINV(η, mean, standard deviation)' for data generation in each cell[3]. Assuming a perfect correlation of isotope ratios and errors in a given blend, only one set of random numbers η had to be generated per blend (Column C for Blend 1 and Column F for Blend 2; not shown in Fig. S-1) This was done using the Excel function '=RAND()' which delivers random numbers for η that follow a rectangular PDF with 0 and 1 as the extreme values. The number of rows M in Fig. S-1 corresponds to the number of Monte Carlo trials used to estimate the combined standard uncertainty. Each trial/row represented one random Monte Carlo simulation of an analytical run. For our purpose, M = 1,000 was found to be sufficient as it only causes changes in the third significant figure of the standard deviation in f_{sample} upon repeated, independent simulations.

In Step 3, generated random numbers for ${}^{x}R_{blend}$ and ${}^{y}R_{blend}$ were used to calculate parameters ${}^{x}A$ and ${}^{y}A$ (Fig, S-1, Columns J-M) for the two blends according to Eqn. (6) as well as the sum over all calculated values of ${}^{x}A$ and ${}^{y}A$ (Column N) and the sum of all $A \cdot \Psi$ (Column O) in each of the rows using the mass ratios Ψ entered in Row 4. Calculated parameters were then used to calculate the intercept for each simulated Monte Carlo trial following Eqn. (9) in Column Q and the difference ${}^{x}A$ - ${}^{y}A$ for each of the two blends in Columns R and S.

In Step 4, parameters calculated in Step 3 were used to find f_{sample} and the two indices of F_{method} by making use of the 'SOLVER' tool in Microsoft Excel for finding numerical solutions by iterative algorithms. For a given trial/row, this was done by setting I = 0 (Column Q) as the objective and allowed for variation of the sample fractionation index f_{sample} and the two method fractionation indices F_{method} (Columns U, V and W). Their initial values were set to zero and ${}^{x}A$ - ${}^{y}A$ = 0 were used as constraints for both of the blends (Columns R and S). As there were 1,000 rows/Monte

Carlo Simulations, a VBA macro was used to loop the SOLVER until all iterations were completed (see Fig. S-2).

```
Sub SOLVER ()
Worksheets("A").Activate
Range(“U12:W1011").Value = 0
RowCount = 12

Do While Not IsEmpty(Worksheets("A").Range(“B" &
RowCount))
   SolverReset
   SolverOptions precision:=0.00000000001
   SolverOptions AssumeNonNeg:=False
   SolverOk SetCell:=Range(“Q" & RowCount), _
   MaxMinVal:=3, _
   ValueOf:="0", _
   ByChange:=Range(“U" & RowCount & ":W" & RowCount)
   SolverAdd CellRef:=Range(“R" & RowCount), _
      Relation:=2, _
      FormulaText:=0
   SolverAdd CellRef:=Range(“S" & RowCount), _
      Relation:=2, _
      FormulaText:=0

   SolverSolve userFinish:=True
   SolverFinish keepFinal:=1
   RowCount = RowCount + 1

Loop
MsgBox "Processing Over"
End Sub
```

Figure S-2. VBA code for the Macro “SOLVER()” used to loop the 'SOLVER' tool in Microsoft-Excel. For implementation, the letter A in the command 'Worksheets(“A”)' must be replaced with the name of the worksheet which utilizes the macro.

In Step 5, Monte Carlo simulations were summarized by calculating the mean and standard deviation of Columns U, V and W containing the fractionation indices. In accordance with GUM, the standard uncertainty in f_{sample} equals the standard deviation defined by the spread of values of f_{sample} as observed in the M conducted Monte Carlo trials in the simulation. In order to optimize the system, a range of spike compositions and mass ratios Ψ must be tested. To scale up the

described Microsoft Excel procedure we used MATLAB. The MATLAB code was written to allow either for variation of spike composition or mass ratios Ψ while keeping the other constant and is available for download.

PART C: Computation of F_{spike} and f_{sample}

The spreadsheet designed for method optimization can also be used to determine the normalized spike fractionation index F_{spike} as the key deliverable of spike calibration as well as the sample fractionation index f_{sample} as the index describing the degree of natural isotope fractionation of the sample. For actual measurements, measured average isotope ratios of the two blends and their standard deviations can be entered as input variables directly into the spreadsheet as described earlier. However, each measurement cycle or block of cycles of a measurement can also be looked at as an individual, repeated measurement. As such, cycle or block data can replace simulated data in the spreadsheet (Fig. S-1, Columns D, E, G and H). In addition, mass ratios of sample to spike solution Ψ are entered. Eqn. (6) is then used to compute ${}^{x}A$ and ${}^{y}A$ in Columns J to M. For spike calibration, f_{sample} is set to zero as the used "sample" is the reference standard which carries by definition a δ-value of zero. Spike calibration will deliver the normalized fractionation index F_{spike} as the output variable. For sample analysis, the determined value of F_{spike} is used in turn in Eqn. (6) to determine the sample fractionation index f_{sample}.

PART D: Magnesium Isotopic Analysis

Reagents and Solutions

All reagents were of analytical grade or better. Concentrated nitric acid and hydrochloric acid were of analytical grade and were cleaned further by surface distillation in a quartz glass still (SAP-900 IR, AHF Analysentechnik, Tuebingen, Germany). Water was cleaned by reversed osmosis to a minimal resistance of 18 MΩ-cm (Millipore, Merck, Darmstadt Germany). 30% H_2O_2 (Merck) and sub-boiled nitric acid were used for microwave acid digestion. HCl of different wt.%

concentrations as required for Mg separation by ion-exchange chromatography were prepared by diluting the sub-boiled acid with Milli-Q water. Our Mg reference standard was $MgCl_2$ (Titrisol®, Merck) stored in 6% HCl. Dilution of the referencing standard to 20 µg/g was carried out using 0.1 M HCl. Tantalum oxide activator used as an ionization enhancer for Mg isotopic analysis was prepared in batch by hydrolyzing 2.0 g $TaCl_5$ (99.999% purity, Sigma-Aldrich, St. Louis, MO, USA) in 30 mL water, followed by the addition of sub-boiled HNO_3 (20 mL), HF (1.2 mL; Suprapur, Merck) and H_3PO_4 (1.2 mL; Suprapur, Merck) and make-up of the solution to a total volume of 100 mL with water. Preparation of the spike involved isotopically enriched oxides, ^{25}MgO and ^{25}MgO purchased from JLD Instruments (Boulogne, France) and Mg turnings of natural isotopic composition from Alfa Aesar (Ward Hill, MA). The oxides and Mg turnings were dissolved first in 1 ml of 21.9 wt.% HCl and then made up to 50 ml with Milli-Q water, respectively, to give an elemental concentration of approximately 200 µg/g. The Mg isotopic spike composed of 10% ^{24}Mg, 10% ^{25}Mg and 80% ^{26}Mg was prepared by mixing appropriate amounts of the isotopically enriched ^{25}Mg and ^{26}Mg solutions as well as the Mg turnings solution, and then diluted to 20 µg/g for preparation of the blends.

Sample preparation

To measure the δ-value of the urine sample, blends were first weighed out in Teflon cups using a micro-analytical balance (Mettler Toledo XP205DR, Greifensee, Switzerland) to reach the desired mass ratios of spike to sample (approximately Ψ_1 = 0.5 and Ψ_2 = 5.0). The Teflon cup was capped and swirled gently for mixing. Each blend was dried down at 70°C, reconstituted in 1 mL 0.1 M HCl and digested in a microwave oven (Ethos One, Milestone, Sorisole, Italy) using a mixture of 2 mL 30% H_2O_2 and 8 mL sub-boiled HNO_3. Digested contents were dried down, reconstituted in 1 mL 2.17 wt.% HCl and Mg was isolated by ion exchange chromatography (Dowex 50WX8, 200-400 mesh) following the protocol of Lim[5] using commercial Columns (Bio-Rad, Hercules, CA) with a resin volume of ca. 1.2 mL. The resin was conditioned with 3 mL of Milli-Q water, 7 mL of 21.9 wt.% HCl and 2 mL of 2.17 wt.% HCl. The sample was loaded and Na and K were removed using

12 mL of 2.17 wt.% HCl and 4 mL of 2.89 wt.% HCl. Mg was eluted using 4 mL of 2.89 wt.% HCl and 4 mL of 5.00 wt.% HCl. The eluent was dried down and then reconstituted in an appropriate volume of 2.89 wt.% HCl to reach a concentration of 30 µg/µL. Blends of reference and spike did not go through digestion or ion-exchange separation.

Filament preparation and heating procedure

Mounted high purity rhenium filaments (99.999%, 20 x 0.03 x 0.76 mm; H Cross Company, Monnachie, NJ) were washed in dilute nitric acid and out-gassed at 4.5 A for 30 min. Filaments were prepared by spot wise loading of samples and reagents in aqueous solution and dry-down by electro-thermal heating. Evaporation filaments were etched with 0.6 µl of concentrated HNO_3 before sample loading and prepared with an aqueous suspension (1 µL) of the tantalum activator suspension to enhance Mg ionization efficiency. The loaded suspension was dried down, followed by drying down of sample magnesium (30 µg, 1 µL) and then finally with another layer of tantalum activator suspension (1 µL). Solutions/suspensions were dried down at a filament current of 1.2 A. Loaded sample filaments were glowed finally to dull red for 10 - 20 s at about 3 A at atmospheric pressure. Ionization filaments were not loaded.

The ionization filament was heated to 1,500 mA at 200 mA/min followed by the evaporation filament to the same current at the same rate. Next, the ionization filament was heated to a filament current of 1,800 mA at 200 mA/min. Then the ionization and evaporation filaments were first heated simultaneously to 2,600 mA and 2,300 mA at 200 mA/min, respectively, and further to 2,800 and 2,500 mA, respectively, at a reduced rate of 100 mA/min. The ionization filament was finally held at a constant current of 2800 mA and the evaporation filament was heated to approximately 2,750 mA at 50 mA/min until a stable emission of Mg^+ ions could be achieved. Temperatures were between 1,400 and 1,500 °C as indicated by the pyrometer. Data acquisition was started when the ion beam of the least abundant isotope of Mg reached an intensity of at least 1 V.

Isotope ratio measurements

All isotopic analysis was carried out with a thermal ionization mass spectrometer (Triton, Thermofisher Scientific, Bremen, Germany). For mass separation, acceleration voltage for generated ions was 10 kV in the positive ionization mode. Ion intensities were measured using Faraday cups in a multi-collector configuration with $^{24}Mg^{+}$ being deflected into the axial cup. Zoom optics parameters were adjusted for the focus lens (~ -10.5V) and the dispersion lens (11.4 – 12.4V) before each measurement to ensure optimal peak overlap and peak shape. Peak centering was done before each block at a mass tolerance of 1% using the instrument software. Three blocks of 10 cycles each were measured for each sample. Interblock baseline measurements were done by defocusing the source lenses. The ion source vacuum was kept at a pressure of less than 2 x 10^{-7} mbar while the analyzer vacuum was kept at less than 3 x 10^{-9} mbar. Amplifier resistance was 10^{11} Ω and amplifier gain was eliminated by virtual amplifier rotation.

Outlier testing by regression analysis

Measurement of isotope ratios at highest precision and minimization of measurement bias is the basic requirement for measuring of isotope abundance variations using established techniques and even more so in GS-IDA. The initial criterion for accepting a measurement is a coefficient of determination (r^2) value of > 0.999 when plotting measured $^{25}Mg/^{24}Mg$ and $^{26}Mg/^{24}Mg$ isotope ratios after logarithmic transformation (three-isotope-plot). For identification of outliers, we applied the robust simple regression technique[6] described below. Residuals larger than the measurement precision are considered indicative of a measurement offset.

Isotope ratios ($^{x}R_m$ and $^{y}R_m$) of a measurement are correlated as they share a common reference isotope (^{24}Mg in the presented study) and isotope fractionation is dependent on the isotopes'

masses. When plotting correlated data in a two dimensional space as in a three-isotope-plot, the slope b_{ij} of a line connecting a pair of data points (x_i, y_i) and (x_j, y_j) is given by Eqn. (S-21)

$$b_{ij} = \frac{y_j - y_i}{x_j - x_i} \tag{S-21}$$

For a total number of *n* cycles per Mg isotope ratio measurement, the total number of data pairs that can be connected in a three-isotope plot is *n(n-1)*, counting b_{ij} and b_{ji} as different combinations. For a measurement in which isotope ratios are measured sequentially 30 times, this translates to 870 (=29x30) data pairs. At the first stage, the median *med* of the slopes of the *n-1* lines that pass through a given point (x_i,y_i) is calculated, followed by calculation of the median of the slope medians as calculated for all *n* datapoints. As a result, the regression slope b_{reg} is obtained as

$$b_{reg} = med_i \left[med_{j \neq i} (b_{ij}) \right] \tag{S-22}$$

To find the intercept of the regression line for all data pairs a_{reg}, we calculate first for each data point y_i the intercept a_i

$$a_i = y_i - b_{reg} \tag{S-23}$$

and then determine

$$a_{reg} = med_i (a_i) . \tag{S-24}$$

The regression line for all data can then be described by

$$y_{reg}(x) = b_{reg}(x) + a_{reg} \tag{S-25}$$

which permits us to calculate the residual *Res* for a given data point (x_i, y_i) as the difference between its measured value and its value according to the regression line

$$\mathrm{Re}\, s(x_i, y_i) = y_i - y_{reg}(x_i) \tag{S-26}$$

As compared to a least square regression line, a robust regression line will tend to produce more residuals of small magnitude, more large residuals and fewer medium sized residuals. For a typical Mg isotope ratio measurement, the majority of the residuals are of the order of 10^{-5} to 10^{-}

[6]. Since the relative standard deviation of our TIMS technique for multiple independent Mg isotope ratio measurements was determined at 0.0018% ($^{26}Mg/^{24}Mg$, 1 SD after internal normalization), we decided to eliminate data points which have residuals > 10^{-4} when plotting logarithmically transformed isotope ratios against each other. We used Microsoft Excel to facilitate our calculations. A copy of the worksheet is available for download.

PART E: Magnesium Isotope Ratio Measurements

Measured isotope ratios of the used reference standard (n = 7; Mg Titrisol Merck), the urine sample (n = 5) and the used Mg isotopic spike (n = 5) are shown in Table S-1. The external RSD of normalized $^{26}Mg/^{24}Mg$ isotope ratios for a urine sample (0.0044%, 1 SD) is about twice that of the reference standard (0.0018%) which is not unexpected as standards can be analyzed more precisely than samples in TIMS. Calculated δ-values for the reference standard and the human urine sample as determined in five fully independent analytical runs are shown in Table S-2. For each analytical run, two blends of spike and sample were prepared and analyzed with mass ratios of spike to standard of approximately 0.5 (Ψ_1) and 5.0 (Ψ_2). Calculation of δ-values was based on un-normalized, average Mg isotope ratios for the reference standard ($^{25/24}\overline{R}_{ref,m}$, $^{26/24}\overline{R}_{ref,m}$) and the spike ($^{25/24}\overline{R}_{spike,m}$, $^{26/24}\overline{R}_{spike,m}$) presented in Table S-1.

Table S-1. Measured isotope ratios of $^{25}Mg/^{24}Mg$ and $^{26}Mg/^{24}Mg$ for the used reference standard (Titrisol, Merck), the analyzed human urine and the used Mg isotopic spike. Measured $^{25}Mg/^{24}Mg$ isotope ratios were normalized to the $^{26}Mg/^{24}Mg$ ratio reported by Catanzarro[4] and vice versa. Measured isotope ratios of the spike were not subjected to internal normalization. Standard deviations (1 SD) in the last two digits of a measurement are reported.

		Unnormalized data		**Normalized data**	
	Run	$^{25}Mg/^{24}Mg$	$^{26}Mg/^{24}Mg$	$^{25}Mg/^{24}Mg$	$^{26}Mg/^{24}Mg$
Reference standard	1	0.12629 ± 24	0.13870 ± 53	0.1265769 ± 11	0.1394343 ± 23
	2	0.12660 ± 31	0.13937 ± 68	0.1265751 ± 30	0.1394383 ± 65
	3	0.12626 ± 24	0.13864 ± 51	0.1265745 ± 25	0.1394395 ± 54
	4	0.12654 ± 33	0.13924 ± 71	0.1265757 ± 22	0.1394370 ± 48
	5	0.12656 ± 32	0.13929 ± 69	0.1265749 ± 22	0.1394386 ± 48
	6	0.12687 ± 24	0.13995 ± 52	0.1265777 ± 23	0.1394326 ± 49
	7	0.12658 ± 21	0.13934 ± 46	0.1265761 ± 19	0.1394362 ± 41
Average		0.12653 ± 21	0.13922 ± 44	0.1265759 ± 12	0.1394366 ± 25
RSD (%)		*0.16*	*0.32*	*0.00091*	*0.0018*
Human Urine	1	0.12641 ± 20	0.13894 ± 43	0.1265857 ± 29	0.1394155 ± 62
	2	0.12672 ± 20	0.13961 ± 43	0.1265829 ± 29	0.1394214 ± 62
	3	0.12680 ± 38	0.13978 ± 82	0.1265840 ± 27	0.1394192 ± 58
	4	0.12673 ± 53	0.1396 ± 11	0.1265846 ± 14	0.1394179 ± 30
	5	0.12736 ± 96	0.1410 ± 21	0.1265784 ± 42	0.1394312 ± 89
Average		0.12680 ± 34	0.13979 ± 75	0.1265831 ± 28	0.1394210 ± 61
RSD (%)		*0.27*	*0.54*	*0.0022*	*0.0044*

Table S-1 (continued)

		Unnormalized data	
	Run	$^{25}Mg/^{24}Mg$	$^{26}Mg/^{24}Mg$
Spike	1	1.0177 ± 29	8.577 ± 47
	2	1.0124 ± 18	8.488 ± 30
	3	1.0233 ± 38	8.669 ± 64
	4	1.0132 ± 24	8.503 ± 40
	5	1.0199 ± 34	8.613 ± 56
Average		1.0173 ± 46	8.570 ± 76
RSD (%)		*0.45*	*0.88*

Table S-2. $\delta^{26}Mg$ (‰) of reference standard and urine sample as determined using the GS-IDA approach. Each line represents an independent analysis consisting of isotope ratio measurements of two blends with a mass ratio of spike to reference or spike to sample of approximately Ψ_1 = 0.5 and Ψ_2 = 5.0, respectively.

	Analysis	$\delta(^{26}Mg)$ ± 1 SD (‰)
Reference Standard	1	0.15 ± 0.18
	2	-0.08 ± 0.17
	3	0.09 ± 0.15
	4	0.00 ± 0.20
	5	-0.16 ± 0.15
Average		0.00 ± 0.12
Urine Sample	1	1.47 ± 0.12
	2	1.26 ± 0.10
	3	1.31 ± 0.12
	4	1.31 ± 0.13
	5	1.46 ± 0.10
Average		1.36 ± 0.10

REFERENCES

1. *International vocabulary of metrology — Basic and general concepts and associated terms (VIM)*. Joint Committee for Guides in Metrology: 2008.
2. *Guide to the Expression of Uncertainty in Measurement*. Joint Committee for Guides in Metrology: 1995.
3. Chew, G.; Walczyk, T., *Anal. Bioanal. Chem.* **2012**, 1-7.
4. Catanzaro, E. J.; Murphy, T. J.; Garner, E. L.; Shields, W. R., *J. Res. Nat. Bur. Stand* **1966**, 453-458.
5. Lim, C. Separation of Magnesium from Urine for Isotope Ratio Analysis. Honours Thesis, National University of Singapore, April 2011.
6. Iglewicz, B.; Hoaglin, D. C., *How to detect and handle outliers*. ASQC Quality Press: Milwaukee, WI, 1993.

MANUSCRIPT 3

Age-dependent Differences in the Natural Isotope Composition of Magnesium in Human Urine

(To be submitted for publication)

Gina Chew[1], Boon Wee Teo[2], Priscilla How[3], Thomas Walczyk[1,4,5*]

[1]NUS Graduate School for Integrative Sciences and Engineering,
National University of Singapore (NUS)

[2]Department of Medicine, Yong Loo Lin School of Medicine (NUS)

[3]Department of Pharmacy, Faculty of Science (NUS)

[4]NutriTrace@NUS, Department of Chemistry, Faculty of Science (NUS),

[5]Department of Biochemistry, Yong Loo Lin School of Medicine (NUS)

*corresponding author: NutriTrace@NUS
Department of Chemistry
National University of Singapore (NUS)
Science Drive 4
Singapore 117543

walczyk@nus.edu.sg

ABSTRACT

In a recent study we found that magnesium (Mg) in human urine is enriched in heavier Mg isotopes. Based on the hypothesis that the Mg isotope effect in urine is determined by preferential reabsorption of lighter Mg isotopes in the kidneys and kidney function is known to decline with age, we investigated if the Mg isotope composition of urine differs between apparently healthy, younger (n = 11) and older males (n = 9) of Chinese descent. Subjects were given a standardized meal for dinner. Urine was collected until the next day morning and a venous blood sample was obtained. Urine and serum were analysed for a range of kidney related parameters. The Mg isotope effect $\delta^{26}Mg$ in urine was measured by gravimetric spiking - isotope dilution analysis (GS-IDA). As hypothesized, we found $\delta^{26}Mg$ in urine to be negatively correlated with age (p = 0.038) but also positively correlated with serum albumin (p = 0.004) and positively correlated with serum (Ca) (p = 0.044) Correlations with estimated glomerular filtration rate (eGFR) nearly reached statistical significance (p = 0.052). With eGFR being an indicator of kidney function declining with age and supposedly with efficiency of renal reabsorption, $\delta^{26}Mg$ is expected to be less positive or isotopically lighter in elderly subjects, which we have observed in our study. Unexpectedly strong correlations between serum albumin concentration and $\delta^{26}Mg$ in urine point to an isotope effect induced by binding of Mg with albumin in serum. If confirmed, the difference in Mg isotopic composition between the ultrafilterable Mg fraction in serum and urinary Mg can serve as a novel marker of renal reabsorption efficiency and, thus, kidney function. Renal reabsorption efficiency is a more sensitive indicator for a decline in kidney function than eGFR but is rarely employed due to the invasiveness of current tests.

INTRODUCTION

Natural magnesium (Mg) is a blend of its three stable isotopes (^{24}Mg, ^{25}Mg and ^{26}Mg). Their mixing proportions, however, are not constants of nature. Transport processes can alter isotope abundances in proportion to the fraction of element transferred if transport rates differ between isotopes due to their different physical masses[1]. Isotope fractionation may occur either through physical transfer of matter from one compartment to another, e.g. passive nutrient absorption through interstitial spaces in the intestine, or in chemical reactions at the moment that the element is transferred or converted from one element species into another. Small variations in the iron isotope composition of blood, as an example, are governed by the efficiency by which iron is absorbed from diet and distributed between organs and tissues within the body and were found to be associated with iron status[2-4].

In a recent survey we found that Mg in urine differs in isotope composition from Mg of non-biological origin[5]. Urinary Mg was found to be enriched in the heavier Mg isotopes and represents the isotopically heaviest form of Mg in nature that has been described so far. While iron homeostasis is maintained exclusively by tight regulation of iron absorption in the gut, Mg homeostasis is maintained primarily by the kidneys by controlling the rate at which Mg is reabsorbed from the glomerular filtrate before excretion[6]. Element uptake by the body appears to favor the lighter isotopes, in general[4, 7]. Preferred uptake of lighter Mg isotopes from the glomerular filtrate in the course of reabsorption would leave more of the heavier Mg isotope behind for excretion, which we have observed. A similar observation has been made for calcium (Ca) for which body homeostasis is also maintained by regulating renal reabsorption[7-10].

As a first step to explore regularities that determine the Mg isotopic composition of urine that may ultimately lead to its use as a biomarker we tried to assess if Mg isotope signatures are age dependent. Fractionation theory dictates that the magnitude of an isotope effect induced by reabsorption of ultrafilterable Mg in the proximal convoluted tubule, thick ascending loop of Henle

and the distal convoluted tubule of the kidneys must be proportional to the efficiency of reabsorption. Ageing is associated with a decline in kidney function and higher urinary losses of Mg[11-12]. For testing our hypothesis that Mg isotope effects in urine are age-dependent, we have administered a standardized meal to young and elderly healthy adult males and measured the Mg isotopic composition of their urine following its intake along with common biomarkers of Mg metabolism and kidney function.

MATERIAL AND METHODS

Study design

A total of 20 healthy Chinese males from 24 to 69 years old were recruited for the study. Subjects were without diagnosed medical conditions that have a relevant impact on kidney function (e.g. hypertension, cardiovascular disease, liver disease, gastrointestinal disorders, osteoporosis or diabetes), without conditions that may potentially interfere with the accuracy of glomerular filtration rate (GFR) measurement (e.g. amputations, edema, pleural effusion, ascites, overly muscular or skinny appearance) and without regular intake of medication or supplements containing Ca, vitamin D and Mg over the past 4 months. Their urine samples were screened negative for microalbuminuria, proteins, red blood cells and white blood cells using reagent strips tested for at least 2 out of 3 occasions, thus indicating normal kidney function.

Participants were given a standardized meal consisting of ready-to-eat fried rice (Yamie Rice, Gan Hup Lee Pte Ltd, Singapore), cream crackers (Jacob's, United Biscuits, UK) and bottled 750 ml water (Ice Mountain, McFine Foods, Singapore) for dinner. All foods were from the same manufacturing batch. Participants were asked to empty their bladder before consuming the standardized meal at home in the evening before urine collection. The meal and all water had to be consumed completely before going to bed. No further drinks, meals or medication was permitted until completion of urine

and blood sampling in the morning of the following day. Subjects were asked to collect all urine in the provided urine bottle after meal intake including the first morning void on the following day. Participants were asked to record the time on the instruction sheet when they emptied their bladder, when they consumed the standardized meal, when they finished consuming all the bottled water and when they collected their urine starting from the time they finished the meal until their first morning void. Venous blood samples were obtained from each subject and the volume of the collected urine determined on the following day. All subjects provided written informed consent before being enrolled in the study, approved by the Domain Specific Review Board (DSRB) of the National Healthcare Group, Singapore.

Sample Analysis

To determine if subjects were eligible for this study, screening of spot-urine samples for microalbuminuria was carried out on an automated analyser (CLINITEK STATUS, Bayer Healthcare, U.S.); screening of urine for proteins, red blood cells and white blood cells was carried out using a dipstick test (Combur® test, Roche, Switzerland). For the study proper, aliquots of collected urine and blood were analyzed at the Laboratory of Clinical Medicine at the National University Hospital (NUH) Singapore. Urine samples were analyzed for albumin and creatinine by colorimetric techniques and for sodium and potassium by potentiometric measurements using a fully automated analyzer (ADVIA 2400, Siemens Healthcare Group, US). Venous blood samples were allowed to clot and centrifuged at 4°C to obtain serum portions. Serum was analyzed using standard automated procedures for albumin, creatinine, phosphate, Ca and Mg by colorimetry (ADVIA 2400), for sodium and potassium by potentiometry (ADVIA 2400), for 25-hydroxy-vitamin-D by electrochemiluminescence (COBAS e411, Roche Diagnostics, Switzerland) and for intact parathyroid hormone (iPTH) by chemiluminescence in chilled blood samples kept on ice (ADVIA Centaur, Siemens Healthcare Group, US). Urinary Mg concentrations and Mg isotopic composition of urine were

determined by Thermal Ionization Mass Spectrometry (TIMS) and Gravimetric Spiking-Isotope Dilution Analysis (GS-IDA) technique[5] at NutriTrace@NUS at the National University of Singapore (NUS).

Sample preparation for isotope ratio mass spectrometry

Samples were prepared for isotopic analysis in class 10 metal free fumehoods in a class 10,000 clean-room. All reagents were of analytical grade or better. Concentrated nitric acid and hydrochloric acid were of analytical grade (Merck, Darmstadt, Germany) and were cleaned further by surface distillation in a quartz glass still (SAP-900 IR, AHF Analysentechnik, Tuebingen, Germany). Water was cleaned by reversed osmosis to a minimal resistance of 18 MΩ-cm (Millipore, Merck, Darmstadt Germany). Only acid washed plastic or teflon containers/labware was used.

The isotopically enriched spike for GS-IDA analysis was prepared from ^{25}MgO and ^{26}MgO (Chemgas, Boulogne, France) and Mg turnings of natural isotopic composition (99.98% purity; Alfa Aesar, Ward Hill, MA). Optimal spike composition (10% ^{24}Mg, 10% ^{25}Mg and 80% ^{26}Mg) and procedures for spike preparation and calibration have been described previously[5].

Urine samples were homogenized by shaking and pouring urine bottle content into a plastic container and stirring of the urine with a 50 mm bar magnet at 500 rpm for at least 3 minutes before sampling. Flame Atomic Absorption Spectroscopy (Agilent, Santa Clara, CA, USA) was used to determine urinary Mg concentration and samples were diluted with water (if necessary) to approximately 20 µg Mg/g to match the Mg concentration of the spike solution. For Mg isotopic analysis by GS-IDA, two different blends of urine and spike at a desired mass ratio of spike to sample solution of approximately 0.5 and 5.0 were prepared gravimetrically using a micro-analytical balance (> 0.5 g per weighing aliquot at a measurement uncertainty of 0.0005 g (k=1); Mettler Toledo XP205DR, Greifensee, Switzerland). Blends were dried down at 70°C after mixing and the content

was pre-digested using 8 mL conc. HNO_3. The pre-digested content was transferred to a Teflon vessel, followed by the addition of 2 mL 30% H_2O_2 for microwave digestion (Ethos One, Milestone, Sorisole, Italy). Contents were transferred to a teflon container. Samples were digested further using aqua regia (0.75 ml conc. HCl and 0.25 ml conc HNO_3; 70°C) if the dried down contents appeared yellow instead of white.

The digested content was reconstituted in 1 mL 0.7 M HCl and Mg was isolated by ion exchange chromatography (Dowex 50WX8, 200-400 mesh) following the protocol of Lim[13] using commercial columns (Bio-Rad, Hercules, CA) with a resin volume of ca. 1.2 mL. The resin was conditioned with 3 mL of Milli-Q water, 7 mL of 7.1 M HCl and 2 mL of 0.7 M HCl. The sample was loaded and Na and K were removed using 12 mL of 0.7 M HCl and 8 mL of 0.9 M HCl. Mg was eluted using 4 mL of 1.6 M HCl. The eluent was dried down and then reconstituted in 0.9 M HCl to reach a concentration of 30 µg/µL for TIMS analysis.

Magnesium isotopic analysis

All isotopic analysis was carried out with a thermal ionization mass spectrometer (Triton, Thermofisher Scientific, Bremen, Germany). Measurement procedures have been described elsewhere in detail[5]. In brief, sample Mg (30 µg Mg, 1 µL) was sandwiched between two layers of TaO activator loaded onto the surface of etched rhenium filaments. Evaporation filaments were prepared by spot wise loading of samples and reagents in aqueous solution and dry-down by electro-thermal heating. Ionization filaments were not loaded. To generate ions for measurement, the ionization filament was heated to 1,500 mA, followed by the evaporation filament, both at a constant rate of 200 mA/min. The ionization and evaporation filaments were then heated stepwise at 100 mA/min until an ion current was detected. Lenses were optimized to obtain a steady signal.

Three blocks of ten cycles each were measured and inter-block baseline was measured for baseline correction.

Measurements were repeated, in general, if they did not fulfil the following criteria: (1) ion signal intensity of the least abundant Mg isotope ≥ 1 V; (2) variations in ion signal intensity within a measurement ≤ 10% RSD; and (3) coefficient of determination (r^2) for the correlation between logarithmically transformed ratios of $^{25}Mg/^{24}Mg$ and $^{26}Mg/^{24}Mg$ (three-isotope plot) ≥ 0.999 for a single measurement. Measured data was subjected to robust outlier testing as stated earlier[5].

Data Reduction and Analysis

Mg isotope ratios of the analyzed urine samples are expressed on a δ-scale as the relative difference in the $^{26}Mg/^{24}Mg$ isotope abundance ratio in the sample relative to its ratio in a reference standard.

$$\delta^{26}Mg = \frac{\left(\frac{^{26}Mg}{^{24}Mg}\right)_{sample}}{\left(\frac{^{26}Mg}{^{24}Mg}\right)_{ref}} - 1 = M^{\,f_{sample}} - 1 \qquad (1)$$

with M as the ratio of the ^{26}Mg to ^{24}Mg nuclides' masses and f_{sample} as the sample fractionation index. Relative differences are reported in parts per thousand (‰) after multiplying calculated δ-values with a factor of 1,000. Ideally, the reference standard for reporting δ-values is an isotopically homogenous material that has been certified for absolute isotope composition to ensure data comparability over space and time and that is freely available. Because of a lack of such a material for Mg, IUPAC has recommended recently DSM-3, an uncertified aqueous Mg standard solution kept at the University of Cambridge (UK), as the anchor point of the δ-scale carrying a δ-value of zero absolute[14]. Because of restrictions in accessing this material, we measured urinary Mg isotope ratios

in our study against a commercial aqueous Mg standard (Titrisol®, Merck, Germany) which we calibrated against an aliquot of DSM-3 kindly provided by Chen-Feng You at the National Cheng Kung University, Tainan, Taiwan. The used in-house Mg standard yielded a $\delta^{26}Mg$ value of 1.59 ± 0.10 ‰ (n = 5) relative to DSM-3 which was used in the following to convert $\delta^{26}Mg$ values for reporting of measured Mg isotope ratios relative to DSM-3.

Measured $^{25}Mg/^{24}Mg$ and $^{26}Mg/^{24}Mg$ ratios do not reflect the true Mg isotope ratios of the sample as they may have been shifted by isotope fractionation during sample preparation or mass spectrometric analysis. The sample fractionation index, f_{sample} as the parameter of interest (see Eqn. 1) was determined from the measured Mg isotope ratios and the mass ratios of sample and spike solution of the two blends using spreadsheet software[5]. The GS-IDA method is based on the principle that calculated molar ratios of spike to sample must be the same using either the $^{25}Mg/^{24}Mg$ or the $^{26}Mg/^{24}Mg$ isotope ratio in the absence of a methodological isotope fraction effect (f_{sample} =0) and that spike-to-sample ratios must plot on a straight line passing through the origin when plotted against the mass ratio of spike to sample solution in the blends. The value of f_{sample} for each sample and thus its δ-value was calculated from the measured isotope ratios of each individual scan (n>30 per measurement) and given as their arithmetic mean with its standard deviation.

RESULTS

Subject characteristics

Recruited subjects were of a wide age range, from 24 to 69 years old with an eGFR range from 77 to 119 ml/min/1.73m^2. Anthropometric measurements such as blood pressure, Waist-to-Hip Ratio (WHR), Body Mass index (BMI), as well as serum and urine measurements are summarized in Table 1. Urinary sodium, potassium and Mg concentrations were normalized to urinary creatinine concentration U_{Cr} to control for variations in urine volume and reported as normalized urinary

sodium ($U_{Na,norm}$), potassium ($U_{K,norm}$) and Mg ($U_{Mg,norm}$). The Mg isotope fractionation effect in urine, reported as $\delta^{26}Mg$ ranged from -0.93 to 0.46 ‰ relative to DSM-3 as the referencing standard. Repeatability of $\delta^{26}Mg$ measurements was of the order of ±0.10 ‰ (1 SD) for independent analysis of the same sample.

Mann-Whitney U test was used to compare the differences between the younger (<42 years old) and older subjects (>52 years old). The younger subjects were significantly different from the older subjects in terms of systolic blood pressure $(S.BP)$, serum albumin (S_{Alb}), serum Mg (S_{Mg}), serum phosphate (S_{PO4}), normalized urinary potassium ($U_{K,norm}$) and normalized urinary Mg ($U_{Mg,norm}$) at $p < 0.05$ (2-sided). They were highly significantly different in terms of age, eGFR, urine volume (U_{vol}) and urine creatinine concentration (U_{Cr}) ($p < 0.01$, 2-sided), see Table 1.

Table 1. Characteristics of all subjects and grouped by age (<42 years for younger subjects and > 52 years for older subjects). Parameters are given as arithmetic means (± SD) with the range in brackets.

Parameter	All subjects	Younger subjects	Older subjects
No. of subjects, *n*	20	11	9
Age (years) ††	46 ± 17 (24 – 69)	32.2 ± 7.0 (24 – 42)	62.7 ± 6.0 (52 - 69)
Systolic Blood pressure (mmHg), $S.BP$†	122 ± 13 (108 – 153)	117 ± 10 (108 – 138)	128 ± 13 (113 – 153)
Diastolic Blood pressure (mmHg), $D.BP$	72.0 ± 7.0 (60 – 84)	70.0 ± 6.4 (60 – 80)	74.2 ± 7.0 (66 – 84)
Waist-to-Hip Ratio	0.881 ± 0.042 (0.806 – 0.940)	0.866 ± 0.043 (0.806 – 0.932)	0.900 ± 0.035 (0.837 – 0.940)
Body Mass Index (kg/m^2)	23.5 ± 3.0 (18.0 – 28.0)	22.4 ± 3.0 (18.0 – 27.0)	25.0 ± 2.5 (21.0 – 28.0)
eGFR (mL/min/1.73m^2)* ††	101 ± 10 (77 - 119)	108.7 ± 5.4 (100 – 119)	92.1 ± 7.4 (77 - 102)
Serum measurements			
Creatinine (µmol/L), S_{Cr}	77.9 ± 8.9 (63 – 92)	80.6 ± 7.9 (66 – 91)	74.7 ± 9.4 (63 – 92)
Albumin (g/L), S_{Alb}†	45.5 ± 2.2 (42- 50)	46.6 ± 2.0 (44 – 50)	44.1 ± 1.5 (42 – 47)
Sodium (mmol/L), S_{Na}	141.3 ± 1.4 (138 - 144)	141.6 ± 1.4 (140 – 144)	141.0 ± 1.4 (138 – 143)
Potassium (mmol/L), S_K	4.25 ± 0.27 (3.7 – 4.8)	4.25 ± 0.31 (3.7 – 4.8)	4.23 ± 0.22 (3.9 – 4.6)
Magnesium (mmol/L), S_{Mg}†	0.913 ± 0.061 (0.79 – 1.00)	0.886 ± 0.059 (0.79 – 0.95)	0.944 ± 0.048 (0.86 – 1.00)
Calcium (mmol/L), S_{Ca}	2.338 ± 0.082 (2.21 – 2.54)	2.366 ± 0.090 (2.21 – 2.54)	2.302 ± 0.057 (2.22 – 2.38)
Phosphate (mmol/L), S_{PO4}†	1.10 ± 0.14 (0.85 – 1.32)	1.16 ± 0.13 (0.87 – 1.32)	1.03 ± 0.11 (0.85 – 1.19)
Intact parathyroid hormone (pmol/L), S_{iPTH}	3.9 ± 1.4 (2.2 – 7.9)	3.53 ± 0.88 (2.2 – 4.6)	4.4 ± 1.7 (2.3 – 7.9)
25-hydroxy Vitamin D (µg/L), S_{VitD}	23.3 ± 9.3 (11.9 – 45.2)	19.7 ± 7.8 (11.9 – 34.9)	27.6 ± 9.5 (13.1 – 45.2)
Urine measurements			
Urine volume (ml), U_{vol}††	880 ± 300 (300 - 1425)	720 ± 280 (300 – 1200)	1075 ± 200 (875 – 1425)

Table 1 (continued)

Parameter	All subjects	Younger subjects	Older subjects
Urine measurements			
Creatinine concentration †† (mmol/L), U_{Cr}	7.1 ± 2.9 (3.8 – 13.9)	8.7 ± 2.8 (4.7 – 13.9)	5.0 ± 1.2 (3.8 – 7.1)
Total urinary sodium (mmol), $U_{Na,total}$	46 ± 20 (11.4 – 79.8)	43 ± 22 (11.4 – 78.6)	49 ± 17 (31.5 – 79.8)
Normalized urinary sodium, $U_{Na,norm}$	8.1 ± 3.0 (3.4 – 13.7)	7.0 ± 2.5 (3.4 – 11.1)	9.5 ± 3.1 (5.2 – 13.7)
Total urinary potassium (mmol), $U_{K,total}$	14.3 ± 5.1 (7.1 – 23.1)	13.0 ± 5.4 (7.1 – 21.5)	15.9 ± 4.3 (9.9 – 23.1)
Normalized urinary potassium, $U_{K,norm}$†	2.60 ± 0.81 (1.49 – 4.23)	2.24 ± 0.68 (1.49 – 3.51)	3.04 ± 0.76 (1.96 – 4.23)
Total urinary magnesium (mmol), $U_{Mg,total}$	1.45 ± 0.61 (0.35 – 2.88)	1.27 ± 0.55 (0.35 – 2.27)	1.66 ± 0.64 (0.59 – 2.88)
Normalized urinary magnesium, $U_{Mg,norm}$†	0.255 ± 0.085 (0.15 – 0.42)	0.212 ± 0.055 (0.15 – 0.32)	0.309 ± 0.086 (0.17 – 0.42)
$\delta^{26}Mg$ in urine (‰)	-0.11 ± 0.35 (-0.93 – 0.46)	0.01 ± 0.27 (-0.45 – 0.46)	-0.25 ± 0.40 (-0.93 – 0.22)

* eGFR was calculated using the CKD-EPI equation for Chinese males[15] ($S_{Cr} \leq 80$ µmol/L: eGFR = 141 x $(S_{Cr}/80)^{-0.411}$ x $(0.993)^{Age}$; $S_{Cr} > 80$ µmol/L: eGFR = 141 x $(S_{Cr}/80)^{-1.209}$ x $(0.993)^{Age}$)

†,†† statistical significant difference between the younger and older subjects based on 2-sided Mann-Whitney U test: †p-value < 0.05,††p-value < 0.01

Correlation analysis

Spearman rank correlation analysis was used to examine the relationship among all the measured parameters. Spearman rank correlation test was given preference over Pearson correlation test because of the relatively small number of subjects in the study (n < 30). There were several correlations between variables that were significant at p < 0.05 (2-sided). We observed three major clusters of correlations related to age, serum albumin and eGFR as shown in Fig. 1. Correlations are tabulated in the Appendix Table A1. Serum sodium, serum potassium and serum iPTH concentrations are not shown in Fig. 1 because they are not found to be correlated with any parameter.

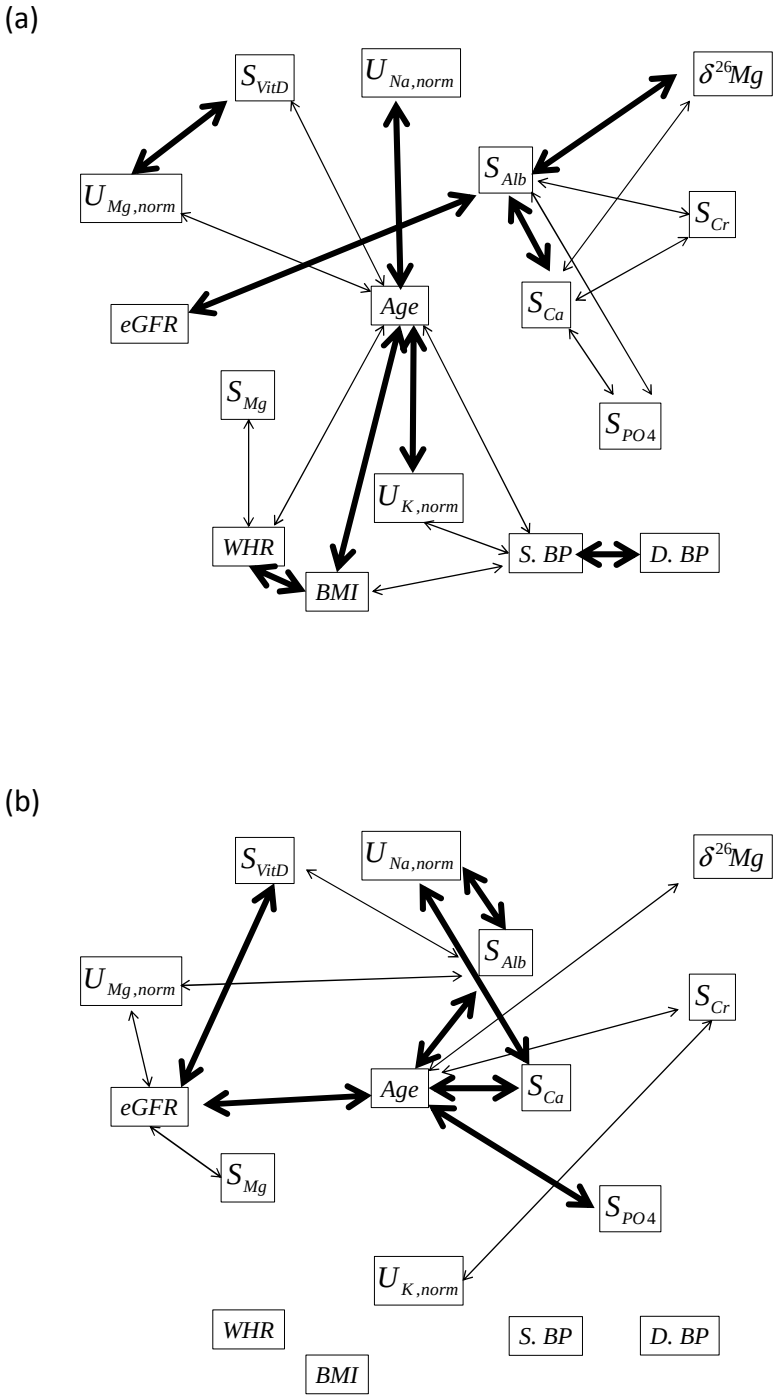

Figure 1. Spearman rank correlations between age, anthropometric measurements, measured parameters related to kidney function and $\delta^{26}Mg$ in urine that are (a) positively correlated and (b) negatively correlated. Bold arrows refer to statistically significant correlations at $p < 0.01$ (2-sided). Normal arrows refer to statistical significance at $p < 0.05$ (2-sided). Refer to Table 1 for the list of abbreviations.

The negative correlation between $\delta^{26}Mg$ in urine and age (ρ = -0.47, p = 0.038) for all 20 subjects shown in Fig. 2(a) confirmed our hypothesis that the Mg isotope composition of urine is age-dependent. However, age is not the most highly correlated variable with $\delta^{26}Mg$ in urine. Instead, it was found that $\delta^{26}Mg$ in urine was highly significantly correlated with serum albumin concentration (ρ = 0.62, p =0.004), see Fig. 2(b). Mg isotopic composition of urine was also found to be correlated with serum Ca concentration (ρ = 0.46, p = 0.044), see Fig. 2(c). The correlation between $\delta^{26}Mg$ in urine and eGFR was marginally significant (ρ = 0.37, p = 0.052), see Fig. 2(d) using a one-sided test based on the hypothesis that a stronger kidney function (higher eGFR value) will result in urine that is enriched in the heavier ^{26}Mg isotope based on our earlier observations[5].

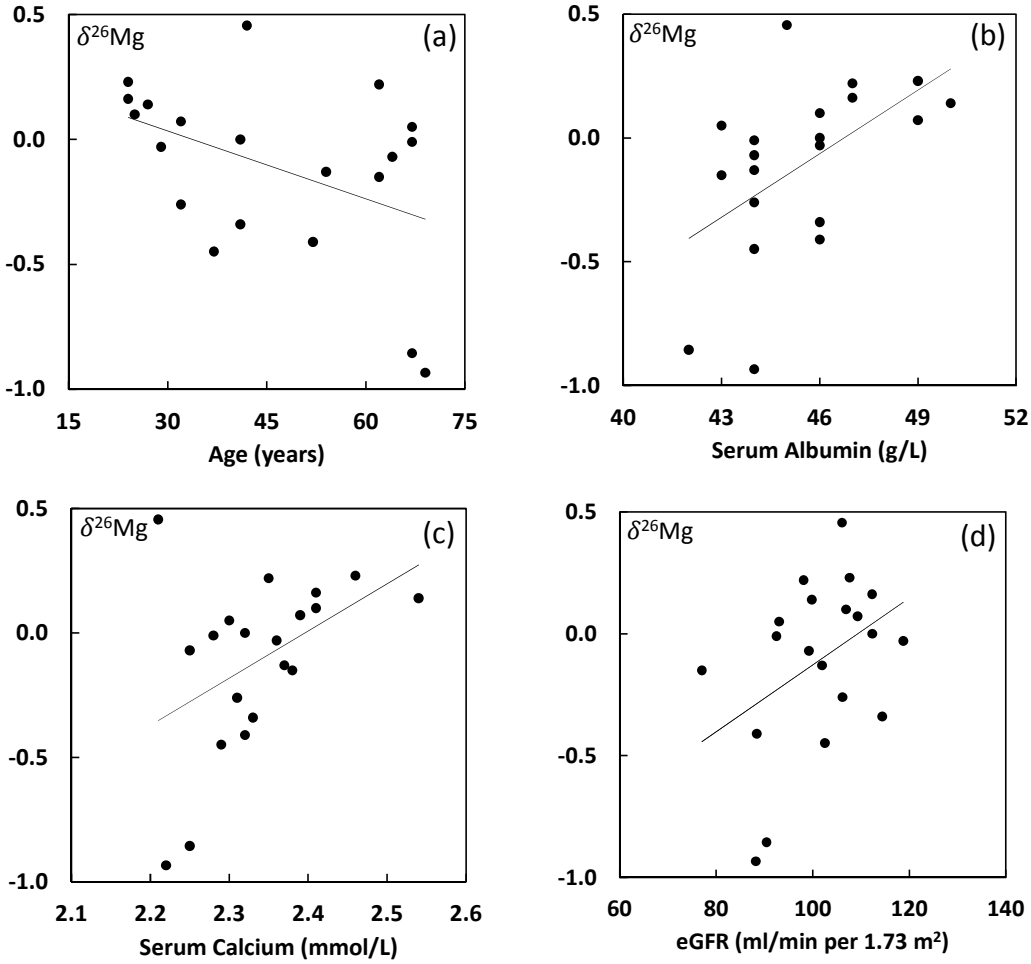

Figure 2. Statistically significant correlations of $\delta^{26}Mg$ in urine with age (p=0.038; Fig. 2a), serum albumin concentration (p=0.004; Fig. 2b), serum Ca concentration (p= 0.044; Fig. 2c) and eGFR (p= 0.052; Fig. 2d). Each symbol (●) represents an individual subject.

DISCUSSION

Mg in human urine was found to be among the isotopically heaviest forms of Mg in nature that have been described until now in the literature (see Fig. 3). Samples from the hydrosphere and geosphere are mostly isotopically lighter than DSM-3, i.e they contain proportionally more ^{24}Mg and ^{25}Mg than ^{26}Mg. In the biosphere, plant roots are isotopically heavy as there is a preferential uptake of the lighter isotopes during absorption by the plant. With chlorophyll from leafy vegetables being a major Mg source in the human diet , urinary Mg appear to be isotopically heavier than dietary Mg, although data for food sources (biosphere and hydrosphere), are still limited.

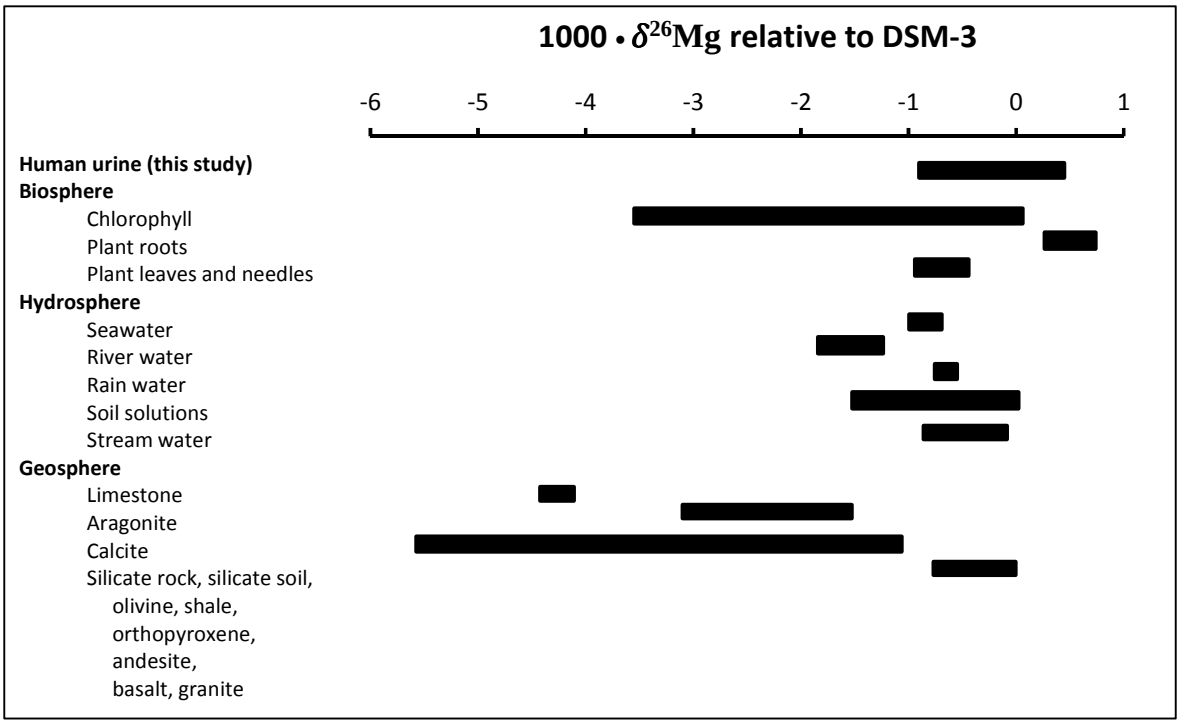

Figure 3. Mg isotopic composition of samples in the biosphere[16-19], hydrosphere[19-23] and geosphere[21, 24-29].

Our hypothesis that Mg isotope composition of urine is age-dependent has been confirmed and we found indications through a weak correlation with eGFR ($p = 0.052$) that this might be due to a decline in kidney function which was also found to be strongly correlated with age ($p < 0.001$). Decline in kidney function as estimated via eGFR with age is well documented[30-31]. Correlations for other parameters related or unrelated to kidney function in our study follow common observations

reported in the literature, e.g. BMI, WHR and systolic blood pressure are known to be correlated with age[32]. Increased normalized urinary losses of Na, K and Mg with age have also been reported[11, 33]. The declines in serum Ca and serum phosphate have also been observed with age[34].

Correlations between $\delta^{26}Mg$ and eGFR were rather weak for kidney function as a major determinant of the isotope composition of urine as our initial hypothesis. To some extent, this might be due to inherent limitations of assessing kidney function using eGFR. GFR is a sum of the filtration rates of all functioning nephrons. Physicians rely on GFR to determine the onset and severity of kidney disease. GFR is most accurately estimated when measured directly via urinary clearance of intravenously administered exogenous substances, e.g. inulin or radiolabeled markers such as ^{125}I-iothalamate. A much less invasive, indirect measure of GFR is to estimate it from serum creatinine as an endogenous marker using empirically derived equations. The CKD-EPI equation[15] is now widely used for eGFR calculation as in our study. The use of serum creatinine, however, has its limitations because it is affected by non-GFR determinants such as muscle mass and meat ingestion, and is secreted at variable rates in different individuals[35]. Furthermore, eGFR is only a proxy for glomerular function but not for kidney function in general which involves both glomerular filtration and tubular reabsorption.

The observed Mg isotope effect in urine is unlikely to be associated directly with glomerular filtration but with reabsorption. Non-albumin bound Mg which comprises of Mg complexed to carbonate, phosphate and other large anions as well as free ionized Mg, represent the majority of Mg in serum, and are ultrafilterable. They can be expected to pass through the glomerulus without being fractionated due to the small size of the complexed or hydrated Mg ion (4.28 Å)[36] relative to the glomerular pore size (48 – 60 Å)[37]. Renal reabsorption changes in the same direction as glomerular filtration when kidney function is declining but not necessarily in the same proportion. The fact that eGFR - as our main parameter to assess kidney function - is only an estimate for glomerular filtration rate as a process that is supposedly associated but not causally related to

$\delta^{26}Mg$ in urine may explain the weak correlation that we have observed with serum creatinine derived eGFR values in our study.

A possible mechanism by which Mg isotope fractionation takes place in the nephron could be driven by its large hydration shell which consists of two layers of water molecules. Due to its high charge-to-size ratio, its hydration radius is approximately 400 times larger than its ionic radius and is the largest among other electrolytes such as Na, K and Ca. Mg is reabsorbed by two pathways, namely the paracellular pathway[38] (pore size = 3.5 Å) via the Proximal Convoluted Tubule and the Thick Ascending Loop of Henle, and the transcellular pathway in the distal tubule. Both the paracellular and transcellular transport of Mg would involve the removal of its large hydration shell[39]. Such a process is energy demanding. We deduced that the heavier Mg ion would prefer to remain in its hydrated state as it is more thermodynamically stable, based on principles of isotope fractionation theory[1]. Hence the lighter Mg isotope may be preferentially reabsorbed, leaving behind the heavier Mg isotope to be excreted in urine. Calcium, like Mg, also has a hydration shell (but consisting of only a single layer of water molecules) to remove before passing through the cell membrane via their transport channels. This could explain why the Ca isotope composition of urine is heavier than that of soft tissues as observed in several studies[7, 9-10, 40].

The renal reabsorption process may be represented by a Rayleigh fractionation process[41] illustrated in Fig. 4, in which ultrafilterable Mg is reabsorbed from tubular fluid (source) into serum (target) before excretion of remaining Mg in the tubular fluid into urine. The renal reabsorption of filtered Mg which occurs in the proximal convoluted tubule (PCT, 15 – 20% filtered Mg) followed by the thick ascending loop of Henle (TALH, 65 – 75% filtered Mg) and, finally, the distal convoluted tubule (DCT, 5 – 10% filtered Mg), is represented on the x-axis. As the extent of renal reabsorption is close to 100%, the difference in $\delta^{26}Mg$ for ultrafilterable (UF) Mg in serum and Mg in the tubular fluid (TF), Δ_{UF-TF} is large while the impact of an isotope effect during tubular reabsorption on ultrafilterable Mg in serum is only small following mass balance principles.

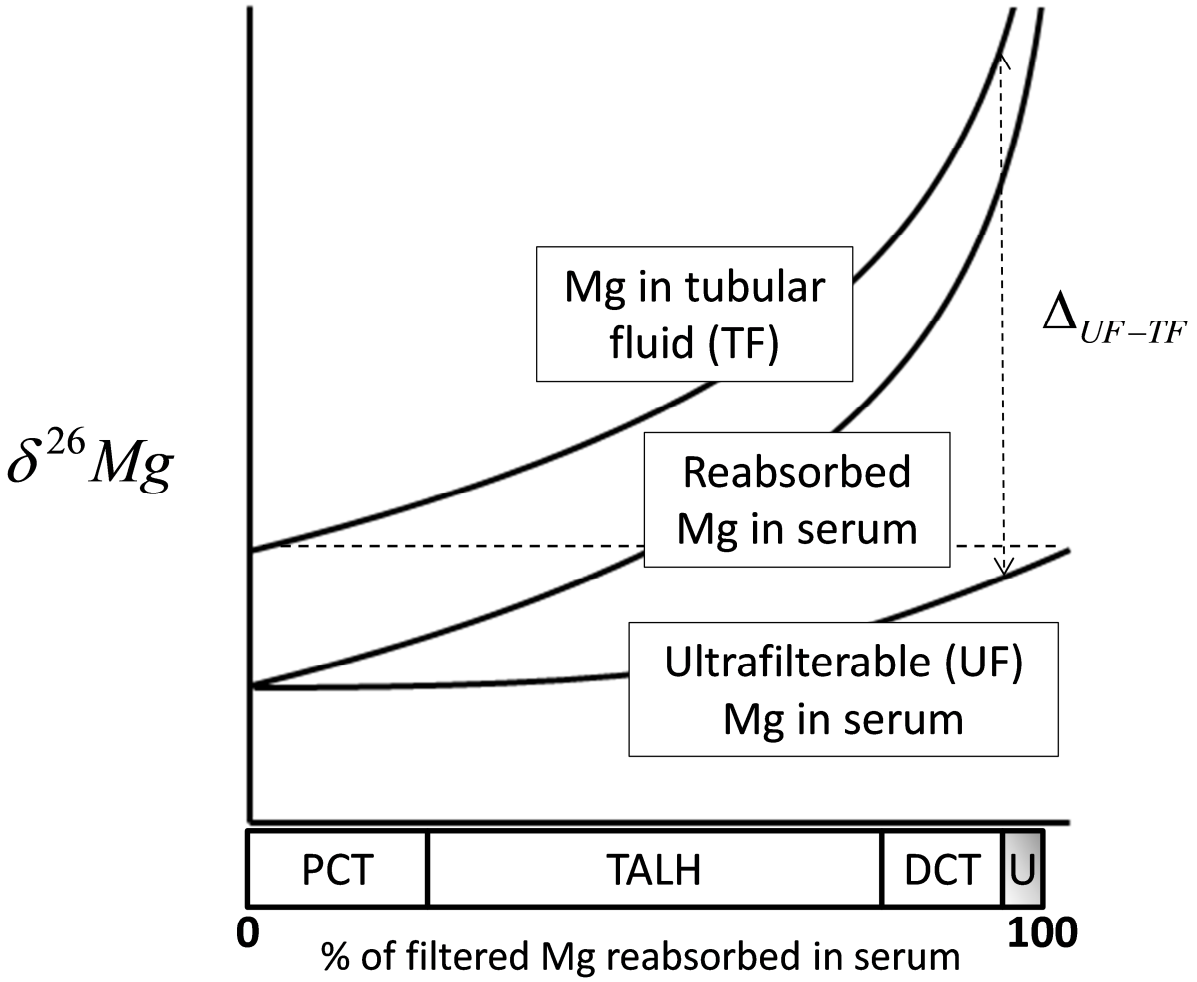

Figure 4. Plot of change in $\delta^{26}Mg$ for Mg in tubular fluid, reabsorbed Mg in serum (portion that is instantaneously reabsorbed) and ultrafilterable Mg in serum, following a Rayleigh fractionation process. The percentage of filtered Mg reabsorbed in serum is increased from the proximal convoluted tubule (PCT, 15 – 20% filtered Mg), thick ascending loop of Henle (TALH, 65 – 75% filtered Mg) and the distal convoluted tubule (DCT, 5 – 10% filtered Mg), is represented on the x-axis. Approximately 5% is excreted (shaded and denoted as U to represent urine). Since approximately 95% of filtered Mg is reabsorbed, Δ_{UF-TF} is likely to be large and differ between individuals with different renal reabsorption efficiencies.

From Fig. 4, it is apparent that the difference in isotope composition between the ultrafilterable Mg in serum and urinary Mg is supposedly better correlated with renal reabsorption efficiency than $\delta^{26}Mg$ in urine alone. Due to the limited mass spectrometric sensitivity of TIMS as employed in this study, we were not able to measure the isotope composition of ultrafilterable Mg. Amounts of

ultrafilterable Mg in serum are very small as Mg is primarily an intracellular ion. However, ultrafilterable $\delta^{26}Mg$ in serum may vary between individuals not only because of differences in the Mg isotope composition of diet as the source of body Mg. Variations may also be induced at the stage of intestinal Mg absorption and/or delivery of serum Mg to muscle tissue and bone as the major Mg compartments in the body.

We expect, however, that induced isotope effects at absorption are small. For an average adult human, the efficiency of Mg intestinal absorption is rather effective at 20-75%[42]. Mass balance principles dictate that an isotope effect becomes weaker in the target compartment of a transfer process, i.e. serum, when less is transferred. Similar to Ca, only a small fraction of body Mg (0.3%) circulates in serum. Most body Mg (ca. 60%) is present in bone of which about 30% are readily exchangeable. Remaining Mg is equally distributed between muscle tissue and other soft tissues. Cellular uptake of serum Mg or ionic exchange processes at the bone surface may induce an isotope effect in serum but as for Ca we expect the effect to be small as compared to the change in isotope composition induced at the level of the kidneys. The Ca isotope composition in blood was found to be close to diet and not significantly different among individuals of the same species[10, 40]. Since Ca and Mg homeostasis are coupled, variations in $\delta^{26}Mg$ in serum between individuals induced by bone deposition/release for Mg are probably small.

We have observed a correlation between age/eGFR and $\delta^{26}Mg$ as we have hypothesized, although weaker than expected for the above reasons. Surprisingly, we have also found a statistically significant correlation between $\delta^{26}Mg$ and serum Ca but the by far strongest correlation - even stronger than age - was with serum albumin concentration. The correlation observed between serum Ca and $\delta^{26}\mathrm{Mg}$ in urine could be due to serum albumin as a confounder since serum albumin is more highly correlated to serum Ca than $\delta^{26}Mg$ in urine (refer to Appendix Table A1). Exact mechanisms which cause serum albumin to decline with age are not entirely clear. Protein intake

may play a role but there are other age related factors that may affect albumin which cannot be separated from a diet effect[43]. Mg is known to be bound unspecifically to albumin. When serum albumin is increased, complexation with serum Mg may also increase. Studies of other cations e.g. Fe and Zn show that complexation with anions can favour either the lighter or heavier isotope based on theoretical *ab initio* calculations and experimental verification[44-45]. Our observations show that complexation may favour the lighter isotopes in serum as urine becomes isotopically heavier when serum albumin concentration is increased. A direct measure of $\delta^{26}Mg$ of ultrafilterable (non-albumin bound) Mg and non-ultrafilterable (albumin bound) Mg would help us to confirm if there is a preferential binding of the lighter Mg isotopes with serum albumin. This would be possible by using MC-ICP-MS to determine $\delta^{26}Mg$ of ultrafilterable Mg and non-ultrafilterable Mg in serum as a more sensitive technique compared to TIMS.

CONCLUSION

We have detected in human urine one of the isotopically heaviest forms of Mg described so far in nature. The effect is age-related and observed correlations point to reabsorption efficiency as the most probable mechanism. Parallel determination of $\delta^{26}Mg$ in the ultrafilterable fraction of Mg in serum would control for factors other than renal reabsorption. If confirmed, we would have found a measure of reabsorption in addition to glomerular filtration as the current standard parameter for kidney function. As reabsorption efficiency is supposed to decline earlier than GFR, Mg isotope effects will be a more sensitive marker of kidney function. Since the difference in $\delta^{26}Mg$ of ultrafilterable Mg in serum and urine can only be related to reabsorption, it is potentially more robust than a measure of eGFR based on serum creatinine concentration that is also affected by non-GFR determinants. Mg isotope composition is a property of the element itself and information is

not obtained from its concentration in body fluids and, based on first principles, determined solely by the efficiency of transport or transfer processes.

ACKNOWLEDGMENT/DECLARATION

Sample preparation steps which included microwave acid digestion and purification of Mg by ion-exchange chromatography were developed by Lim Li Yan Clare as an Honours Year Thesis. Optimization of the MC-TIMS technique for the measurement of Mg isotope ratios was carried out by Go Jun Hong, also as an Honours Year Thesis. Both honours projects were conducted at NutriTrace@NUS (Department of Chemistry/Biochemistry) under supervision of Gina Chew and Thomas Walczyk. Derivation of GS-IDA equations and optimization of spike and blend compositions using MATLAB was done by Gina Chew in collboration with Thomas Walczyk. The clinical study was carried out as a collaborative project between the author, Jimmy Teo (Department of Medicine, NUS), Priscilla How (Department of Pharmacy) and Thomas Walczyk. Toh Qi Chun assisted in the submission of relevant documents to the Domain Specific Review Board of the National Healthcare Group to obtain approval for the clinical study. Gina Chew was the main study coordinator who screened and recruited all the subjects and analyzed urine samples for $\delta^{26}Mg$. Serum and urine biochemistry measurements were done at NUH (Department of Laboratory Medicine).

REFERENCES

1. Hoefs, J., *Stable isotope geochemistry*. Springer: 2009.
2. Walczyk, T.; von Blanckenburg, F., *Science* **2002,** *295* (5562), 2065-2066.
3. Hotz, K.; Augsburger, H.; Walczyk, T., *J. Anal. At. Spectrom.* **2011,** *26* (7), 1347-1353.
4. Hotz, K.; Krayenbuehl, P. A.; Walczyk, T., *J. Biol. Inorg. Chem.* **2012,** *17* (2), 301-309.
5. Chew, G.; Walczyk, T., *Anal. Chem.* **2013,** *85* (7), 3667-3673.
6. Quamme, G. A., *Miner. Electrol. Metab.* **1993,** *19* (4-5), 218-225.
7. Heuser, A.; Eisenhauer, A., *Bone* **2010,** *46* (4), 889-896.
8. Skulan, J.; Bullen, T.; Anbar, A. D.; Puzas, J. E.; Shackelford, L.; LeBlanc, A.; Smith, S. M., *Clin. Chem.* **2007,** *53* (6), 1155-1158.
9. Heuser, A.; Eisenhauer, A.; Scholz-Ahrens, K. E.; Schrezenmeir, J., *Geochim. Cosmochim. Acta* **2007,** *71* (15), A402-A402.
10. Skulan, J.; DePaolo, D. J., *Proceedings of the National Academy of Sciences* **1999,** *96* (24), 13709-13713.
11. Gullestad, L.; Nes, M.; Rønneberg, R.; Midtvedt, K.; Falch, D.; Kjekshus, J., *J. Am. Coll. Nutr.* **1994,** *13* (1), 45-50.
12. Barbagallo, M.; Belvedere, M.; Dominguez, L. J., *Magnes. Res.* **2009,** *22* (4), 235.
13. Lim, C. Separation of Magnesium from Urine for Isotope Ratio Analysis. Honours Thesis, National University of Singapore, April 2011.
14. Galy, A.; Yoffe, O.; Janney, P. E.; Williams, R. W.; Cloquet, C.; Alard, O.; Halicz, L.; Wadhwa, M.; Hutcheon, I. D.; Ramon, E.; Carignan, J., *J. Anal. At. Spectrom.* **2003,** *18* (11), 1352-1356.
15. Levey, A. S.; Stevens, L. A., *Am. J. Kidney Dis.* **2010,** *55* (4), 622.
16. Galy, A.; Belshaw, N. S.; Halicz, L.; O'Nions, R. K., *Int. J. Mass spectrom.* **2001,** *208* (1), 89-98.
17. Ra, K.; Kitagawa, H., *J. Anal. At. Spectrom.* **2007,** *22* (7), 817-821.
18. Black, J. R.; Yin, Q. Z.; Casey, W. H., *Geochim. Cosmochim. Acta* **2006,** *70* (16), 4072-4079.
19. Bolou-Bi, E. B.; Vigier, N.; Poszwa, A.; Boudot, J. P.; Dambrine, E., *Geochim. Cosmochim. Acta* **2012**.
20. Chang, V. T. C.; Makishima, A.; Belshaw, N. S.; O'Nions, R. K., *J. Anal. At. Spectrom.* **2003,** *18* (4), 296-301.
21. Bolou-Bi, E. B.; Vigier, N.; Brenot, A.; Poszwa, A., *Geostand. Geoanal. Res.* **2009,** *33* (1), 95-109.
22. Ling, M. X.; Sedaghatpour, F.; Teng, F. Z.; Hays, P. D.; Strauss, J.; Sun, W., *Rapid Commun. Mass Spectrom.* **2011,** *25* (19), 2828-2836.
23. Tipper, E. T.; Galy, A.; Bickle, M. J., *Geochim. Cosmochim. Acta* **2008,** *72* (4), 1057-1075.
24. Wombacher, F.; Eisenhauer, A.; Bohm, F.; Gussone, N.; Regenberg, M.; Dullo, W. C.; Ruggeberg, A., *Geochim. Cosmochim. Acta* **2011,** *75* (19), 5797-5818.
25. Tipper, E. T.; Galy, A.; Bickle, M. J., *Earth. Planet. Sci. Lett.* **2006,** *247* (3-4), 267-279.
26. Teng, F. Z.; Wadhwa, M.; Helz, R. T., *Earth. Planet. Sci. Lett.* **2007,** *261* (1), 84-92.
27. Huang, F.; Zhang, Z. F.; Lundstrom, C. C.; Zhi, X. C., *Geochim. Cosmochim. Acta* **2011,** *75* (12), 3318-3334.
28. Opfergelt, S.; Georg, R.; Delvaux, B.; Cabidoche, Y. M.; Burton, K.; Halliday, A., *Earth. Planet. Sci. Lett.* **2012,** *341*, 176-185.
29. Choi, M. S.; Ryu, J.-S.; Lee, S.-W.; Shin, H. S.; Lee, K.-S., *J. Anal. At. Spectrom.* **2012,** *27* (11), 1955-1959.
30. Coresh, J.; Selvin, E.; Stevens, L. A.; et al., *JAMA* **2007,** *298* (17), 2038-2047.
31. Lindeman, R. D., Renal and Urinary Tract Function. In *Comprehensive Physiology*, John Wiley & Sons, Inc.: 2010.
32. Fliser, D.; Franek, E.; Joest, M.; Block, S.; Mutschler, E.; Ritz, E., *Kidney Int.* **1997,** *51* (4), 1196-1204.
33. Musso, C.; Macías-Núñez, J., *Int. Urol. Nephrol.* **2011,** *43* (1), 249-252.

34. Jorde, R.; Sundsfjord, J.; Bønaa, K. H., *Eur. J. Epidemiol.* **2001,** *17* (12), 1117-1123.
35. Ferguson, M. A.; Waikar, S. S., *Clin. Chem.* **2012,** *58* (4), 680-689.
36. Nightingale, E. R., *The Journal of Physical Chemistry* **1959,** *63* (9), 1381-1387.
37. Thomson, S. C.; Blantz, R. C., Biophysics of Glomerular Filtration. In *Comprehensive Physiology*, John Wiley & Sons, Inc.: 2012.
38. Gunzel, D.; Yu, A. S. L., *Pflugers Arch. EJP* **2009,** *458* (1), 77-88.
39. Jahnen-Dechent, W.; Ketteler, M., *Clinical Kidney Journal* **2012,** *5* (Suppl 1), i3-i14.
40. Hirata, T.; Tanoshima, M.; Suga, A.; Tanaka, Y.-k.; Nagata, Y.; Shinohara, A.; Chiba, M., *Anal. Sci.* **2008,** *24* (11), 1501-1507.
41. Johnson, C. M.; Beard, B. L., *Rev. Mineral. Geochem.* **2004,** *55*, 1-24.
42. Swaminathan, R., *Clin. Biochem. Rev.* **2003,** *24* (2), 47.
43. Thalacker-Mercer, A. E.; Campbell, W. W., *Nutr. Rev.* **2008,** *66* (2), 91-95.
44. Moynier, F.; Fujii, T.; Wang, K.; Foriel, J., *Comptes Rendus Geoscience* **2013,** *345* (5-6), 230-240.
45. Fujii, T.; Albarède, F., *PLoS ONE* **2012,** *7* (2), e30726.

Appendix

Table A1. Spearman rank correlations, ρ of variables with a) age b) serum albumin and c) eGFR

(a) Variables correlated with age	**ρ**	**(b) Variables correlated with S_{Alb}**	**ρ**	**(c) Variables correlated with eGFR**	**ρ**
BMI	0.48	Age	-0.72*	Age	-0.75*
WHR	0.54	S_{Ca}	0.67*	S_{Alb}	0.56
Systolic BP	0.51	S_{PO4}	0.56	S_{VitD}	-0.58*
S_{Alb}	-0.72*	S_{VitD}	-0.49	S_{Mg}	-0.50
S_{Ca}	-0.73*	$eGFR$	0.56	U_{vol}	-0.58*
S_{Cr}	-0.49	U_{vol}	-0.56	U_{Cr}	0.59*
S_{PO4}	-0.57*	U_{Cr}	0.51	$U_{Mg,norm}$	-0.52
S_{VitD}	0.50	$U_{Na,norm}$	-0.57*		
$eGFR$	-0.75*	$U_{Mg,norm}$	-0.52		
U_{vol}	0.58*	$\delta^{26}\mathrm{Mg}$	0.615*		
U_{Cr}	-0.67*				
$U_{Na,norm}$	0.57*				
$U_{K,norm}$	0.60*				
$U_{Mg,norm}$	0.51				
$\delta^{26}\mathrm{Mg}$	-0.47				

* indicate p-value < 0.01 (2-sided), otherwise, p-value < 0.05

4. CONCLUSION

We have successfully derived and validated a novel mass bias correction technique known as Gravimetric Spiking-Isotope Dilution Analysis (GS-IDA, Manuscript 2) to determine isotope fractionation effects of Mg in nature, using MC-TIMS, that was never previously done before. The use of tantalum oxide as the ionizing agent improved the precision of Mg isotope ratio measurements. The external precision of $^{26}Mg/^{24}Mg$ was 0.0018% (n = 7) after internal normalization to $^{25}Mg/^{24}Mg$ = 0.12663. It is the highest possible precision achieved thus far among publications related to MC-TIMS for a Mg load of 30 µg. Optimization of parameters for GS-IDA using Monte Carlo Simulations was carried out as shown in Manuscript 1.

We are the first group to explore Mg isotope fractionation effects in a higher organism (human urine) using the GS-IDA technique. $\delta^{26}Mg$ = 1.36 ± 0.10 ‰ (1 SD, n = 5) relative to Mg Titrisol standard. The external standard deviation of ±0.10 ‰ shows that our technique is capable of distinguishing between inter-individual differences. Our Mg Titrisol standard relative to the currently accepted reporting standard DSM-3 was $\delta^{26}Mg$ =1.59 ± 0.10 ‰ (1 SD, n = 5). The spike that was calibrated against Mg Titrisol was used to prepare the blends for measurement of $\delta^{26}Mg$ in urine of subjects recruited for our clinical study (Manuscript 3). Measured $\delta^{26}Mg$ in urine were then converted from the Mg Titrisol scale to the DSM-3 scale by subtracting 1.59 ‰, which allowed us to compare our data against samples found in the geosphere, biosphere and hydrosphere.

We found that Mg in urine is one of the isotopically heaviest form in nature. The results of our clinical study showed an age-related dependence of $\delta^{26}Mg$ in urine relative to DSM-3 in urine (Spearman rank correlation, ρ = -0.47, p = 0.038, 2-sided test) and a weak association with estimated glomerular filtration rate (eGFR), an index of kidney function (ρ = 0.37, p = 0.052, 1-sided test). It is also known that kidney function declines with age (ρ =- 0.75, p < 0.001, 2-sided test). The age-related dependence of $\delta^{26}Mg$ could be due to a parallel decline in kidney function. Rayleigh fractionation

dictates that a large extent of transfer of a substance from source to target will give rise to a large difference in delta-value between the source and target. Since approximately 95% of filtered Mg is reabsorbed and 5% is excreted in urine, an isotope fractionation effect in urine due to the renal reabsorption process is highly possible. It is the difference in $\delta^{26}Mg$ between ultrafilterable Mg in serum and Mg in urine that would be a true measure of renal reabsorption. eGFR is a measure of only one facet of kidney function which is glomerular filtration and not reabsorption. Since we lack measurements of $\delta^{26}Mg$ in ultrafilterable Mg in serum and eGFR is not a true measure of renal reabsorption, we only obtained a weak correlation between eGFR and $\delta^{26}Mg$ in urine.

As the difference in $\delta^{26}Mg$ between ultrafilterable Mg in serum and Mg in urine can only be related to reabsorption, it is potentially more robust than other measures such as eGFR which rely on measurement of concentration of endogenous markers which are influenced by non-GFR determinants and therefore not ideal. Magnesium isotope composition is a property of the element itself and information is not through its concentration in body fluids but based on first principles, determined solely by the efficiency of transfer processes.

5. RESEARCH PARTNERS AND CONTRIBUTIONS

Sample preparation steps which included microwave acid digestion and purification of Mg by ion-exchange chromatography were developed by Lim Li Yan Clare as an Honours Year Thesis. Optimization of the MC-TIMS technique for the measurement of Mg isotope ratios was carried out by Go Jun Hong, also as an Honours Year Thesis. Both honours projects were conducted at the NutriTrace Laboratory at NUS (Department of Chemistry/Biochemistry) under supervision of Gina Chew and Assoc. Prof Thomas Walczyk. Derivation of GS-IDA equations and optimization of spike and blend compositions using MATLAB was done by Gina Chew. The clinical study was carried out as a collaborative project between Gina Chew, Dr Jimmy Teo (Department of Medicine, NUS), Dr Priscilla How (Department of Pharmacy) and Assoc. Prof Thomas Walczyk. Toh Qi Chun assisted in the submission of relevant documents to the Domain Specific Review Board of the National Healthcare Group to obtain approval for the clinical study. Gina Chew was the main study coordinator who screened and recruited all the subjects and analyzed urine samples for $\delta^{26}Mg$. Serum and urine biochemistry measurements were done by NUH (Department of Laboratory Medicine).